Prediction of Drying Shrinkage Cracking of Steel Chip Reinforced Polymer Cementitious Composites Considering Bond and Tensile Creep

2015

Sunhee Hong

TABLE OF CONTENTS

Chapter 1   Introduction

1.1   Background and objective

The development of material civilization and industrialization since the industrial revolution caused various environmental problems, such as global warming, the destruction of the ecosystem, resource depletion and waste accumulation, etc. Since the adoption of Kyoto Protocol in 1997, reducing of CO_2 emission became important tasks in the entire industry (AIJ 2008). Among others, iron and steel industry represents one of the major constituents of industrial waste. Therefore, the reuse of steel materials contributes to a reduction in the environmental load.

Over the years, numerous attempts have been made to reuse the waste produced by the iron and steel industry. For example, there is an idea of using steel chips as a replacement material for sand in concrete (Zainab and Enas 2008, Alwaeli and Nadziakiewicz 2012). As part of research on using steel chips as a reinforcing material, there is a study on the shape memory alloy machining chips used in reinforcing smart composites (Wakatsuki et al. 2006). However, their application to building structures is not economically practical. Therefore, the use of steel chips, which are waste products of the iron and steel industry, is economically efficient and environmentally sound because it reduces the total amount of industrial waste.

Recently, many studies related to fiber reinforced cementitious composites (FRCC) have been conducted, and various structures have been built with FRCC. The fibers used for FRCC, which improve the bond strength of mortar or concrete, tend to be expensive. As a result, it was attempted to develop and implement steel chip reinforced cementitious composite (SCRCC), which is reinforced with steel chips instead of conventional steel fibers. The steel chips are produced when steel plates are precisely machined on NC lathes. If the use of SCRCC is economically practical, it will also contribute to reducing the environmental load by reusing steel chips, which are currently being disposed of as industrial waste. But it is a serious problem that their consistency grows worse remarkably because of addition of steel chips. By means of modification of SCRCC with polymer dispersions for cement modifier, it is expected that not only the consistency but also the physical properties of the hardened cementitious composites are improved. For this reason, not only SCRCC but also steel chip reinforced polymer cementitious composites (SCRPCC) were examined in this study.

In a previous study (Kanada et al. 2011), fundamental material tests clarified that SCRCC has properties that are similar to FRCC. Based on these results, it was set out to examine the drying shrinkage cracking behavior of SCRCC to determine its long-term durability.

An experiment based on the research of Koyanagi et al. (1990) and Kheder (1997) was conducted in an attempt to predict the shrinkage strain and cracking behavior of SCRCC. However, the prediction did not correspond to the experimental result (Hong et al. 2014).

It was determined that the drying shrinkage and cracking characteristics of the restraint SCRCC

members were influenced by tensile creep and bond with the reinforcement. As a result, the drying shrinkage cracking behavior was predicted analytically by considering tensile creep based on studies by Kojima et al. (2008), Kumano et al. (1999), and Ranaivomanana et al. (2013).

1.2   Organization

This dissertation consists of eight chapters, and the schematic diagram of organization is shown in Figure 1.1.
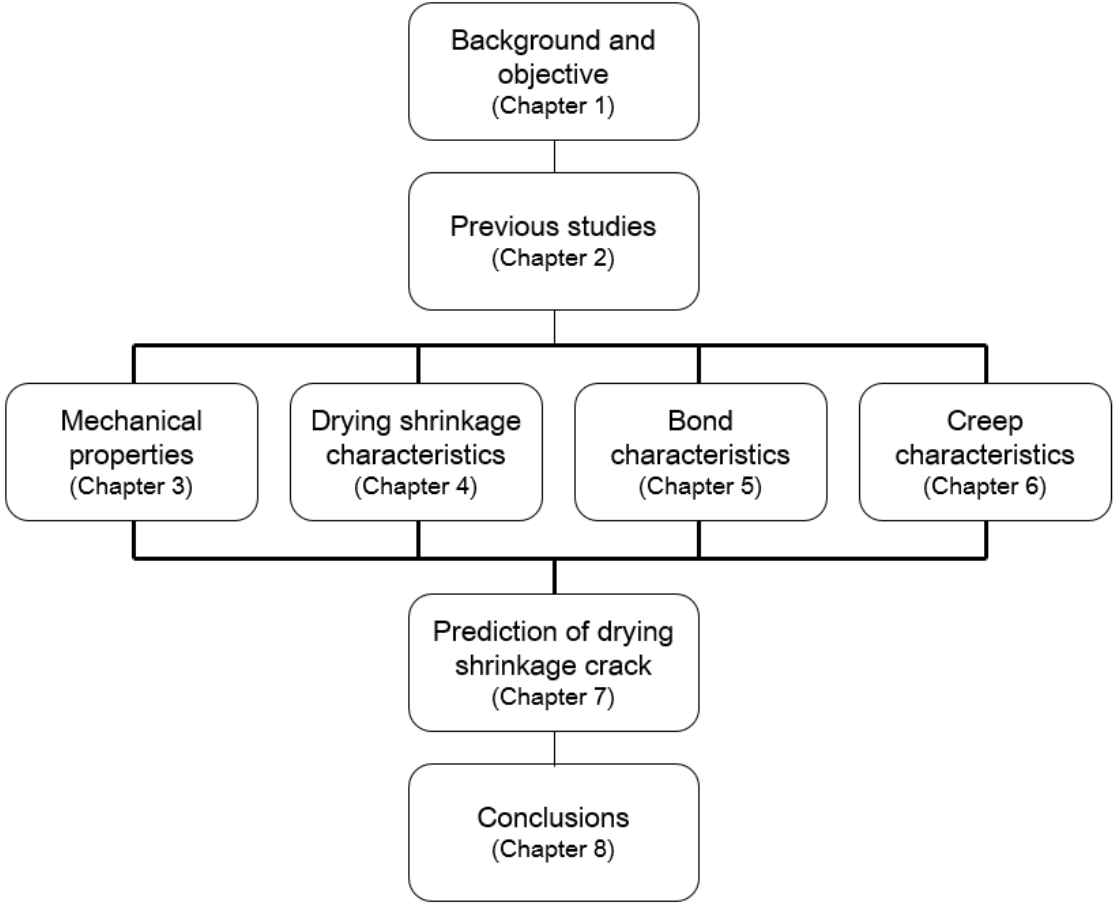
Figure 1.1 Organization and flow chart of this study

Chapter 1 is the background of this study, while Chapter 2 summarizes the previous researches on fiber reinforced cementitious composites, steel chip, concrete-polymer composites and shrinkage cracking. And Chapter 8 is the summary and conclusions. Chapter 3 to 7 constitute the main part of the dissertation: (1) compressive and flexural strength properties, (2) drying shrinkage cracking characteristics through the free and restrained shrinkage test, (3) bond characteristics through the pull-out and uniaxial tension test, (4) creep characteristics to predict the drying shrinkage crack. (5) prediction of drying shrinkage cracking behavior based on the experiment results. The contents of the five chapters are summarized as follows.

In Chapter 3, compressive strength tests and three point flexural tests were conducted to understand the

mechanical properties of SCRCC and SCRPCC.

In Chapter 4, the drying shrinkage cracking behavior of SCRCC and SCRPCC were examined to determine its long-term durability.

In Chapter 5, it is examined about fundamental properties of bond stress-slip relationships between steel bar and SCRCC or SCRPCC by means of the pull-out test. Also, uniaxial tension tests were conducted to examine the cracking characteristics of SCRCC and SCRPCC.

In Chapter 6, flexural creep tests of SCRCC and SCRPCC were conducted with varying loading period in order to clarify how the reinforcing with steel chip impacts on the creep behavior.

In Chapter 7, prediction of the drying shrinkage cracking behavior of SCRCC and SCRPCC was attempted to verify the long-period durability of SCRCC and SCRPCC based on the experiment results of the previous chapters.

Chapter 2   Previous studies

2.1   Fiber reinforced cementitious composites

Concrete is relatively brittle, and its tensile strength is typically only about one tenths of its compressive strength. Therefore regular concrete is normally reinforced with steel reinforcing bars. For many applications, it is becoming increasingly popular to reinforce the concrete with small, randomly distributed fibers. Their main purpose is to increase the energy absorption capacity and toughness of the material, but also increase tensile and flexural strength of concrete.

2.1.1 Historical aspects of fiber reinforced concretes

Since ancient times, fibers have been used to reinforce brittle materials. Straw was used to reinforce sun-baked bricks, and horsehair was used to reinforce masonry mortar and plaster. In more recent times, large scale commercial use of asbestos fibers in a cement paste matrix began with the invention of the Hatschek process in 1898. Asbestos cement construction products are widely used throughout the world today. However, primarily due to health hazards associated with asbestos fibers, alternate fiber types were introduced throughout the 1960s and 1970s.

In modern times, a wide range of engineering materials (including ceramics, plastics, cement, and gypsum products) incorporate fibers to enhance composite properties. The enhanced properties include tensile strength, compressive strength, elastic modulus, crack resistance, crack control, durability, fatigue life, resistance to impact and abrasion, shrinkage, expansion, thermal characteristics, and fire resistance (ACI committee 544 1996).

Experimental trials and patents involving the use of discontinuous steel reinforcing elements (such as nails, wire segments, and metal chips) to improve the properties of concrete date from 1910 (Naaman 1985). During the early 1960s in the United States, the first major investigation was made to evaluate the potential of steel fibers as a reinforcement for concrete (Romualdi 1963). Since then, a substantial amount of research, development, experimentation, and industrial application of steel fiber reinforced concrete has occurred.

Use of glass fibers in concrete was first attempted in the USSR in the late 1950s (Biryukovich et al. 1965). It was quickly established that ordinary glass fibers, such as borosilicate E-glass fibers, are attacked and eventually destroyed by the alkali in the cement paste. Considerable development work was directed towards producing a form of alkali-resistant glass fibers containing zirconia (Majumdar 1975). This led to a considerable number of commercialized products. The largest use of glass fiber reinforced concrete in the U.S. is currently for the production of exterior architectural cladding panels. Initial attempts at using synthetic fibers (nylon, polypropylene) were not as successful as those using glass or steel fibers (Goldfein 1963, Monforce 1968). However, better understanding of the concepts behind fiber reinforcement, new methods of fabrication, and new types of organic fibers have led researchers to

conclude that both synthetic and natural fibers can successfully reinforce concrete (Krenchel and Shah 1985, Naaman et al. 1982). Considerable research, development, and applications of FRC are taking place throughout the world. Industry interest and potential business opportunities are evidenced by continued new developments in fiber reinforced construction materials. These new developments are reported in numerous research papers, international symposia, and state-of-the-art reports issued by professional societies. The ACI Committee 544 published a state-of-the-art report in 1973 (ACI Committee 544 1973). RILEM's committee on fiber reinforced cement composites has also published a report (RILEM Technical Committee 19-FRC 1977). A Recommended Practice and a Quality Control Manual for manufacture of glass fiber reinforced concrete panels and products have been published by the Precast/Prestressed Concrete Institute (PCI Committee on Glass Fiber Reinforced Concrete Panels 1991, 1993).

2.1.2 Steel fiber reinforced concretes

There are numerous fiber types available for commercial and experimental use. The basic fiber categories are steel, glass, synthetic, and natural fiber materials. Among them, previous researches of steel fiber reinforced concrete were reviewed in this part.

Steel fiber reinforced concrete (SFRC) is concrete made of hydraulic cements containing fine or fine and coarse aggregate and discontinuous discrete steel fibers. In tension, SFRC fails only after the steel fiber breaks or is pulled out of the cement matrix. Figure 2.1 shows a typical fractured surface of SFRC.

Figure 2.1 Fracture surface of steel fiber reinforced concrete (ACI committee 544 1996)

Properties of SFRC in both the freshly mixed and hardened state, including durability, are a consequence of its composite nature. The mechanics of how the fiber reinforcement strengthens concrete or mortar, extending from the elastic precrack state to the partially plastic post-cracked state, is a continuing research topic. One approach to the mechanics of SFRC is to consider it a composite material whose properties can be related to the fiber properties (volume percentage, strength, elastic modulus, and a fiber bonding parameter of the fibers), the concrete properties (strength, volume percentage, and elastic

modulus), and the properties of the interface between the fiber and the matrix. A more general and current approach to the mechanics of fiber reinforcing assumes a crack arrest mechanism based on fracture mechanics. In this model, the energy to extend a crack and debond the fibers in the matrix relates to the properties of the composite (ACI committee 544 1996).

Types of steel fibers

Round, straight steel fibers are produced by cutting or chopping wire, typically wire having a diameter between 0.25 and 1.00 mm. Flat, straight steel fibers having typical cross sections ranging from 0.15 to 0.64 mm thickness by 0.25 to 2.03 mm width are produced by shearing sheet or flattening wire (Figure 2.2a). Crimped and deformed steel fibers have been produced with both full-length crimping (Figure 2.2b), or bent or enlarged at the ends only (Figure 2.2 c and d). Some fibers have been deformed by bending or flattening to increase mechanical bonding. Some fibers have been collated into bundles to facilitate handling and mixing. During mixing, the bundles separate into individual fibers (Figure 2.2c). Fibers are also produced from cold drawn wire that has been shaved down in order to make steel wool. The remaining wires have a circular segment cross-section and may be crimped to produce deformed fibers. Also available are steel fibers made by a machining process that produces elongated chips. These fibers have a rough, irregular surface and a crescent−shaped cross section (Figure 2.2e).

Steel fibers are also produced by the melt-extraction process. This method uses a rotating wheel that contacts a molten metal surface, lifts off liquid metal, and rapidly solidifies it into fibers. These fibers have an irregular surface, and crescent shaped cross-section (Figure 2.2f) (ACI committee 544 1996).
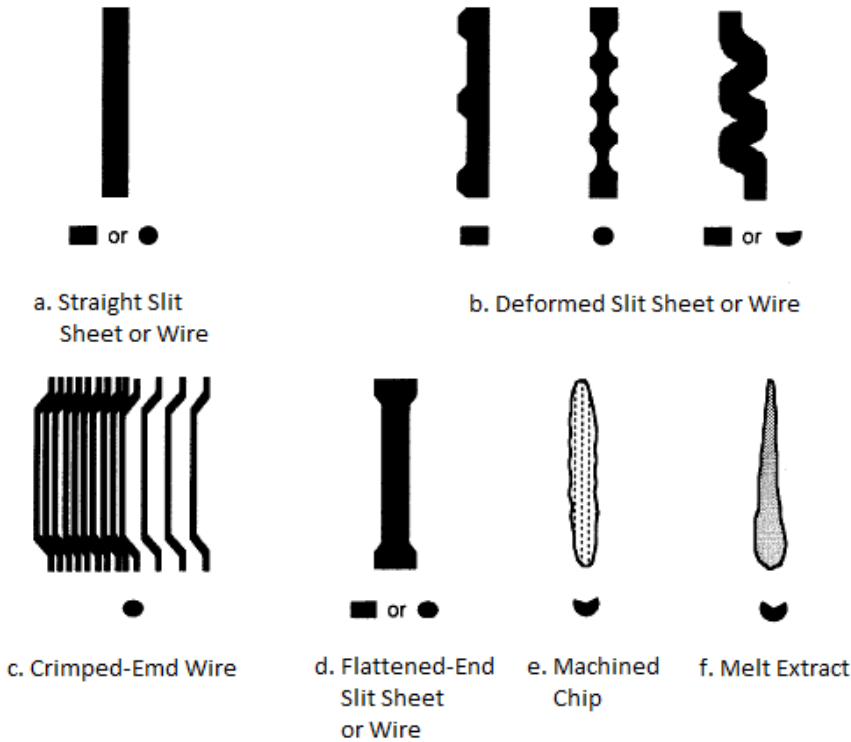

Figure 2.2 Various steel fiber geometries (ACI committee 544 1996)

History of steel fibers

Research on closely-spaced wires and random metallic fibers in the late 1950s and early 1960s was the basis for a patent on SFRC based on fiber spacing (Romualdi and Batson 1963, Romualdi and Mandel 1964, Bettelle Memorial Institute 1969, 1970, U.S. Steel Corporation 1972). The Portland Cement Association investigated fiber reinforcement in the late 1950s (Monfore 1968). Principles of composite materials were applied to analyze fiber reinforced concrete (Shah and Rangan 1970, 1971). The addition of fibers was shown to increase toughness much more than the first crack strength in these tests. Additional data on patents are documented in the reference by Naaman (1985). Since the time of these original fibers, many new steel fibers have been produced.

Applications of SFRC since the mid-1960s have included road and floor slabs, refractory materials and concrete products (Hoff 1986).

The usefulness of SFRC has been aided by other new developments in the concrete field. High-range water reducing admixtures increase the workability of some harsh SFRC mixtures (Ramakrishnan et al. 1981) and have reduced supplier and contractor resistance to the use of SFRC. Silica fume and accelerators have enabled steel fiber reinforced shotcrete to be placed in thicker layers. Silica fume also reduces the permeability of the shotcrete material (Morgan et al. 1987).

Properties of fresh SFRC

The properties of SFRC in its freshly mixed state are influenced by the aspect ratio of the fiber, fiber geometry, its volume fraction, the matrix proportions, and the interfacial bond characteristics of fiber and matrix (Ramakrishnan 1987).

Since compaction by mechanical vibration is recommended in most SFRC applications, assessing the workability of a SFRC mixture with either the Vebe consistometer, as described in the British Standards Institution Standard BS 1881, or by ASTM C 995 Inverted Slump-Cone Time is recommended rather than the conventional slump measurement. A typical relationship between slump, Vebe time, and Inverted Slump-Cone time is shown in Figure 2.3 (Johnston 1984). Studies have established that a mixture with a relatively low slump can have good consolidation properties under vibration (Balaguru and Ramakrishnan 1987). Slump loss characteristics with time for SFRC and non-fibrous concrete are similar (Balaguru and Ramakrishnan 1988). In addition to the above considerations, the balling of fibers must be avoided. A collection of long thin steel fibers with an aspect ratio greater than 100 will, if shaken together, tend to interlock to form a mat, or ball, which is very difficult to separate by vibration alone. On the other hand, short fibers with an aspect ratio less than 50 are not able to interlock and can easily be dispersed by vibration (Hannant 1978). However, a high aspect ratio is desired for many improved mechanical properties in the hardened state.
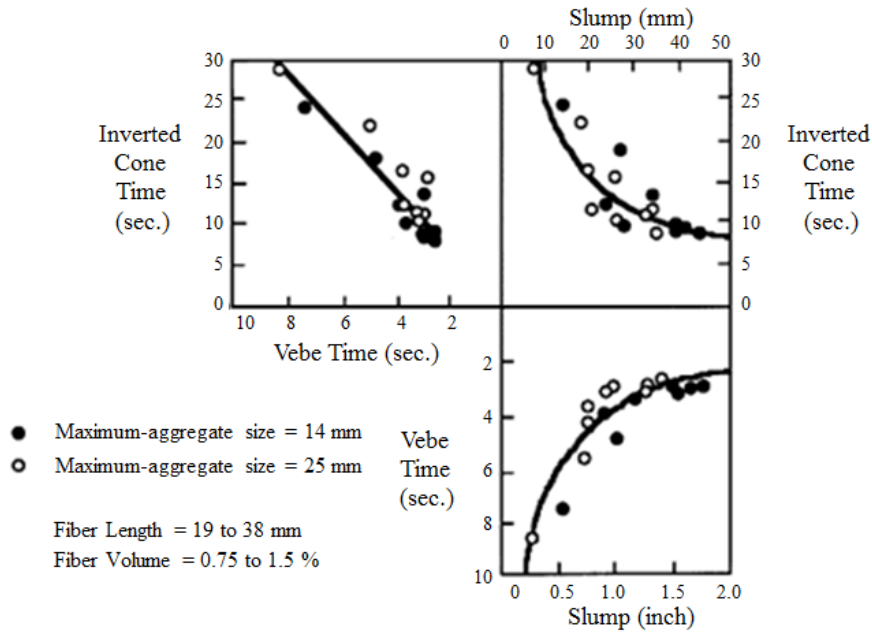
Figure 2.3 Relationship between slump, vebe time and inverted cone time (Johnson 1984)

Properties of the hardened composites

The mechanism of fiber reinforcement of the cementitious matrix in concrete has been extensively studied in terms of the resistance of the fibers to pullout from the matrix resulting from the break-down of the fiber-matrix interfacial bond. Attempts have been made to relate the bond strength to the composite mechanical properties of SFRC (Shah and McGarry 1971, Shah 1971, Shah 1983, Naaman and Shah 1975, Naaman and Shah 1976, Shah and Naaman 1976, Stang and Shah 1986, Morrison et al. 1988, Gray and Johnston 1984).

Steel fibers improve the ductility of concrete under all modes of loading, but their effectiveness in improving strength varies among compression, tension, shear, torsion and flexure.

In compression, the ultimate strength is only slightly affected by the presence of fibers, with observed increases ranging from 0 to 15 percent for up to 1.5 percent by volume of fibers (Johnston 1974, Dixon and Mayfield 1971).

In direct tension, the improvement in strength is significant, with increases of the order of 30 to 40 percent reported for the addition of 1.5 percent by volume of fibers in mortar or concrete (Williamson 1974).

In flexure, the flexural strength of SFRC is about 50 to 70 percent more than that of the unreinforced concrete matrix in the normal three-point bending test (Shah and Rangan 1971, Works and Untrauer 1964). Use of higher fiber volume fractions, or center-point loading, or small specimens and long fibers with significant fiber alignment in the longitudinal direction will produce greater percentage increases up to 150 percent (Snyder and Lankard 1972, Johnston 1989).

In fatigue behavior, it has been shown that the addition of fibers to conventionally reinforced beams increases the fatigue life and decreases the crack width under fatigue loading (Kormeling et al. 1980)

2.2   Steel chip

Over the years, numerous attempts have been made to reuse the waste produced by the iron and steel industry. For example, there is an idea of using steel chips as a replacement material for sand in concrete (Zainab and Enas 2008, Alwaeli and Nadziakiewicz 2012).

As part of research on using steel chips as a reinforcing material, there is a study on the shape memory alloy machining chips used in reinforcing smart composites (Wakatsuki et al. 2006). However, their application to building structures is not economically practical.

Therefore, the use of steel chips, which are waste products of the iron and steel industry, is economically efficient and environmentally sound because it reduces the total amount of industrial waste. There is a research about steel chip reinforced cementitious composites (SCRCC) as a substitution material of steel fiber reinforced cementitious composites (SFRCC) by Kanada (2012). However, the study on the durability of SCRCC was not conducted in this research. So it is necessary to investigate the durability of SCRCC thoroughly.

2.3   Concrete-polymer composites

Cement mortar and concrete have some disadvantages such as delayed hardening, low tensile strength, large drying shrinkage, and low chemical resistance. To reduce these disadvantages, many attempts to use polymers have been made. One such attempt is polymer-modified (or polymer-cement) mortar or concrete, which is made by the modifying ordinary cement mortar or concrete with polymer additives such as latexes, redispersible polymer powders, water-soluble polymers, liquid resins, and monomers (Ohama 1995a).

2.3.1 Historical background

The use of polymers as an admixture to cementitious materials is not new. In Babylonia in 4000 B.C. and in Indus Valley in 3000 B.C., clay brick walls were produced by using natural polymers such as albumen and rice paste (Chandra and Ohama 1994, Kardon 1997). More recently, in 1923, the first patent of a polymer-hydraulic-cement system, issued to Cresson (1923), refers to paving materials with natural rubber latexes where cement was used as filler. The first patent of the modern concept of a polymer-modified system was granted to Lefebure in 1924 (Lefebure 1924). Lefebure appears to be the first worker who intended to produce a Polymer-Modified Concrete (PMC) using natural rubber latexes by proportioning latex on the basis of cement content; Cresson, in contrast, based his mixture on the polymer content. In 1925, Kirkpatrick patented a similar idea (Kirkpatrick 1925). Throughout the 1920s and 1930s, Latex-Modified Mortar (LMM) and concrete using natural rubber latexes were developed. Bond's patent in 1932 (Bond 1932) suggested the use of synthetic rubber latexes, and Rodwell's patent in 1939 (Rodwell 1939) first claimed to use synthetic resin latexes, including polyvinyl acetate latexes, to produce polymer-modified systems.

In the 1940s, patents on polymer-modified systems with synthetic latexes, such as poly-chloroprene rubber latexes (Neoprene) (Cooke 1941) and poly-acrylic ester latexes (Jaenicke et al. 1943) were published. Also, polyvinyl acetate-modified mortar and concrete were actively developed for practical applications. Since the late 1940s, polymer modified mixtures have been used in various applications such as deck coverings for ships and bridges, paving, floorings, anti-corrosives, and adhesives. In the United Kingdom, feasibility studies on the applications of natural rubber-modified systems were conducted by Stevens (1948) and Griffiths (1951). Also, a strong interest was focused on the use of synthetic latexes in the polymer-modified systems. Geist et al. (1953) reported a detailed fundamental study on polyvinyl acetate-modified mortar and provided a number of valuable suggestions for later research and development of polymer-modified systems. The first use of epoxy resins to modify hydraulic cement was reported by Lezy and Paillere (1967).

Research efforts in the 1970s, 80s, and 90s were focused on examining the properties of Latex-Modified LMC and selecting the most suitable polymer latex for modifying cement in polymer-modified mortar (PMM) and PMC (Popovics and Tamas 1978, Lavelle 1988, Ohama 1995a, Okba et al. 1997). A major milestone during that time period was revealing the principles of latex modification of the cement hydration and identifying the mechanism of polymer-cement co-matrix formation (Ohama 1987, Su et al. 1991, 1996, Puterman and Malorny 1998, Jenni et al. 2006). Later efforts examined the long-term behavior of PMC with focus on durability and deterioration resistance aspects as a main characteristic of PMC (Ohama et al. 1985, Shaker et al. 1997, Mirza et al. 2002) and on controlling the rheological properties of LMC (Barluenga and Hernández-Olivares 2004).

Recently, researchers developed and examined very early-strength LMC using rapid hardening cement (Sprinkel 1999). The use of the new very-early-strength LMC proved efficient for replacing bridge deck overlays. Moreover, the use of fiber-reinforced LMC has been recently promoted (Cao and Chung 2001, Issa et al. 2007). The use of glass and carbon fiber-reinforced LMC provides a watertight microstructure of LMC with very low permeability and the ability of the chopped fibers to limit plastic shrinkage cracking. Such combined benefits make fiber-reinforced LMC an excellent alternative for bridge deck slabs (Issa et al. 2007). Finally, a bibliography developed and updated by Ohama (2007) represents an excellent source of information on historical and recent developments of PMC.

2.3.2 Properties of Polymer-modified mortars and concretes

Polymer modified mortars and concretes (PMM and PMC) are widely used in various building constructions such as surface preparation materials, finishing materials, self-leveling materials, patching materials for deteriorated RC structures, etc. Generally, Polymer modifiers are classified broadly into four types; Polymer dispersion, redispersible polymer powder, water-soluble polymer, liquid polymer. In this part, previous researches on polymer-modified cementitious composites with polymer dispersion among them were reviewed.

Polymer modifiers

Table 2.1 lists the various polymers that have been used to modify cementitious materials. The materials in italics are the ones that are in general use today, and those marked with an asterisk are available in a redispersible powder form.

Table 2.1 Polymers used to modify cementitious mixtures (ACI committee 548 2009)

Elastomeric	Natural rubber latex	
	Synthetic latexes	*Styrene-butadiene, polychloro-prene (Neoprene), acrylonitrile-butadiene*
Thermoplastic	*Polyacrylic ester,* styrene-acrylic,* polyvinyl acetate,* vinyl acetate copolymers,* polyvinyl propionate, vinyli-dene chloride copolymers, polypropylene*	
Thermosetting	*Epoxy resin*	
Bituminous	Asphalt, rubberized asphalt, coal-tar, paraffin	
Mixed latexes		

*Available in a redispersible powder form.
Note: Italics = in general use today.

Principle of polymer modification

Polymer modification of hydraulic cementitious mixtures is governed by two processes: cement hydration and polymer coalescence. Generally, cement hydration occurs first. As the cement particles hydrate and the mixture sets and hardens, the polymer particles become concentrated in the void spaces. Figures 2.4 indicate the type of change that occurs during polymer modification (Ohama 1973, 1995a). With continuous water removal by cement hydration, evaporation, or both, the polymer particles coalesce into a polymer film that is interwoven in the hydrated cement, resulting in a mixture or comatrix that coats the aggregate particles and lines the interstitial voids (Fessenden and Fessenden 1998, Afridi et al. 2003).
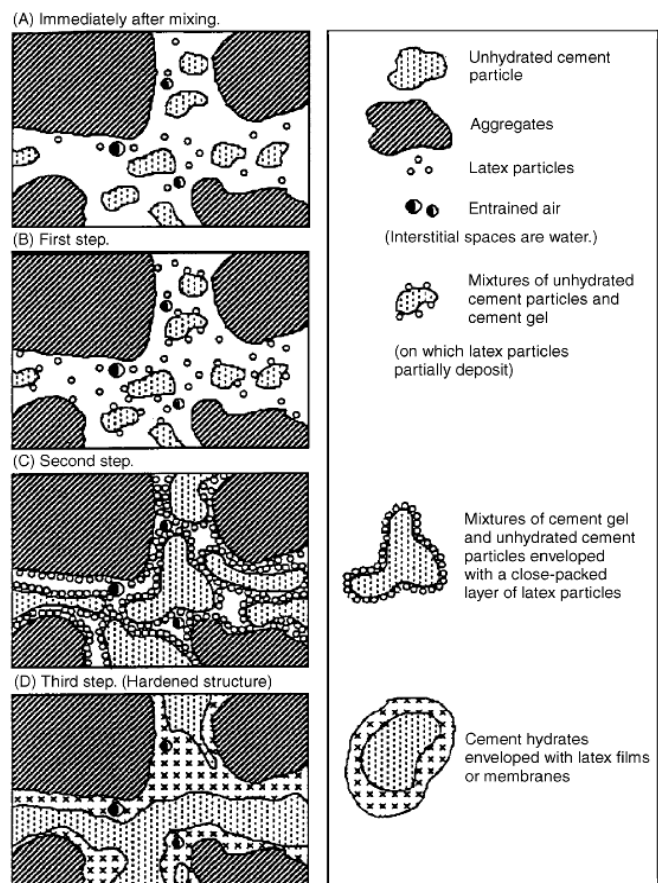

Figure 2.4 Simplified model of formation of polymer-cement comatrix (Ohama 1987)

Properties of fresh PMM and PMC

Unlike conventional cementitious mixtures, PMC does not produce bleed water and, during its fresh state, polymermodified mixtures are more sensitive to plastic-shrinkage cracking than unmodified mortar or concrete because of the water-reducing influence of the polymer's surfactant system (De Puy 1996, Beeldens et al. 2001). This phenomenon is caused by water evaporation at the surface.

Properties of the hardened PMM and PMC

Hardened portland cement paste is predominantly an agglomerated structure of calcium silicates, aluminates, and hydroxides bound together by relatively weak van der Waals forces. Consequently, microcracks are induced in the paste by stresses such as those caused by evaporation of excess mixing water (drying shrinkage). Polymer modification helps in two ways. Not only do the polymer particles reduce the rate and extent of moisture movement by blocking the passages, but when microcracks form, the polymer film bridges the cracks and restricts propagation. Figure 2.5 shows electron micrographs of polymer-modified and unmodified concrete; the micrograph of the PMC shows latex strands bridging a microcrack while such strands are absent in the unmodified concrete.

This results in increased tensile strength and flexural strength. The moisture-movement- blocking property naturally works both ways and also restricts the ingress of most fluids (Ohama 1995b), thus reducing permeability and increasing resistance to both chemicals and freezing-and-thawing resistance. PMC does not require additional air entrainment because of its typically high air content of approximately 6%. There is little or no free water in PMC and the polymer restricts ingress and movement of water. The resistance to freezing and thawing of PMC has been shown to be superior to that of unmodified concrete due to the ability of the polymer latex to block water transport in concrete and the air entrained by the polymer latex in the concrete (Maultzsch 1989, Ohama and Shiroishida 1984).

Kim et al. (1999) experimentally investigated the fracture surface of PMC. They observed that the fracture surface of PMC was propagated through the aggregate instead of around the aggregate, and that debonding of the aggregate was rarely observed compared with unmodified concrete. This
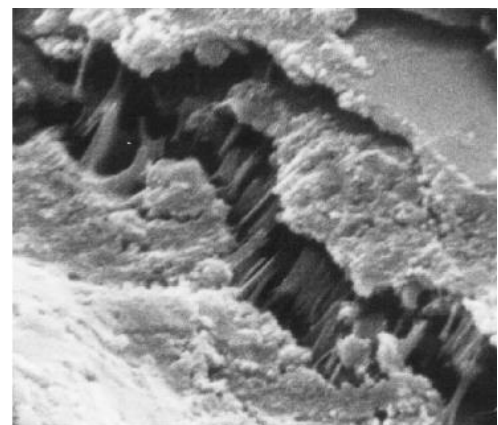
Latex-modified concrete

Portland cement concrete

Figure 2.5 Electron micrograph of latex-modified and portland-cement concrete (magnification=12,000X) (Dow Chemical Co. 1985)

observation was not reported by other researchers examining fracture of PMC. However, PMC and PMM were reported to have relatively higher fracture toughness compared with normal concrete and mortar (Chou et al. 1990, Bureau et al. 2001, Xu et al. 2004).

The optimum degree of polymer modification is usually achieved between 5 and 20% dry polymer solids by mass of cement in the mixture (AIJ 2011). Optimal polymer content is related to enhancing water tightness, durability, cracking strength, and fracture toughness of concrete while maintaining an acceptable compressive strength and workability. The use of excess polymer is not economical, can cause excessive air entrainment, and can cause the mixture to behave like a polymer filled with aggregates and cement. Levels of polymer lower than the recommended optimal content cannot achieve the level of modification necessary for producing the unique characteristics of PMC previously described.

2.4   Shrinkage cracking

2.4.1 Plastic shrinkage cracking

When moisture evaporates from the surface of freshly placed concrete faster than it is replaced by bleed water, the surface concrete shrinks. Due to the restraint provided by the concrete below the drying surface layer, tensile stresses develop in the weak, stiffening plastic concrete. This results in shallow cracks of varying depths that may form a random, polygonal pattern, or be essentially parallel to one another (Figure 2.6). These cracks may be fairly wide (as much as 3 mm) at the surface. They range from a few inches to many feet in length, and are spaced from a few millimeters to as much as 3 m apart. Plastic shrinkage cracks begin as shallow cracks, but can become full-depth cracks later in the life of the concrete. (Price 1982)
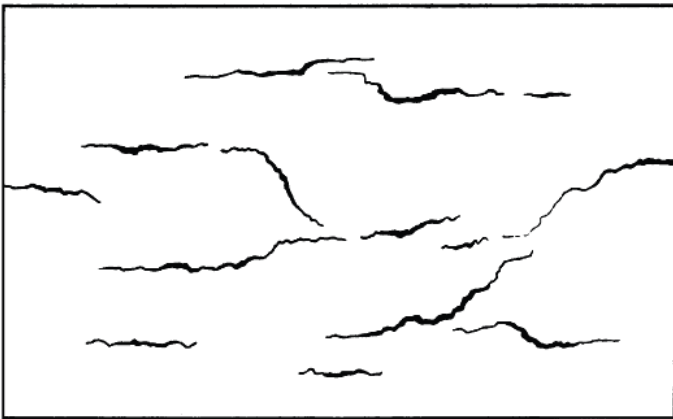

Figure 2.6 Typical plastic shrinkage cracking (Price 1982)

Plastic shrinkage cracking is usually associated with the rapid loss of moisture caused by a combination of factors that include high air and concrete temperatures, low relative humidity, and high wind velocity at the surface of the concrete. Concrete with lower amounts of bleed water, such as those containing mineral admixtures (especially silica fume) have a greater tendency to undergo plastic shrinkage cracking

than concrete with a greater tendency to bleed.

2.4.2 Drying shrinkage cracking

A common cause of cracking in concrete is restrained drying shrinkage. Drying shrinkage is caused by the loss of moisture from the cement paste constituent, which can shrink by as much as 1%. Fortunately, aggregate particles provide internal restraint that reduces the magnitude of this volume change to about 0.06%. On the other hand, concrete tends to expand when wetted.

These moisture-induced volume changes are a characteristic of concrete. If the shrinkage of concrete could take place without restraint, the concrete would not crack. It is the combination of shrinkage and restraint that causes tensile stresses to develop. When the tensile strength of the material is exceeded, concrete will crack. Cracks may propagate at much lower stresses than are required to cause crack initiation (ACI Committee 446 1999).

The amount of drying shrinkage is influenced mainly by the amount and type of aggregate and the cement paste content of the mixture. As the quantity of aggregate increases, the shrinkage decreases (Pickett 1956). The higher the stiffness of the aggregate, the more effective it is in reducing the shrinkage of the concrete; that is, the shrinkage of concrete containing sandstone aggregate may be more than twice that of concrete with granite, basalt, or high quality limestone (Carlson 1938). The higher the water and cement contents, the greater the amount of drying shrinkage (Schmitt and Darwin 1999, Darwin et al. 2004).

Surface crazing on walls and slabs is an example of drying shrinkage on a small scale. Crazing usually occurs when the surface layer of the concrete has a higher water content than the interior concrete. The result is a series of shallow, closely spaced, fine cracks.

2.4.3 Autogenous shrinkage cracking

Autogenous shrinkage "is a special case of drying shrinkage" (Mindess et al. 2003) that results from self-desiccation (internal drying) in concretes with water-cement ratios (W/C) below 0.42, but most often observed at a W/C below 0.30. Thus, it is a problem often associated with high-strength concretes. Autogenous shrinkage occurs without the loss of moisture from the bulk concrete.

The self-desiccation occurs as the relative humidity in interior voids drops to 75 to 80%, which results in bulk shrinkage (Davis 1940). Houk et al. (1969) found that autogenous shrinkage increases with increasing temperature, cement content, and cement fineness.

Chapter 3 Mechanical properties of SCRPCC

3.1 Background and objective

The objective of this chapter is to understand the mechanical properties of SCRCC and SCRPCC. In this chapter, compressive strength test and three point flexural test were conducted.

3.2 Experimental program

3.2.1 Materials

Cementitious composites were prepared with four different types of binder. Among these binders, normal mortar (NM) and SCRCC contain silica fume and superplasticizer for high strength development, but polymer cement mortar (PCM) and SCRPCC don't contain silica fume and superplasticizer for high durability considering the general use of PCM and an economical efficiency. The mix proportions of cementitious composites used in this study are given in Table 3.1.

For the mix proportions of SCRCC, Ordinary Portland cement (Density : $3.14g/cm^3$) and silica fume (Density : $2.2g/cm^3$)   were used as a binder. River sand (Density : $2.69g/cm^3$) of saturated surface dry condition was used as a fine aggregate. And superplasticizer (Density : $1g/cm^3$) was used to reduce the unit water content of cementitious composites. Steel chip (Density : $7.86g/cm^3$)   content of 3% by volume were used in this test.

For the mix proportions of SCRPCC, Ordinary Portland cement was used. And ethylene vinyl acetate emulsion was used as a polymeric admixture. This is a fluid milk-white solution with a solid content of 45% and the density $1.07g/cm^3$. River sand of saturated surface dry condition was used as a fine aggregate. Steel chip content of 3% by volume was used in this test.

Table 3.1 Mix proportions of cementitious composites

	Normal Mortar (NM)	SCRCC (SC)	Polymer Cement Mortar (PCM)	SCRPCC (SCP)
W/B (%)	23.30	23.30	30.00	30.00
Water (kg/m^3)	222.35	222.35	205.92	205.92
Cement (kg/m^3)	754.40	754.40	686.40	686.40
Fine aggregate (kg/m^3)	1152.35	1044.07	1372.80	1220.08
Silica fume (kg/m^3)	199.90	199.90	0.00	0.00
Polymer (kg/m^3)	0.00	0.00	68.64	68.64
Steel chip (Vol. %)	0.00	3.00	0.00	3.00
Antifoaming Agent (kg/m^3)	0.00	0.00	0.69	0.69
Chemical admixture (kg/m^3)	20.79	20.79	0.00	0.00

3.2.2 Specimens

Cylindrical specimens of size of φ100mm×200mm were prepared for compression test. And beam specimens of size of 100×100×500mm were prepared for three point flexural test.

3.2.3 Test procedures

Flow test

After mixing with hand mixer, flow test was conducted as shown in Photo 3.1.

Photo 3.1 Flow test

Compression test

Loading was applied using a 2000kN universal testing machine. Measuring of compressive strain was conducted as follows. Pre-peak was measured with three displacement transducers that were set on the specimen before the compressive strength is reached. After the compressive strength was reached, the post-peak was measured with two displacement transducers that were set on the top and bottom of loading plate as shown in Photo 3.2. And the compressive stress-strain relationships were obtained.

Photo 3.2 Compression test

Three point flexural test

Loading was applied using a 2000kN universal testing machine. Measuring of flexural strain was conducted as follows. Beam specimens of size $100 \times 100 \times 500$ mm were notched to a depth of 20mm, and a U type clip gauge was set on the notched surface of specimen as shown in Photo 3.3. Also, a displacement transducer that was set on the top of loading plate was used for measuring of flexural strain. And load-crack opening displacement relationships were obtained from the test.

Photo 3.3 Three point flexural test

3.3.1 Steel Chip Reinforced Cementitious Composites

Flow

   NM showed flow of 190 X 200mm as shown in Photo 3.4. NM had a proper consistency. However, SC didn't have enough flowability because of tangled steel chips as shown in Photo 3.5. Distribution of fibers in the cementitious composites is a problem to solve.

Photo 3.4 Flow of NM (190 X 200mm)

Photo 3.5 Flow of SC (170 X 170mm)

Compressive strength

Compressive strength was tested at 3, 7 and 28 days. The test results are listed in Table 3.2. And the schematic graphs of stress-strain relationships are shown in Figure 3.1

Table 3.2 Test results of compression test (SCRCC)

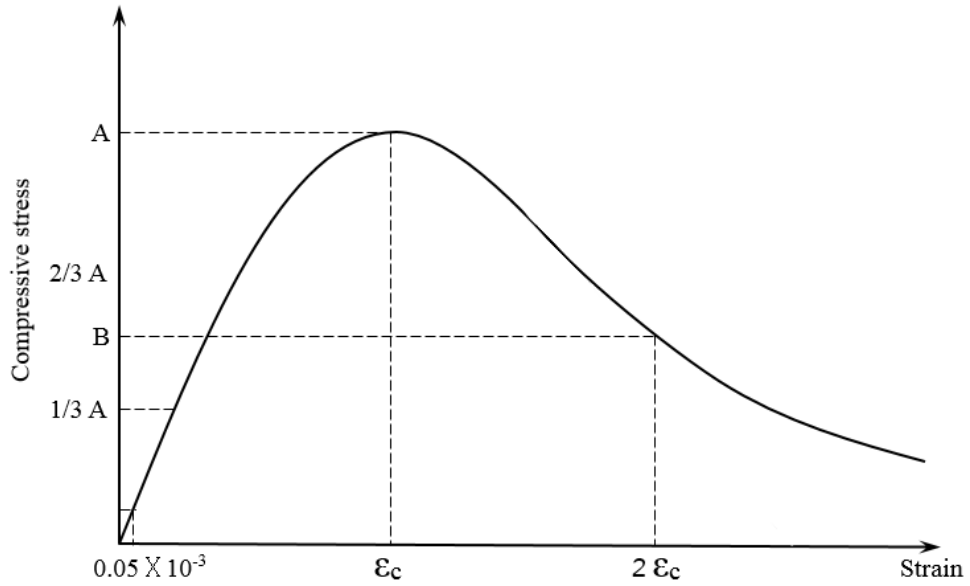| Curing day	Binder	No.	Compressive strength (N/mm²)	Elastic modulus (kN/mm²)	Strain at peak stress (X 10⁻³)	Strength residual rate when 2ε_c
3 day	NM	1	80.96	46.16	2.73	0.00
		2	76.06	32.62	3.04	0.00
		3	76.77	33.06	3.22	0.00
		4	71.46	31.73	3.03	0.00
	SC	1	73.67	34.48	3.30	0.49
		2	68.14	35.41	2.92	0.85
		3	76.26	33.48	3.83	0.60
		4	83.57	35.94	4.54	0.58
7 day	NM	1	97.62	36.70	3.41	0.00
		2	95.97	35.34	2.59	0.00
		3	92.63	35.57	3.52	0.00
		4	94.94	32.59	3.49	0.00
	SC	1	91.62	36.61	3.68	0.17
		2	95.79	51.61	2.53	0.34
		3	103.11	38.35	4.91	0.63
		4	99.35	37.81	4.33	0.63
28 day	NM	1	115.66	37.07	3.58	0.00
		2	119.78	37.72	3.67	0.00
		3	101.81	39.08	3.04	0.00
		4	119.99	38.47	3.60	0.00
	SC	1	114.21	39.57	3.68	0.50
		2	110.69	38.82	3.73	0.28
		3	133.84	62.66	4.23	0.62
		4	131.36	65.47	2.97	0.69

Figure 3.1 Schematic graph of stress-strain relationship

Specimens after test are shown in Photo 3.6. NM specimens were that there was spalling. In contrast, there was no spalling in the SC specimens. It is considered that it was attributed to the effect of reinforcing with steel chip.

| 3day_NM_1 | 3day_NM_2 | 3day_NM_3 | 3day_NM_4 |
| 3day_SC_1 | 3day_SC_2 | 3day_SC_3 | 3day_SC_4 |

Photo 3.6 Specimens after compressive strength test

Compressive stress-strain relationships are shown in Figure 3.2. Compressive strengths of all specimens were increased with increasing of curing day. And brittle fracture occurred in the all NM specimens after maximum stress, however SC specimens maintained strength for some time after maximum stress. It was confirmed that the spalling of NM specimens was surely prevented by reinforcing with steel chip.
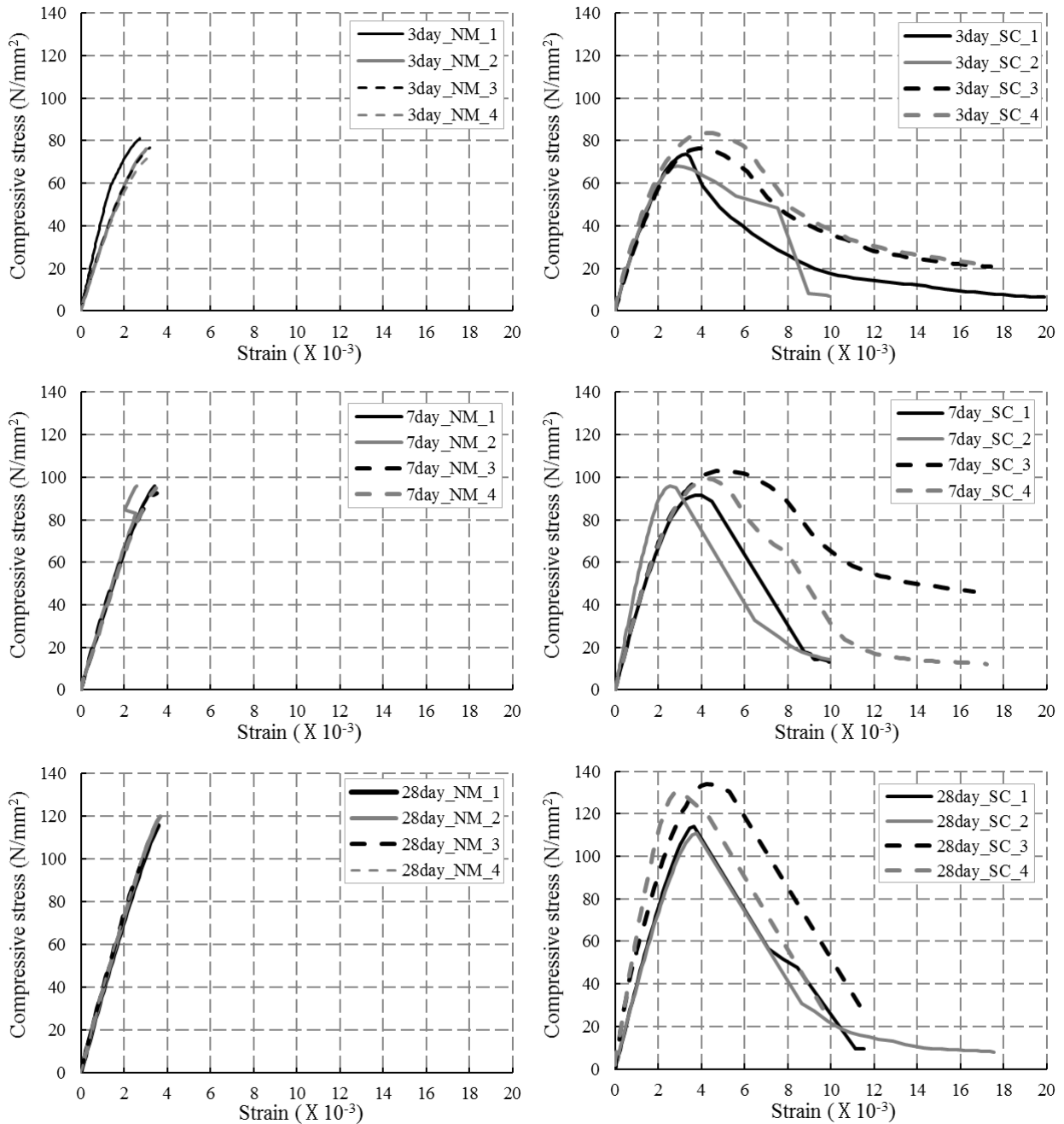
Figure 3.2 Compressive stress-strain relationship (SCRCC)

Three point flexural test

Flexural strength was tested at 3, 7 and 28 days. The test results are listed in Table 3.3. Specimens after three point flexural test are shown in Photo 3.7. Flexural strength of NM specimens were improved by reinforcing with steel chip at every curing days. And it was confirmed that SC specimen was not broken in spite of large crack in contrast with NM specimen as shown in Photo 3.7.

Table 3.3 Test results of flexural strength test (SCRCC)

Curing day	Binder	No.	Flexural strength (N/mm^2)
3 day	NM	1	5.51
		2	4.77
		3	3.68
	SC	1	7.93
		2	8.25
		3	7.54
7 day	NM	1	4.97
		2	4.16
		3	3.91
	SC	1	8.47
		2	9.33
		3	5.72
28 day	NM	1	5.21
		2	4.89
		3	4.77
	SC	1	8.50
		2	10.57
		3	10.93

3day_SC_2

3day_NC_2

Specimens after test   Cross-section

Photo 3.7 Specimens after flexural strength test

3.3.2 Steel Chip Reinforced Polymer Cementitious Composites

Flow

PCM showed flow of 270 X 265mm as shown in Photo 3.8. PCM had a proper consistency. However, SCP didn't have enough flowability because of tangled steel chips as shown in Photo 3.9. Distribution of fibers in the cementitious composites is a problem to solve.
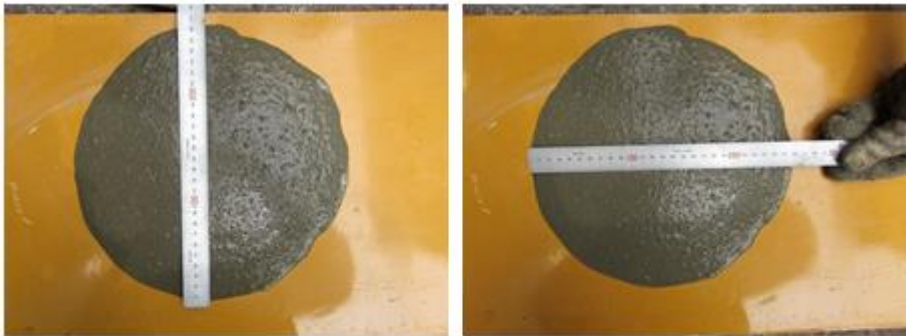

Photo 3.8 Flow of PCM (270 X 265mm)

Photo 3.9 Flow of SCP (190 X 190mm)

Compressive strength

    Compressive strength was tested at 3, 7 and 28 days. The test results are listed in Table 3.4. And the schematic graphs of stress-strain relationships are shown in Figure 3.1

Table 3.4 Test results of compression test (SCRCC)

Curing day	Binder	No.	Compressive strength (N/mm^2)	Elastic modulus (kN/mm^2)	Strain at peak stress ($\times 10^{-3}$)	Strength residual rate when 2ε
3 day	NM	1	23.7	17.5	2.4	0.5
		2	23.3	16.9	2.6	0.5
		3	25.1	18.8	2.8	0.5
		4	23.7	18.4	2.3	0.6
	SC	1	25.4	18.3	2.6	0.6
		2	26.1	16.9	2.8	0.6
		3	29.9	21.6	2.6	0.6
		4	29.9	20.6	2.7	0.6
7 day	NM	1	32.4	18.0	3.2	0.2
		2	31.9	19.4	2.9	0.3
		3	28.1	18.8	2.7	0.5
		4	32.7	20.7	2.9	0.4
	SC	1	35.5	22.9	3.1	0.6
		2	33.8	21.7	3.1	0.6
		3	35.4	21.8	2.9	0.6
		4	35.7	21.0	3.1	0.5
28 day	NM	1	42.6	22.1	3.5	0.2
		2	41.9	21.4	3.4	0.2
		3	40.5	21.8	3.4	0.3
		4	42.3	22.8	3.0	0.3
	SC	1	46.4	23.5	3.6	0.4
		2	45.0	23.1	3.5	0.4
		3	43.5	22.9	3.3	0.5
		4	44.4	37.7	2.6	0.5

Specimens after test are shown in Photo 3.9. PCM specimens were that there was spalling. In contrast, there was no spalling in the SCP specimens. It is considered that it was attributed to the effect of reinforcing with steel chip.

3day_PCM_1, 2   3day_PCM_3, 4

3day_SCP_1, 2   3day_SCP_3, 4

Photo 3.9 Specimens after compressive strength test

Compressive stress-strain relationships of SCRPCC are shown in Figure 3.3. Compressive strength of all specimens were increased with increasing of curing day. And compressive strength of PCM was slightly improved by reinforcing with steel chip. Regardless of reinforcing with steel chip, brittle fracture didn't occur in the PCM and SCP specimens. That's because polymer makes cement matrix more flexible than Ordinary Portland cement mortar. Also, it was confirmed that the ductility of PCM specimens was improved by reinforcing with steel chip.
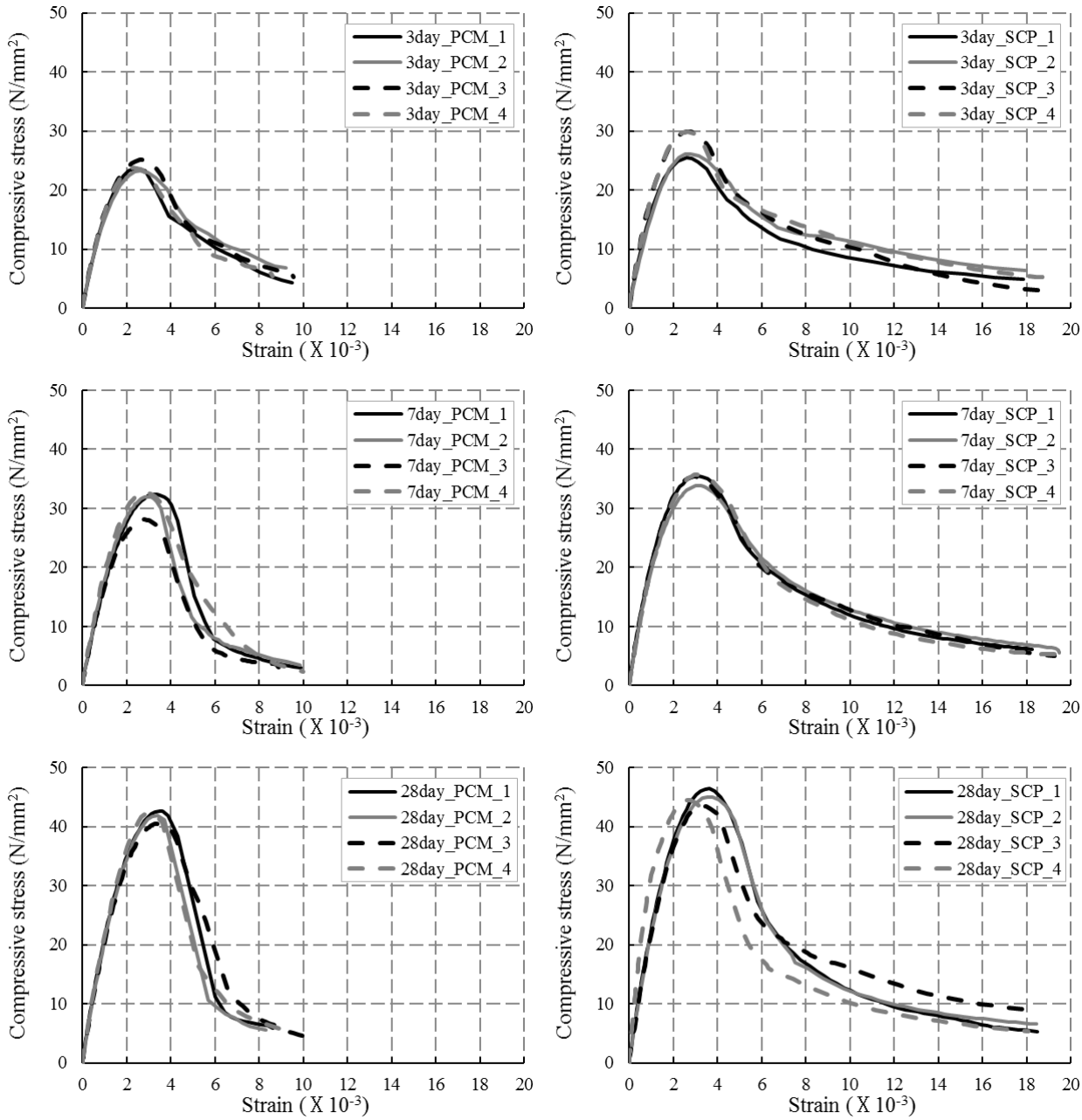
Figure 3.3 Compressive stress-strain relationship (SCRPCC)

Three point flexural test

Flexural strength was tested at 3, 7 and 28 days. The test results are listed in Table 3.5. Specimens after three point flexural test are shown in Photo 3.10. Flexural strength of PCM specimens were improved by reinforcing with steel chip at every curing days. And it was confirmed that SCP specimen was not broken in spite of large crack in contrast with PCM specimen as shown in Photo 3.7. It is attributed to the bridging effect by reinforcing with steel chip.

Table 3.5 Test results of flexural strength test (SCRPCC)

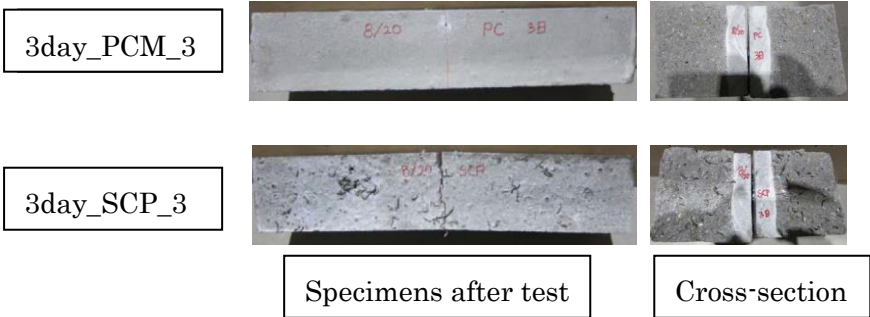| Curing day	Binder	No.	Flexural strength (N/mm^2)
3 day	PCM	1	2.78
		2	3.09
		3	3.06
	SCP	1	3.58
		2	3.52
		3	4.05
7 day	PCM	1	2.75
		2	3.33
		3	3.51
	SCP	1	3.22
		2	4.34
		3	4.11
28 day	PCM	1	3.39
		2	4.25
		3	3.22
	SCP	1	4.10
		2	5.12
		3	5.45

3day_PCM_3

3day_SCP_3

Specimens after test   Cross-section

Photo 3.7 Specimens after flexural strength test

3.4   Conclusions

In this chapter, compression tests and three point flexural tests were conducted to examine the material properties and fracture mode of SCRCC (SC) and SCRPCC (SCP). The following conclusions were obtained from the results.

1) It was confirmed that the spalling of NM specimens was surely prevented by reinforcing with steel chip in the compressive strength test.

2) Flexural strengths of NM specimens were improved by reinforcing with steel chip at every curing days. And it was confirmed that SC specimen was not broken in spite of large crack in contrast with NM specimen.

3) Regardless of reinforcing with steel chip, brittle fracture didn't occur in the PCM and SCP specimens after compressive strength test. Also, it was confirmed that the ductility of PCM specimens was improved by reinforcing with steel chip.

4) It was confirmed that SCP specimen was not broken in spite of large crack in contrast with PCM specimen. It is attributed to the bridging effect by reinforcing with steel chip.

Chapter 4　Drying shrinkage characteristics of SCRPCC

4.1　Background and objective

A free shrinkage test cannot give the true potential of fiber reinforcement to resist restrained shrinkage stresses and to control shrinkage cracking (Swamy and Stavrides 1979). Therefore, it is necessary to examine not only free shrinkage, but also restrained drying shrinkage.

The objective of this chapter is to understand the drying shrinkage characteristics of SCRCC and SCRPCC. In this chapter, the drying shrinkage cracking behavior of SCRCC and SCRPCC were examined to determine its long-term durability.

4.2　Experimental programs

4.2.1 Materials

Cementitious composites were prepared with four different types of binder. Among these binders, normal mortar (NM) and SCRCC contain silica fume and superplasticizer for high strength development, but polymer cement mortar (PCM) and SCRPCC don't contain silica fume and superplasticizer for high durability considering the general use of PCM and an economical efficiency. The mix proportions of cementitious composites used in this study are given in Table 4.1.

For the mix proportions of SCRCC, Ordinary Portland cement (Density : $3.14g/cm^3$) and silica fume (Density : $2.2g/cm^3$) were used as a binder. River sand (Density : $2.69g/cm^3$) of saturated surface dry condition was used as a fine aggregate. And superplasticizer (Density : $1g/cm^3$) was used to reduce the unit water content of cementitious composites. Steel chip (Density : $7.86g/cm^3$) content of 3% by volume were used in this test.

Table 4.1 Mix proportions of cementitious composites

	Normal Mortar (NM)	SCRCC (SC)	Polymer Cement Mortar (PCM)	SCRPCC (SCP)
W/B (%)	23.30	23.30	30.00	30.00
Water (kg/m^3)	222.35	222.35	205.92	205.92
Cement (kg/m^3)	754.40	754.40	686.40	686.40
Fine aggregate (kg/m^3)	1152.35	1044.07	1372.80	1220.08
Silica fume (kg/m^3)	199.90	199.90	0.00	0.00
Polymer (kg/m^3)	0.00	0.00	68.64	68.64
Steel chip (Vol. %)	0.00	3.00	0.00	3.00
Antifoaming Agent (kg/m^3)	0.00	0.00	0.69	0.69
Chemical admixture (kg/m^3)	20.79	20.79	0.00	0.00

For the mix proportions of SCRPCC, Ordinary Portland cement was used. And ethylene vinyl acetate emulsion was used as a polymeric admixture. This is a fluid milk-white solution with a solid content of 45% and the density 1.07g/cm^3. River sand of saturated surface dry condition was used as a fine aggregate. Steel chip content of 3% by volume was used in this test.

4.2.2 Specimens

Specimens for free shrinkage test are beam specimens of size 100×100×500mm. On the other hand, four large specimens of 2,500 mm length for restrained drying shrinkage test are prepared as shown in Figure 4.1. These restrained shrinkage specimens were prepared with larger size than normal based on a study by Koyanagi *et al* (1990) to guarantee certain cracking behavior. The parameters of specimens are listed in Table 4.2.
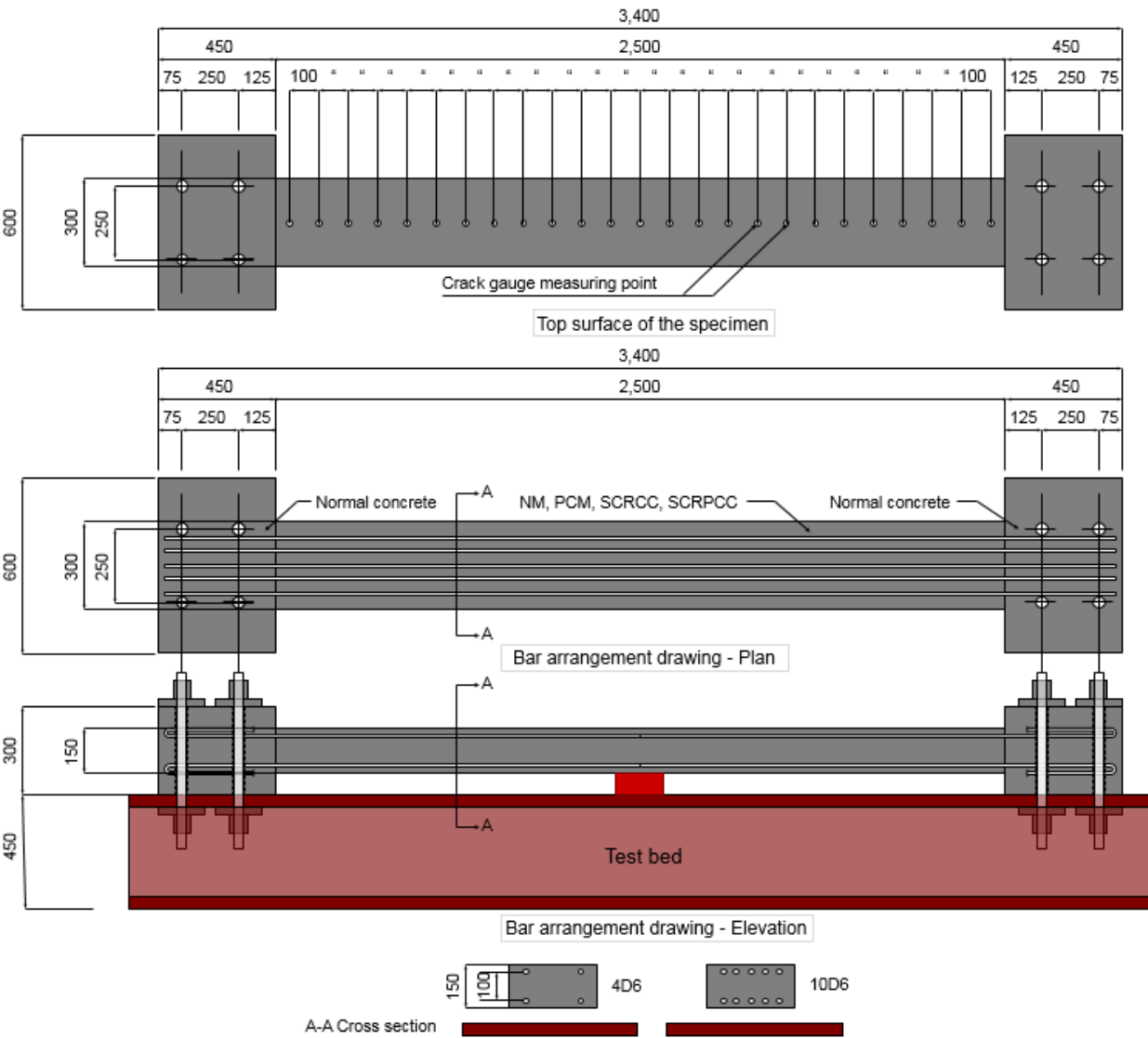
Figure 4.1 Specimens of restrained drying shrinkage test

Table 4.1 Parameters of drying shrinkage specimens

Specimen	Curing condition	Restrain	Mortar	Bar
NM-In	20°C, 60% R.H	Free	NM	-
SC-In	20°C, 60% R.H	Free	SCRCC	-
NM-Out	Outside	Free	NM	-
SC-Out	Outside	Free	SCRCC	-
NM4	Outside	Restrained	NM	4D6
SC4	Outside	Restrained	SCRCC	4D6
NM10	Outside	Restrained	NM	10D6
SC10	Outside	Restrained	SCRCC	10D6
PCM-In	20°C, 60% R.H	Free	PCM	-
SCP-In	20°C, 60% R.H	Free	SCRPCC	-
PCM-Out	Outside	Free	PCM	-
SCP-Out	Outside	Free	SCRPCC	-
PCM4	Outside	Restrained	PCM	4D6
SCP4	Outside	Restrained	SCRPCC	4D6
PCM10	Outside	Restrained	PCM	10D6
SCP10	Outside	Restrained	SCRPCC	10D6

4.2.3 Test procedures

Firstly, the casting form was arranged and restraining steel bars were placed. The steel bars were consisted of four or ten deformed bars of 6mm diameter with 180°hooks in the both ends. Secondly, the restraining block (450 mm x 600 mm x 300 mm) was casted with normal concrete (NC). Each block was fixed with four prestressing bars of 32 mm diameter, to which 250 kN tensile force was applied. Thirdly, the center part (2500 mm x 300 mm x 15 0mm) was casted with normal mortar (NM) or SCRCC (SC). After the casting form was removed (curing 5days), Beam specimens (100×100× 500mm) for free shrinkage and wall specimens (300×150×2500mm) for restrained drying shrinkage were cured for 5 days at the each curing conditions. Then 25 measuring targets were bonded on the surface of specimen with every 100 mm. And initial measurement was started (curing 7 days). Then this point was fixed as a standard point (drying period 0day). The measuring of strains and the observation of crack patterns were conducted every 7 days during first 56 days, every 14 days during next 56days and every 28 days after 112 days.

4.3.1 Steel Chip Reinforced Cementitious Composites

Curing and drying condition

Two beam specimens for the free shrinkage test (NM-In and SC-In) were subjected to a constant temperature and humidity condition of 20℃ and 60R.H.. On the other hand, two beam specimens (NM-Out and SC-Out) and four wall specimens (NM4, SC4, NM10 and SC10) were subjected to the outside condition and kept from the rain.

Average daily temperature and average daily humidity of the outside that specimens were exposed to during drying period are shown in Figure 4.2.
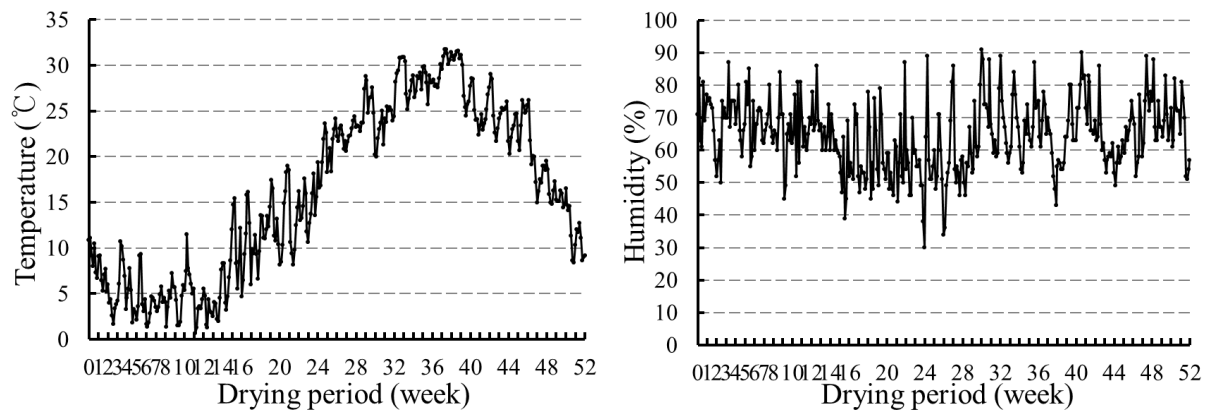
Figure 4.2 Average daily temperature and average daily humidity

Free shrinkage

Figure 4.3 represents the relationship between drying shrinkage of free shrinkage specimens and drying shrinkage of free shrinkage specimens and drying period. Overall, drying shrinkage of all specimens was increased with drying period. And the drying shrinkage was decreased by reinforcing with steel chip. Effect of curing condition on drying shrinkage is that drying shrinkage of specimens in the outside condition was lower than indoor specimens. This is explained by the reason that the temperature and humidity of outdoor were irregular, however, indoor was always maintained constant condition of 20°C, 60% R.H.
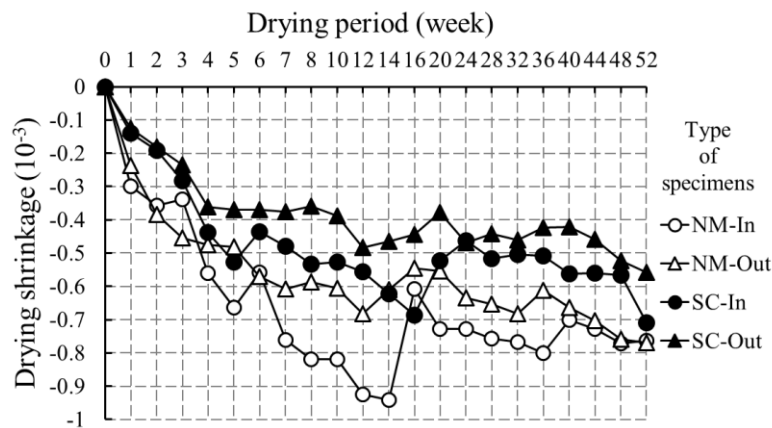
Figure 4.3 Free shrinkage-drying period relationship

Restrained shrinkage and cracking characteristic

Figure 4.4 shows the drying shrinkage and crack patterns for three sides (top and sides) of each specimen. The drying shrinkage of the restrained NM specimens tended to decrease with the steel chip reinforcement and increased number of reinforcing bars. The reason for this decrease is that a bridging effect was provided by reinforcing with steel chips, and the bond strength of the binder increased in the cement matrix. The cracking characteristic is that the occurrence of cracks in the SC specimens was less than in the NM specimens and increasing the number of reinforcing bars increased the occurrence of cracks.
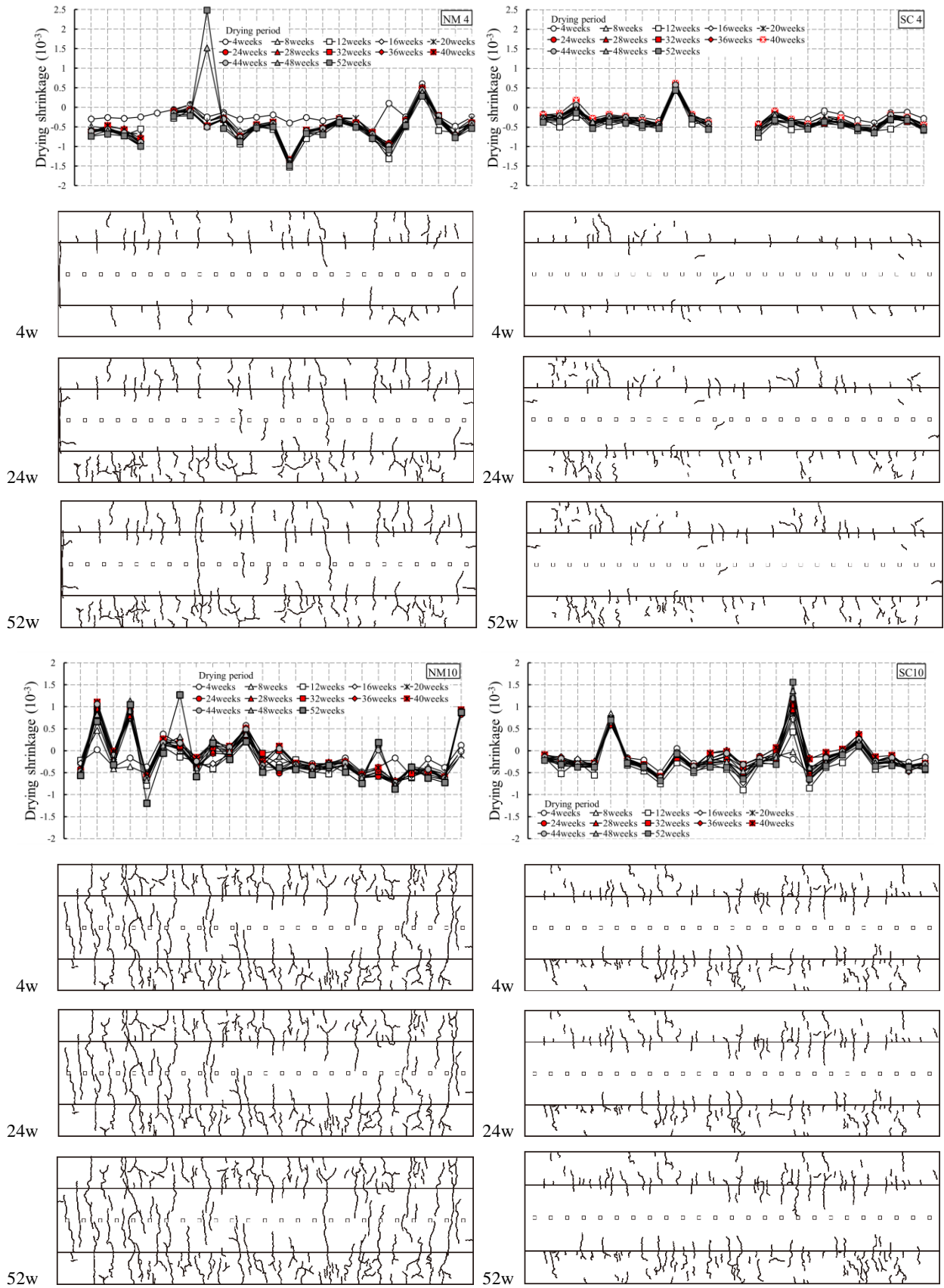
Figure 4.4 Drying shrinkage and crack patterns of specimen NM4, SC4, NM10 and SC10

Figure 4.5 shows the average crack width-drying period relationship. In order to calculate w_{cr}, first of all, equivalent number of cracks was calculated by *Eq(4.1)*. After that, average crack width was calculated by *Eq(4.2)*. The number of cracks N_{cre} is defined as total lengths of cracks on the top surface of the specimen divided by the width (300 mm). Equivalent number of cracks N_{cre} is used since only a few cracks penetrate the entire width of the specimen.

$$N_{cre}=\Sigma(l_{cr})/300 \qquad\qquad Eq(4.1)$$
$$w_{cr}=(L\times\mathcal{E}_{cd})/N_{cre} \qquad\qquad Eq(4.2)$$

N_{cre} : equivalent number of cracks

l_{cr} : length of a crack on the top surface of the specimen (mm)

w_{cr} : average crack width of restrained specimen (mm)

L : length of a restrained specimens (= 2500 mm)

$\mathcal{E}_{cd}$: free drying shrinkage of outdoor specimen
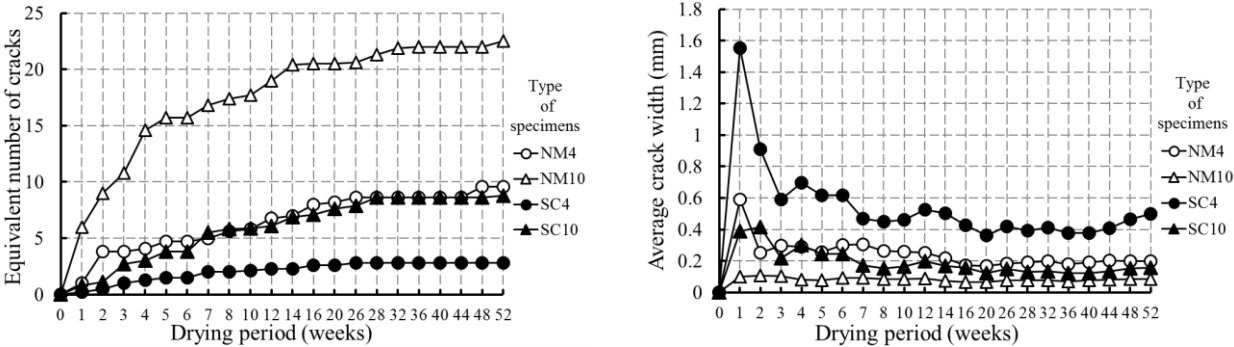
Figure 4.5 Average crack width-drying period relationship

4.3.2 Steel Chip Reinforced Polymer Cementitious Composites

Curing and drying condition

Two beam specimens for the free shrinkage test (PCM-In and SCP-In) were subjected to a constant temperature and humidity condition of 20℃ and 60R.H. On the other hand, two beam specimens (PCM-Out and SCP-Out) and four wall specimens (PCM4, SCP4, PCM10 and SCP10) were subjected to the outdoor condition and kept from the rain. Average daily temperature and average daily humidity of the outdoor that specimens were exposed to during drying period are shown in Figure 4.6.
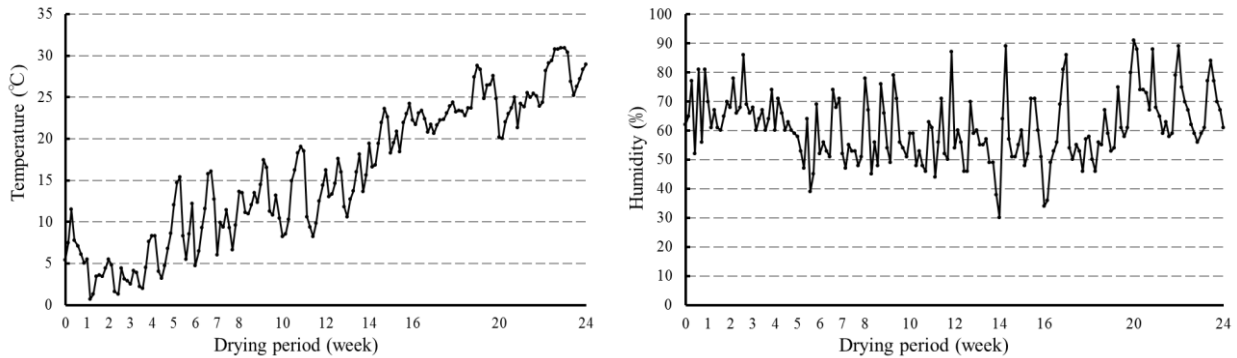
Figure 4.6 Average daily temperature and average daily humidity

Free shrinkage

Figure 4.7 represents the relationship between drying shrinkage of free shrinkage specimens and drying period. Overall, drying shrinkage of all specimens was increased with drying period. And the drying shrinkage was decreased by reinforcing with steel chip at the outside condition. However, the shrinkage of SCRPCC was slightly larger than that of PCM at the indoor condition. Effect of curing condition on drying shrinkage is that drying shrinkage of specimens in the outdoor condition was decreased as compared with that of indoor specimens. This is explained by the reason that the temperature and humidity of outdoor were irregular, and the temperature was always below 20°C until 14 weeks, however, indoor was always maintained constant condition of 20°C, 60% R.H.
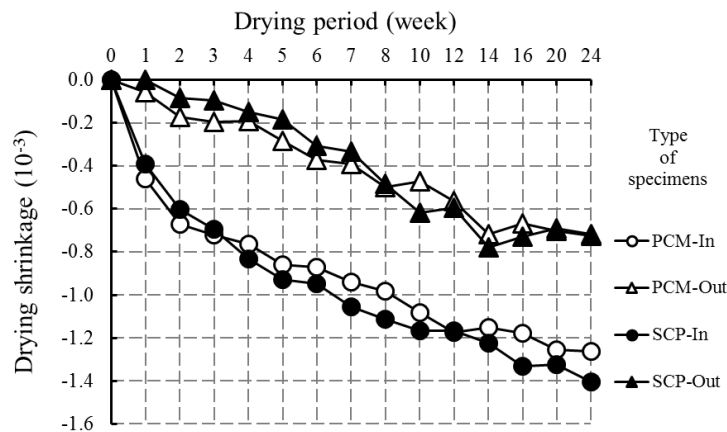

Figure 4.7 Free shrinkage-drying period relationship

Restrained shrinkage and cracking characteristic

Figure 4.8 shows the drying shrinkage and crack patterns for three sides (top and sides) of each specimen. Drying shrinkage of restrained PCM specimens was inclined to decrease with reinforcing with steel chip.
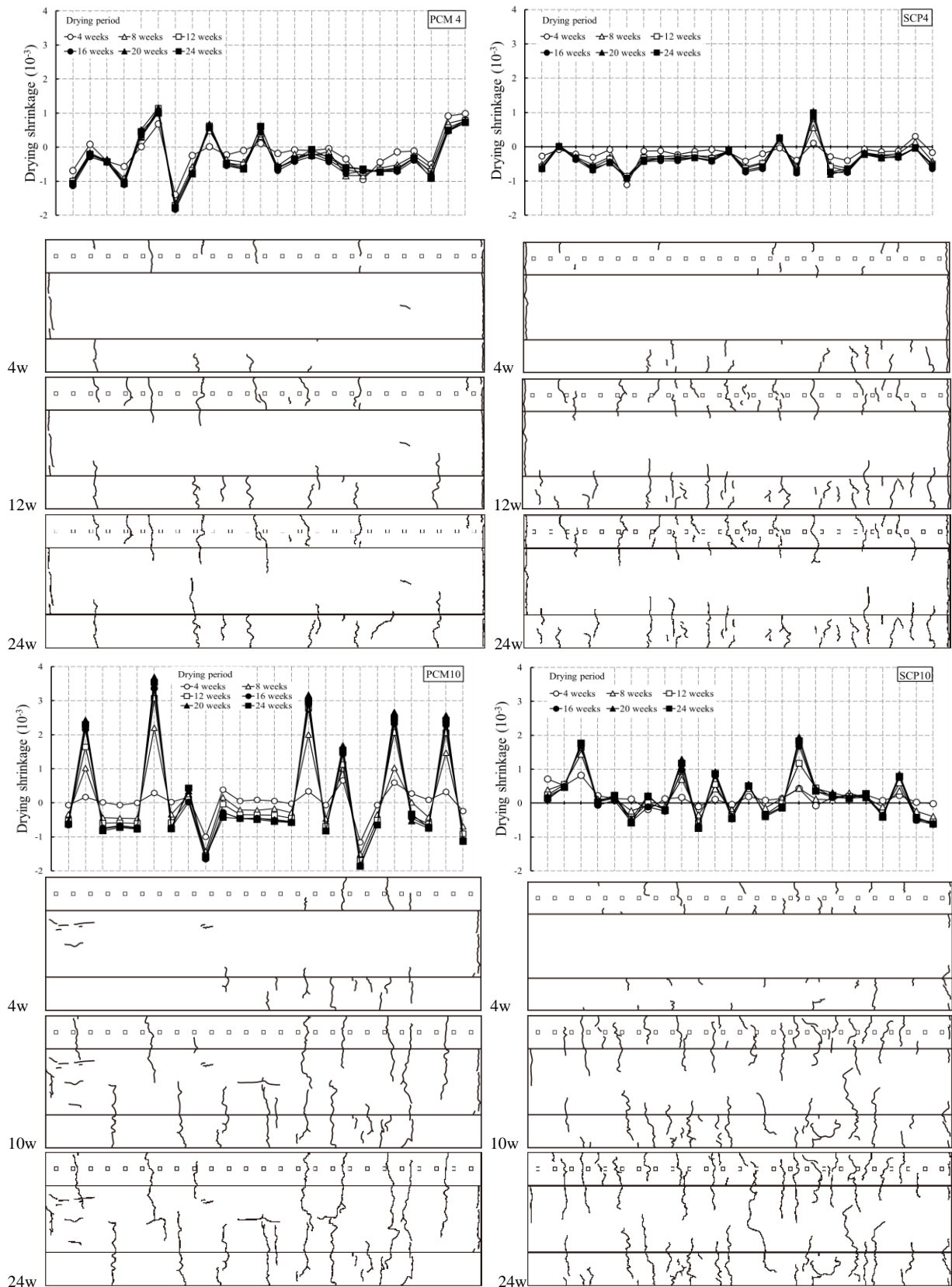

Figure 4.8 Drying shrinkage and crack patterns of specimen PCM4, SCP4, PCM10 and SCP10

The reason for this decrease is because the bridging effect was provided by reinforcing with steel chip, and the bond strength of binder was increased in the cement matrix.

Cracking characteristic is that in the case of specimens with high reinforcement ratio (PCM10, SCP10), the occurrence of cracks of the restrained specimen made of SCRPCC was less than that of PCM, and in the case of specimens with low reinforcement ratio (PCM4, SCP4), there is not so much difference on the number of cracks of both specimens.

Figure 4.9 shows relationship between average crack width and drying period. In order to calculate w_{cr}, first of all, equivalent number of cracks was calculated by *Eq(4.1).* After that, average crack width was calculated by *Eq(4.2).* The number of cracks Ncre is defined as total lengths of cracks on the top surface of the specimen divided by the width (300 mm). Equivalent number of cracks Ncre is used since only a few cracks penetrate the entire width of the specimen.
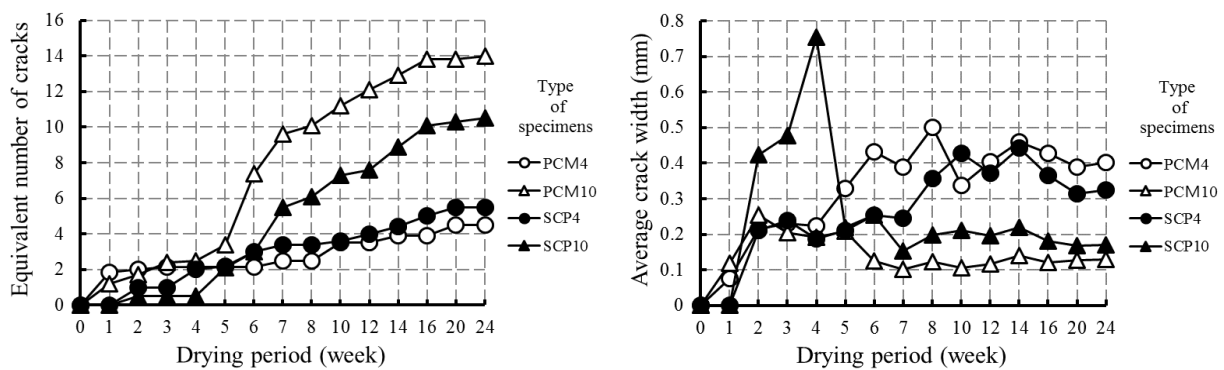
Figure 4.9 Average crack width-drying period relationship

4.4 Conclusions

In this chapter, the drying shrinkage properties and the cracking characteristics of SCRCC and SCRPCC with large scale wall specimen were investigated. The following conclusions were obtained from the results.

1) The drying shrinkage strain of SCRCC was smaller than that of normal mortar.

2) The number of cracks by drying shrinkage of SCRCC was smaller than that of normal mortar. In addition, increasing the reinforcement ratio caused a decrease in crack widths and an increase in the number of cracks.

3) Drying shrinkage of PCM was decreased by reinforcing with steel chip at the outdoor condition. Influence of curing and drying condition on drying shrinkage is that drying shrinkage of outdoor specimens was lower than that of indoor specimens.

4) Drying shrinkage of restrained PCM specimens was reduced by reinforcing with steel chip. And in the case of specimens with high reinforcement ratio, the occurrence of cracks of restrained SCRPCC specimen was less than that of PCM specimen.

5) Average crack width of restrained specimen was decreased by increasing of the amount of reinforcing bar.

Chapter 5　Bond characteristics of SCRPCC

5.1　Background and objective

Recently, numerous fiber reinforced cementitious composites are being developed in many parts of the world. And their applications to RC structures are also being attempted in many different ways. In order to efficiently utilize the fiber reinforced cementitious composites to RC structures, it is necessary to clarify the bond characteristics between steel bar and the composites.

In this chapter, it is examined about fundamental properties of bond stress-slip relationships between steel bar and steel chip reinforced cementitious composite (SCRCC) or steel chip reinforced polymer cementitious composite (SCRPCC) by means of the pull-out tests. Also, uniaxial tension tests were conducted to examine the cracking characteristics of SCRCC and SCRPCC.

Small diameter steel bars (D6, D13) were used in the test. This is because this test is to consider the modeling of bond and pull-out behavior of steel bar when the walls are subjected to in-plane shear, out-of-plane bending, as well as separation from the beams and columns by seismic loading.

5.2　Pull-out tests of small diameter steel bar

In this section, pull-out tests of small diameter steel bar were conducted to examine the fundamental properties of bond stress-slip relationships between small diameter steel bar and SCRCC or SCRPCC.

5.2.1 Experimental programs

Materials

Cementitious composites were prepared with four different types of binder. Among these binders, normal mortar (NM) and SCRCC contain silica fume and superplasticizer for high strength development, but polymer cement mortar (PCM) and SCRPCC don't contain silica fume and superplasticizer for high durability considering the general use of PCM and an economical efficiency. The mix proportions of cementitious composites used in this study are given in Table 5.1.

For the mix proportions of SCRCC, Ordinary Portland cement and silica fume were used as a binder. River sand of saturated surface dry condition was used as a fine aggregate. And superplasticizer was used to reduce the unit water content of cementitious composites. Steel chip content of 3% by volume were used in this test.

For the mix proportions of SCRPCC, Ordinary Portland cement was used. And ethylene vinyl acetate emulsion was used as a polymeric admixture. This is a fluid milk-white solution with a solid content of 45% and the density $1.07 g/cm^3$. River sand of saturated surface dry condition was used as a fine aggregate. Steel chip content of 3% by volume was used in this test.

Table 5.1 Mix proportions of cementitious composites

	Normal Mortar (NM)	SCRCC	Polymer Cement Mortar (PCM)	SCRPCC
W/B (%)	23.30	23.30	30.00	30.00
Water (kg/m³)	222.35	222.35	205.92	205.92
Cement (kg/m³)	754.40	754.40	686.40	686.40
Fine aggregate (kg/m³)	1152.35	1044.07	1372.80	1220.08
Silica fume (kg/m³)	199.90	199.90	0.00	0.00
Polymer (kg/m³)	0.00	0.00	68.64	68.64
Steel chip (Vol. %)	0.00	3.00	0.00	3.00
Antifoaming Agent (kg/m³)	0.00	0.00	0.69	0.69
Chemical admixture (kg/m³)	20.79	20.79	0.00	0.00

Steel bars were prepared with two types (D6, D13) of deformed bars. The properties of steel bars are listed in Table 5.2 and shown in Figure 5.1.

Table 5.2 Mechanical properties of steel bar

Type	Yield load (kN)	Maximum load (kN)	Yield stress σ_y (N/mm²)	Tensile strength σ_u (N/mm²)	Elastic modulus E_s (×10⁵N/mm²)
D6	13.7	17.1	425.9	531.6	1.89
D13	56.2	78.4	423.2	590.7	2.00
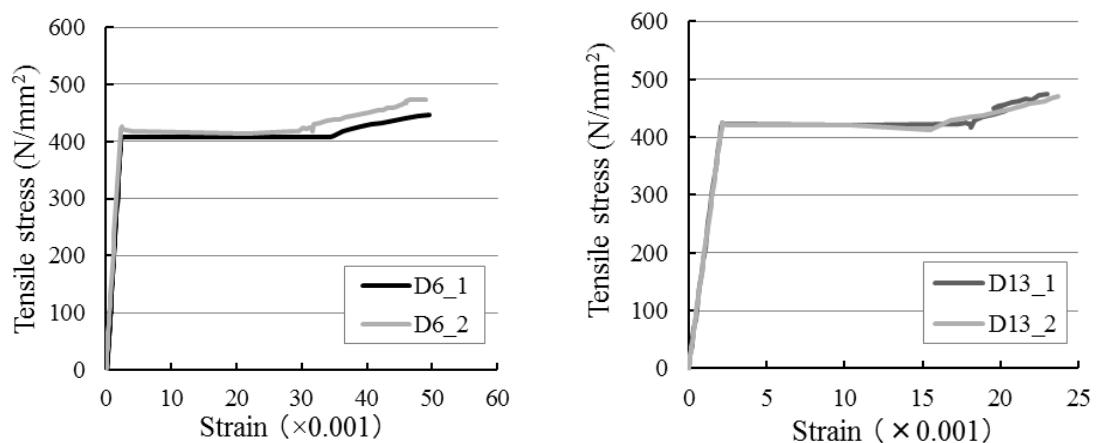
Figure 5.1 Tensile stress-strain relationships of steel bars

Specimens

Specimens were prepared with two types of steel bars, three types of specimen diameter and two types of specimen length as shown in Figure 5.2. In total, 48 specimens were prepared as listed in Table 5.3. NM and PCM were casted in the shape of cylinder type with PVC pipe molds as shown in Photo 5.1. And

SCRCC and SCRPCC were casted in the shape of beam type (same surface area as cylinder type specimens) with wooden molds because of difficulty of casting into the narrow and long PVC pipe molds considering distribution of steel chips in the cementitious composites as shown in Photo 5.2. All the specimens were demolded after three days and cured in the air.
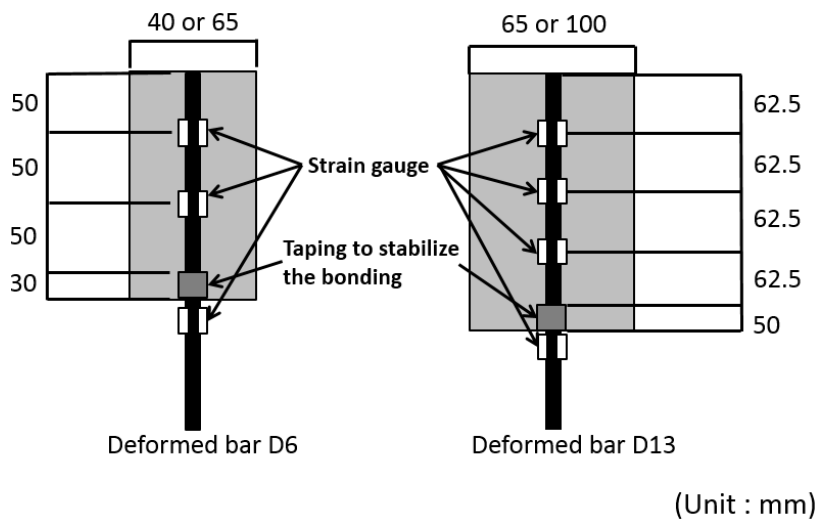

(Unit : mm)

Figure 5.2 Geometry of specimens for pull-out test

Table 5.3 List of specimens

Binder	Diameter of bar (mm)	Length of bar (mm)	Diameter of specimen (mm)	Length of specimen (mm)	Number of specimens	Loading method
NM	6.4	980	40	180	3	Monotonic
			65		3	
	13	1100	65	300	3	
			100		3	
SCRCC (SCP)	6.4	980	40	180	3	
			65		3	
	13	1100	65	300	3	
			100		3	
PCM	6.4	980	40	180	3	
			65		3	
	13	1100	65	300	3	
			100		3	
SCRPCC (SCP)	6.4	980	40	180	3	
			65		3	
	13	1100	65	300	3	
			100		3	

Photo 5.1 NM and PCM specimens for pull-out test
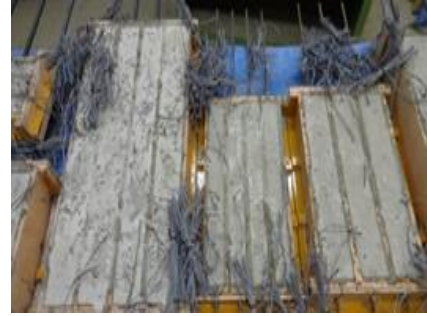
Photo 5.2 SCRCC and SCRPCC specimens

Test procedure

Pull-out test was performed using a 500kN universal testing machine. First, the upper side of a specimen was put on the supporting surface of the machine. Then a tensile loading was applied to the steel bar by pulling the lower part of steel bar downward. Figure 5.3 shows the pull-out test method. The loading method was monotonic. And three specimens were tested for each parameter. Displacement between supporting surface when loaded and measuring point of steel bar was measured. This was conducted by fixing a vice on the proper position, and two displacement transducers were set up as shown in Photos 5.3. The displacement minus elongation of steel bar was determined to the slip between mortar and steel bar. Also, strain of the exposed part and the embedded part of steel bar were measured besides. The pulling-out load was measured by the load cell of the universal testing machine.
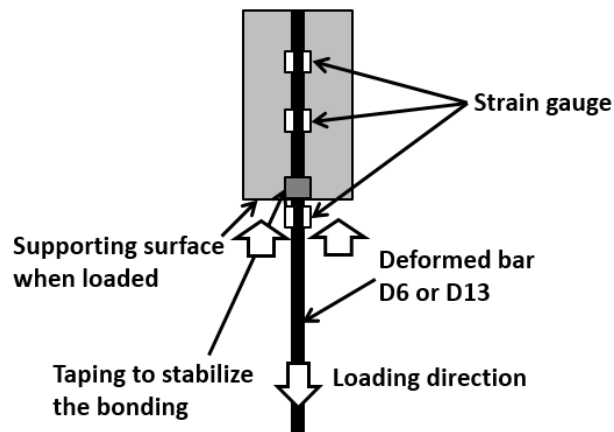
Figure 5.3 Pull-out test method

Photo 5.3 Set up of pull-out test

5.2.2 Test results and discussion

Maximum load · Maximum bond stress · Fracture mode and tensile load-displacement relationships

Pull-out test results are listed in Tables 5.4 and 5.5. And tensile load-displacement relationships are presented in Figures 5.4 to 5.11. The displacement is herein defined as the displacement of measuring point of steel bar minus the displacement of supporting surface when loaded. As a result, some specimens failed by fracture of steel bar or splitting of mortar. The loading of the other specimens were stopped before failure because of over-range of measurement device.

Specimen having splitting failure showed a fracture mode that the mortar split with radially oriented cracks around the steel bar as shown in Photo 5.4. In the fractured part, a bearing failure was observed on the mortar surface corresponding to the transverse rib part of a steel bar. Also, it was observed a steel bar pulled out of mortar in the specimen that the test was finished by over-ranged measurement as shown in Photo 5.5.

Photo 5.4 Specimen having splitting failure   Photo 5.5 Specimen that steel bar was pulled out

Table 5.4 Pull-out test results (D6)

Binder		D6					
		40x180_1	40x180_2	40x180_3	65x180_1	65x180_2	65x180_3
NM	P_{max}	16.0	16.4	15.5	16.2	16.3	15.8
	τb_{max}	8.47	8.46	8.48	8.38	8.44	8.43
	Curing age	39	39	40	41	41	41
	Steel bar yielding	Yield	Yield	Yield	Yield	Yield	Yield
	Number of cracks	3	0	0	0	0	0
	Final result	Split	Fracture	Fracture	Fracture	Fracture	Fracture
SCRCC	P_{max}	16.2	15.7	15.9	16.1	16.1	16.0
	τb_{max}	8.89	7.77	8.27	8.43	7.79	8.32
	Curing age	37	37	37	36	36	37
	Steel bar yielding	Yield	Yield	Yield	Yield	Yield	Yield
	Number of cracks	3	0	0	0	0	0
	Final result	Fracture	Fracture	Fracture	Fracture	Fracture	Fracture
PCM	P_{max}	12.7	16.2	12.4	16.2	15.2	15.7
	τb_{max}	4.78	6.55	0.03	3.93	3.74	4.29
	Curing age	40	40	40	41	41	41
	Steel bar yielding	No yield	Yield	No yield	Yield	Yield	Yield
	Number of cracks	2	2	3	0	0	0
	Final result	Split	Split	Split	Stop	Stop	Stop
SCRPCC	P_{max}	16.0	14.6	13.9	16.1	15.5	14.2
	τb_{max}	5.60	4.35	5.52	6.05	7.83	5.67
	Curing age	37	37	37	36	36	36
	Steel bar yielding	Yield	Yield	Yield	Yield	Yield	Yield
	Number of cracks	0	0	1	0	0	0
	Final result	Stop	Stop	Stop	Stop	Stop	Stop

P_{max} : Maximum load (kN)

τb_{max} : Maximum bond stress (N/mm^2)

Curing age : Curing day (day)

Number of cracks : Number of radial cracks on the supporting surface when loaded

Fracture : End by fracture of steel bar

Split : End by splitting of mortar

Stop : To stop loading at the displacement 20mm after steel bar yielding

Table 5.5 Pull-out test results (D13)

Binder		D13					
		65x300_1	65x300_2	65x300_3	100x300_1	100x300_2	100x300_3
NM	P_{max}	52.2	77.3	69.0	79.3	78.7	77.5
	τb_{max}	11.09	17.00	11.93	16.67	15.78	15.30
	Curing age	41	41	41	42	42	42
	Steel bar yielding	No yield	Yield	Yield	Yield	Yield	Yield
	Number of cracks	4	0	3	0	0	0
	Final result	Split	Fracture	Split	Fracture	Fracture	Fracture
SCRCC	P_{max}	62.1	58.2	77.9	78.4	80.9	79.6
	τb_{max}	9.10	8.85	11.76	13.28	14.59	15.60
	Curing age	37	37	41	41	41	41
	Steel bar yielding	Yield	Yield	Yield	Yield	Yield	Yield
	Number of cracks	1	2	1	0	0	0
	Final result	Split	Split	Split	Fracture	Fracture	Fracture
PCM	P_{max}	27.8	70.7	55.4	73.6	69.8	74.5
	τb_{max}	6.54	9.78	6.69	7.42	24.45	9.05
	Curing age	41	41	41	42	42	42
	Steel bar yielding	No yield	Yield	No yield	Yield	Yield	Yield
	Number of cracks	3	2	2	2	2	0
	Final result	Split	Split	Split	Split	Split	Split
SCRPCC	P_{max}	42.0	39.6	39.0	61.7	64.2	—
	τb_{max}	5.07	0.03	4.21	8.13	10.17	—
	Curing age	37	37	41	41	41	41
	Steel bar yielding	No yield	No yield	No yield	Yield	Yield	Yield
	Number of cracks	1	1	1	2	0	2
	Final result	Stop	Stop	Stop	Stop	Stop	Stop

P_{max}　: Maximum load (kN)

τb_{max}　: Maximum bond stress (N/mm^2)

Curing age　: Curing day (day)

Number of cracks：Number of radial cracks on the supporting surface when loaded

Fracture　: End by fracture of steel bar

Split：End by splitting of mortar

Stop：To stop loading at the displacement 20mm after steel bar yielding
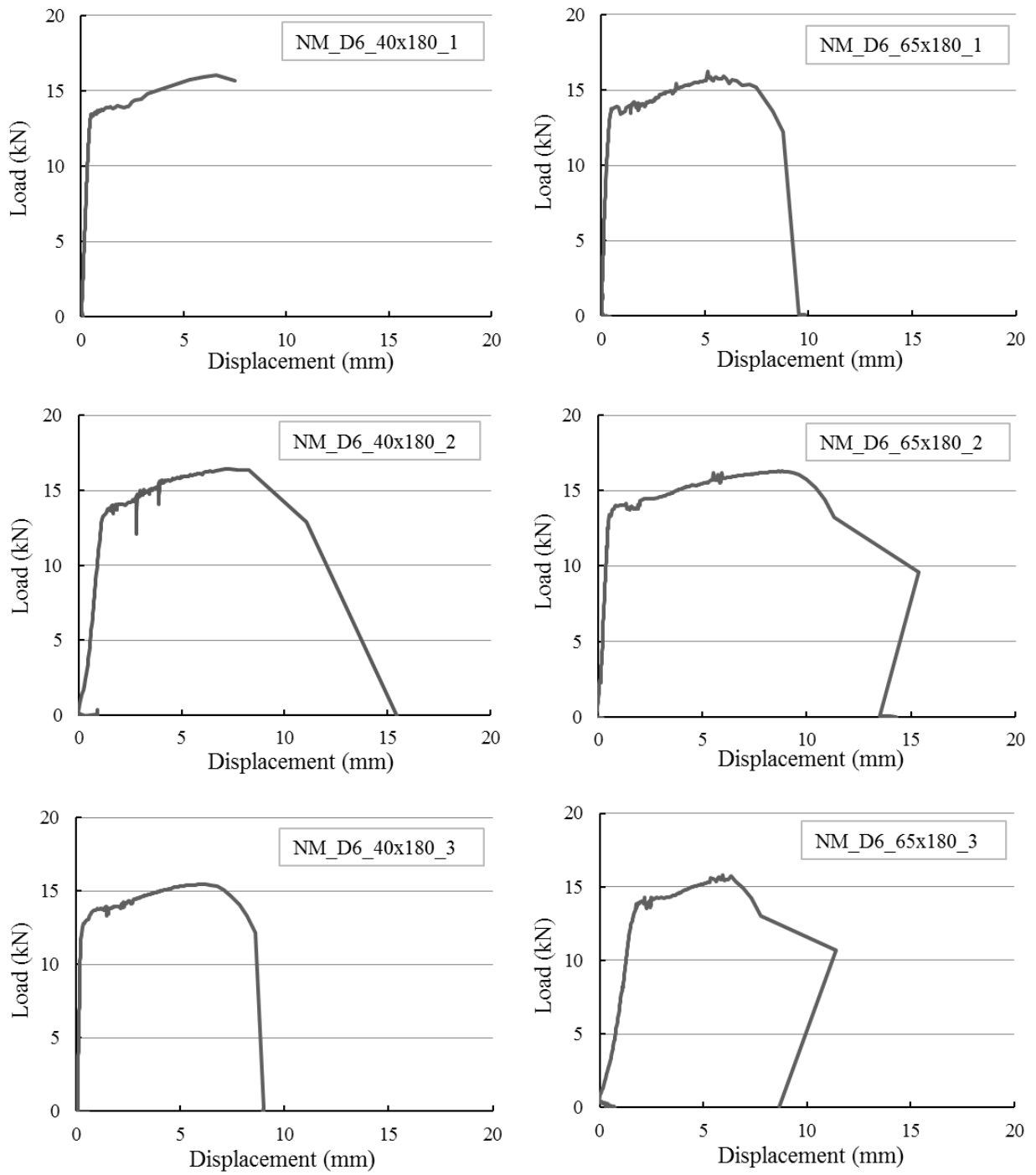
— : Data error

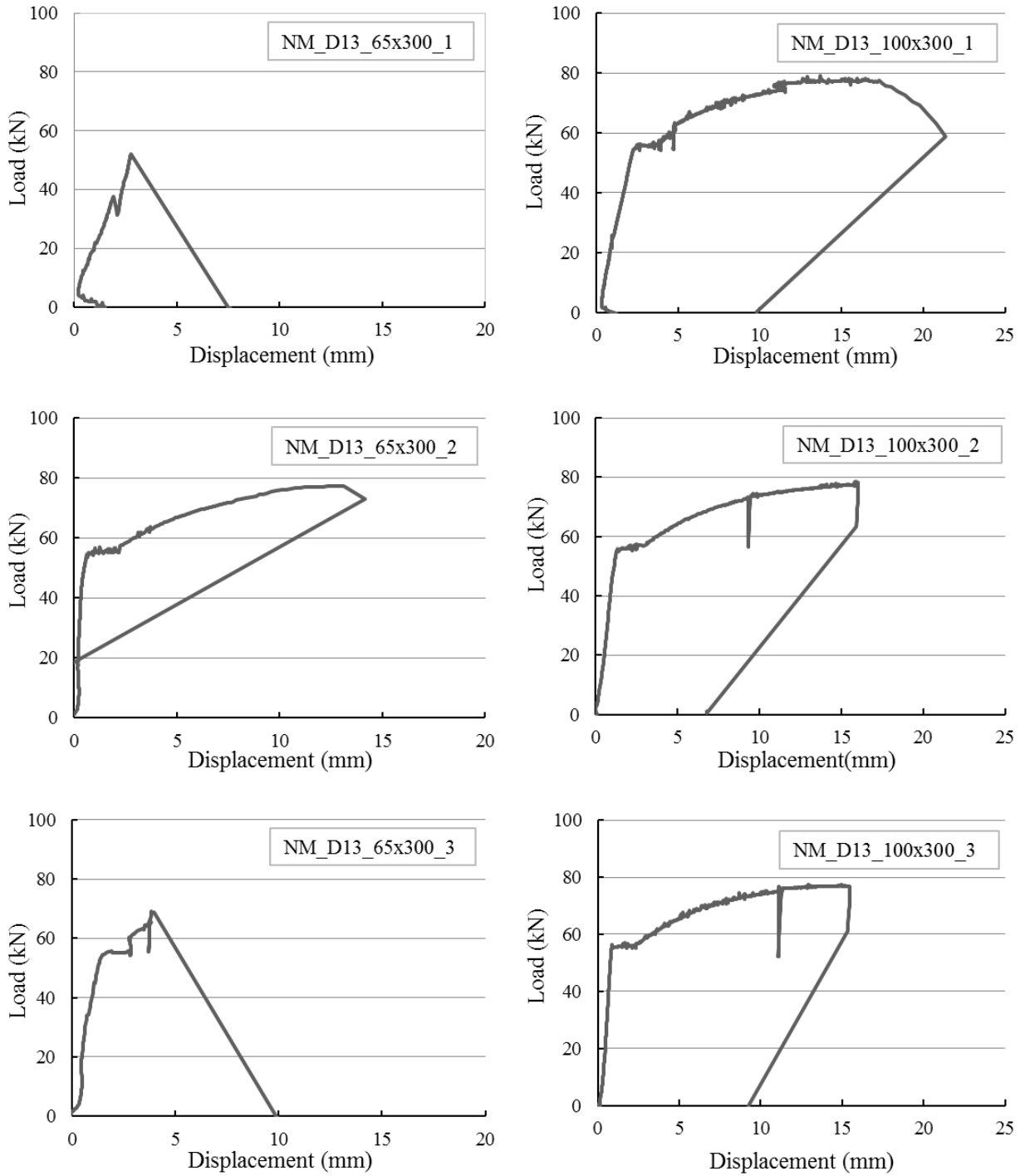Figure 5.4 Tensile load-displacement relationships (NM_D6)

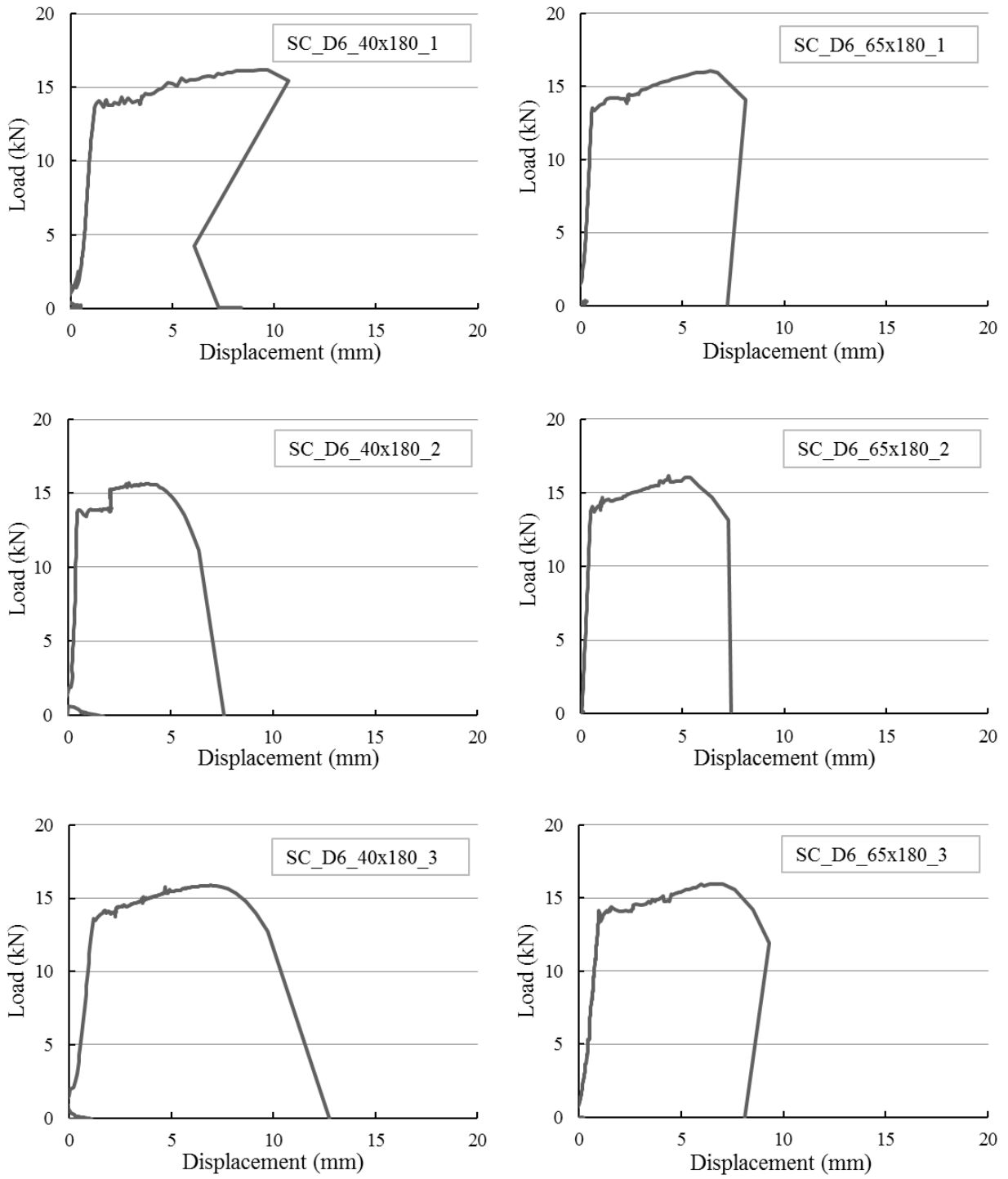Figure 5.5 Tensile load-displacement relationships (NM_D13)

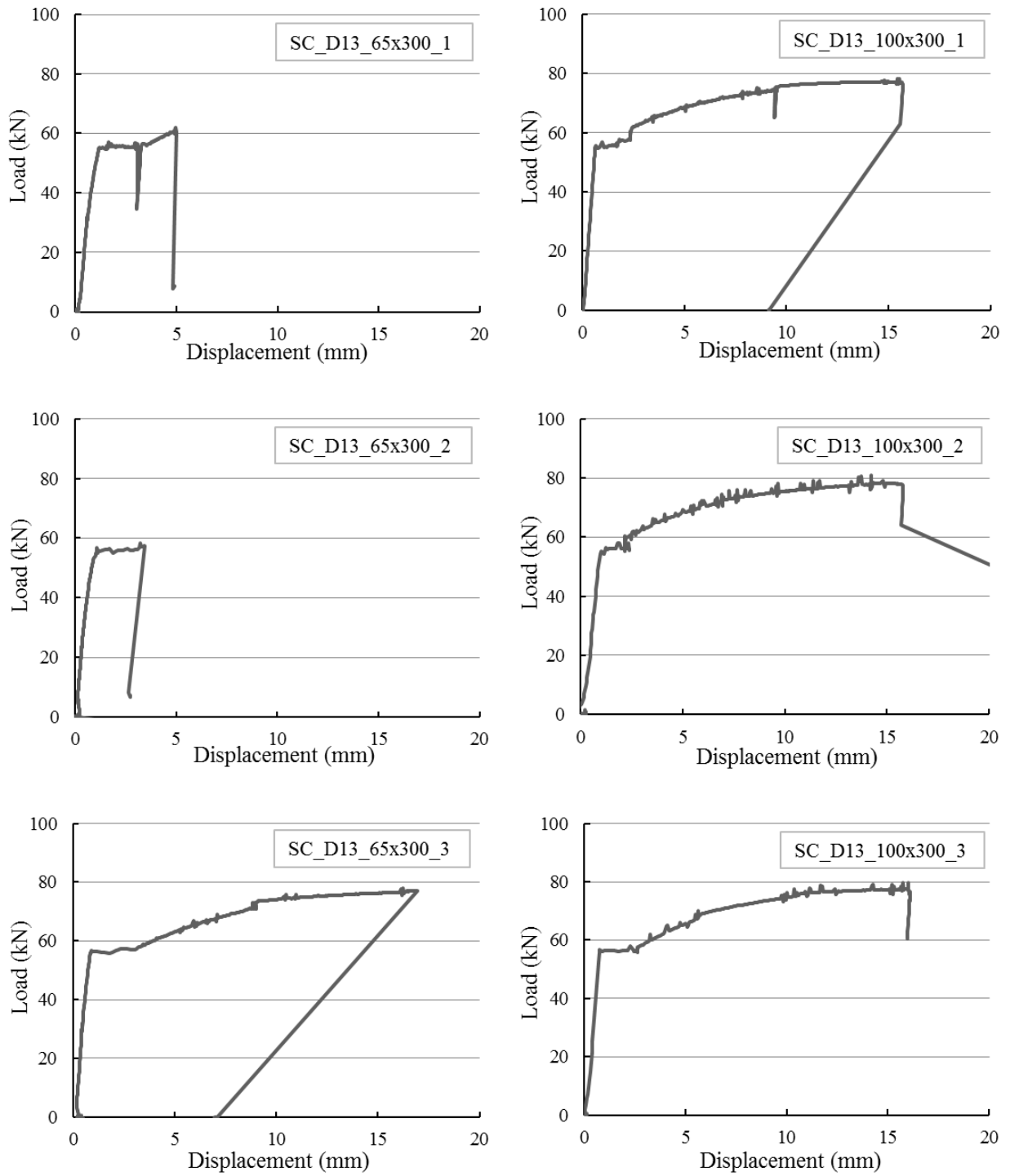Figure 5.6 Tensile load-displacement relationships (SCRCC_D6)

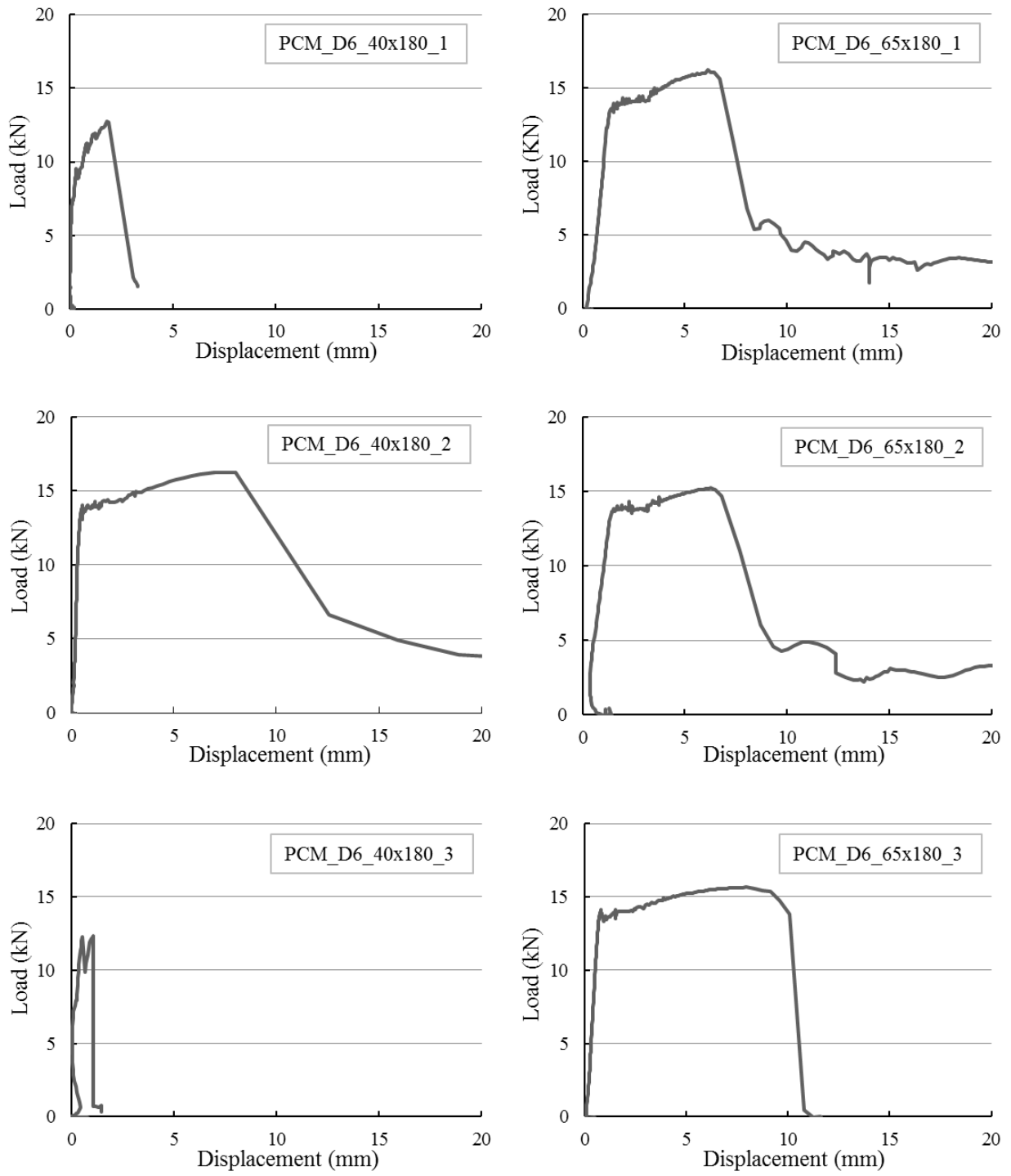Figure 5.7 Tensile load-displacement relationships (SCRCC_D13)

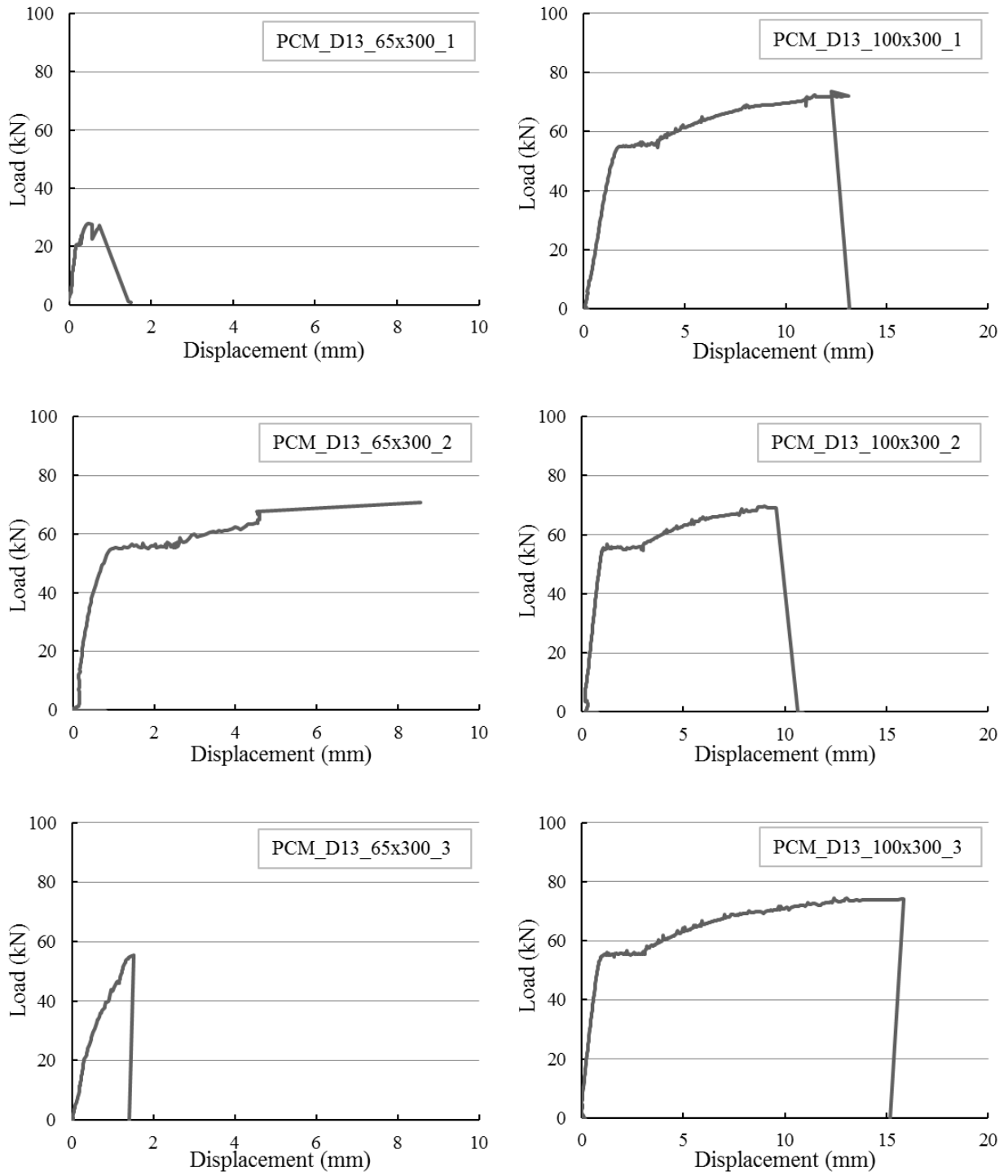Figure 5.8 Tensile load-displacement relationships (PCM_D6)

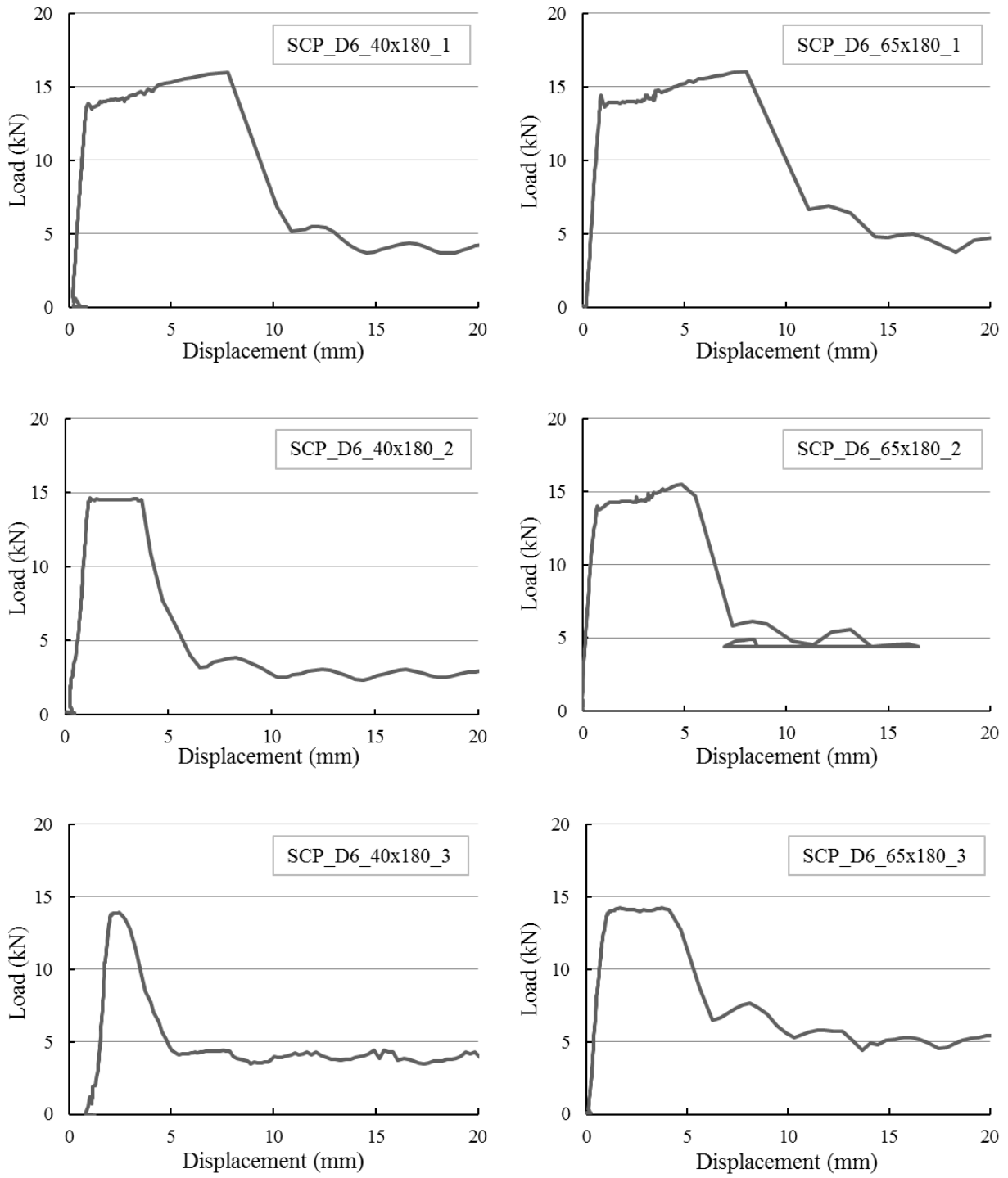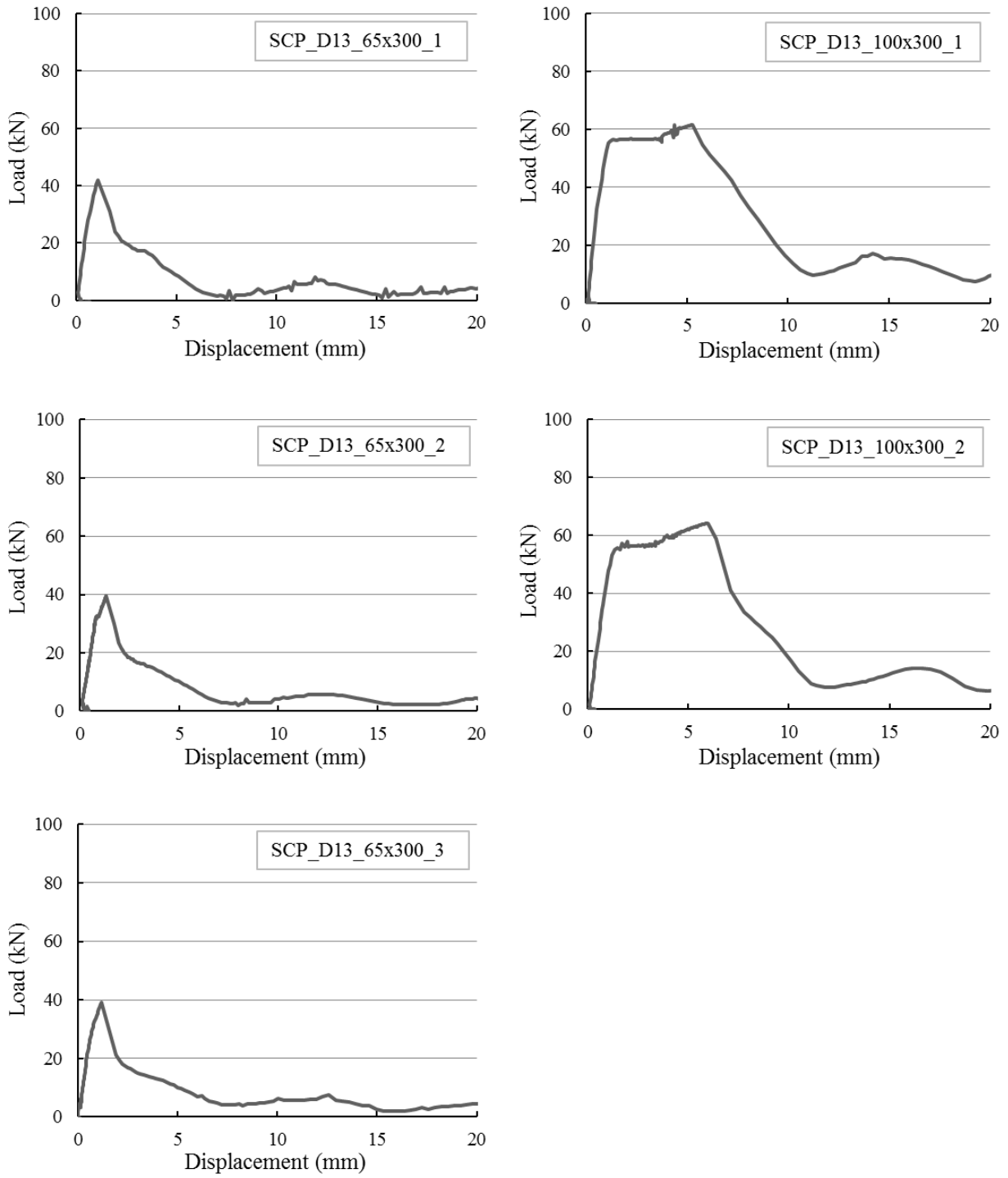Figure 5.9 Tensile load-displacement relationships (PCM_D13)

Figure 5.10 Tensile load-displacement relationships (SCRPCC_D6)

Figure 5.11 Tensile load-displacement relationships (SCRPCC_D13)

It should be noted that, SCP_D13_100x300_3 couldn't be presented in the graph because of data error.

Bond stress-slip relationships

Figure 5.13 indicates the calculation method of bond stress-slip. And bond stress-slip relationships of specimens are shown in Figures 5.14 to 5.21. In the calculation of displacement, it was assumed that strain distribution of each section that strain measurement was performed is linear inside the mortar. It was also assumed that exposed part of steel bar has constant strain distribution. Bond stress was calculated by average stress of steel bar in each measuring point obtained considering *Bauschinger effect* (Vecchio, F.J. 1999) when cyclic load of steel bar.
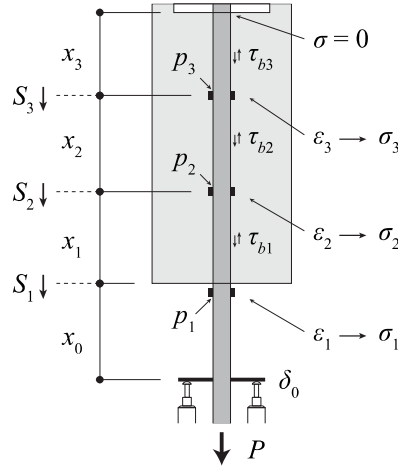
$$\tau_{b1} = (P - \sigma_2 \cdot a_b)/(\phi_b \cdot x_1)$$
$$\tau_{b2} = (\sigma_2 - \sigma_3) \cdot a_b/(\phi_b \cdot x_2)$$
$$\tau_{b3} = \sigma_3 \cdot a_b/(\phi_b \cdot x_3)$$
$$S_1 = \delta_0 - \varepsilon_1 \cdot x_0$$
$$S_2 = S_1 - (\varepsilon_1 + \varepsilon_2)/2 \cdot x_1$$
$$S_3 = S_2 - (\varepsilon_2 + \varepsilon_3)/2 \cdot x_2$$

P : Load a_b : Cross sectional area of steel bar ϕ_b : Diameter of steel bar

δ_0 : Displacement of displacement measuring point from load-supporting surface

x_0 : Distance between displacement measuring point and load-supporting surface

x_1 : Distance between load-supporting surface and p_2

x_2 : Distance between p_2 and p_3

x_3 : Distance between p_3 and the end of embedded steel bar

ε_1, ε_2, ε_3 : Strain at p_1, p_2 and p_3 of steel bar

σ_1, σ_2, σ_3 : Stress at p_1, p_2 and p_3 of steel bar

τ_{b1}, τ_{b2}, τ_{b3} : Average bond stress of section x_1, x_2, x_3

S_1 : Steel bar slip from the load-supporting surface

S_2 : Steel bar slip from p_2

S_3 : Steel bar slip from p_3

Figure 5.13 Calculation method of bond stress-slip relationship
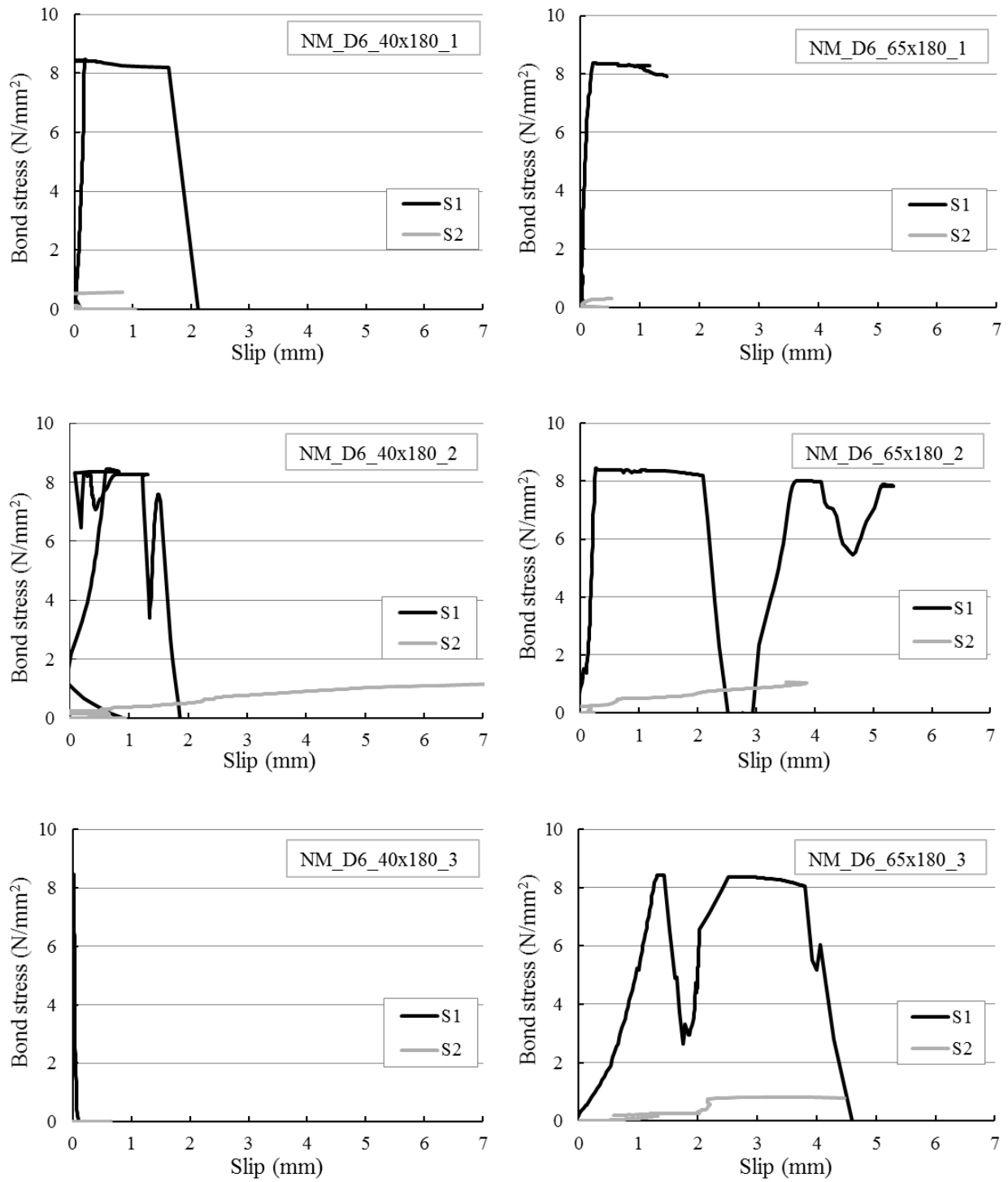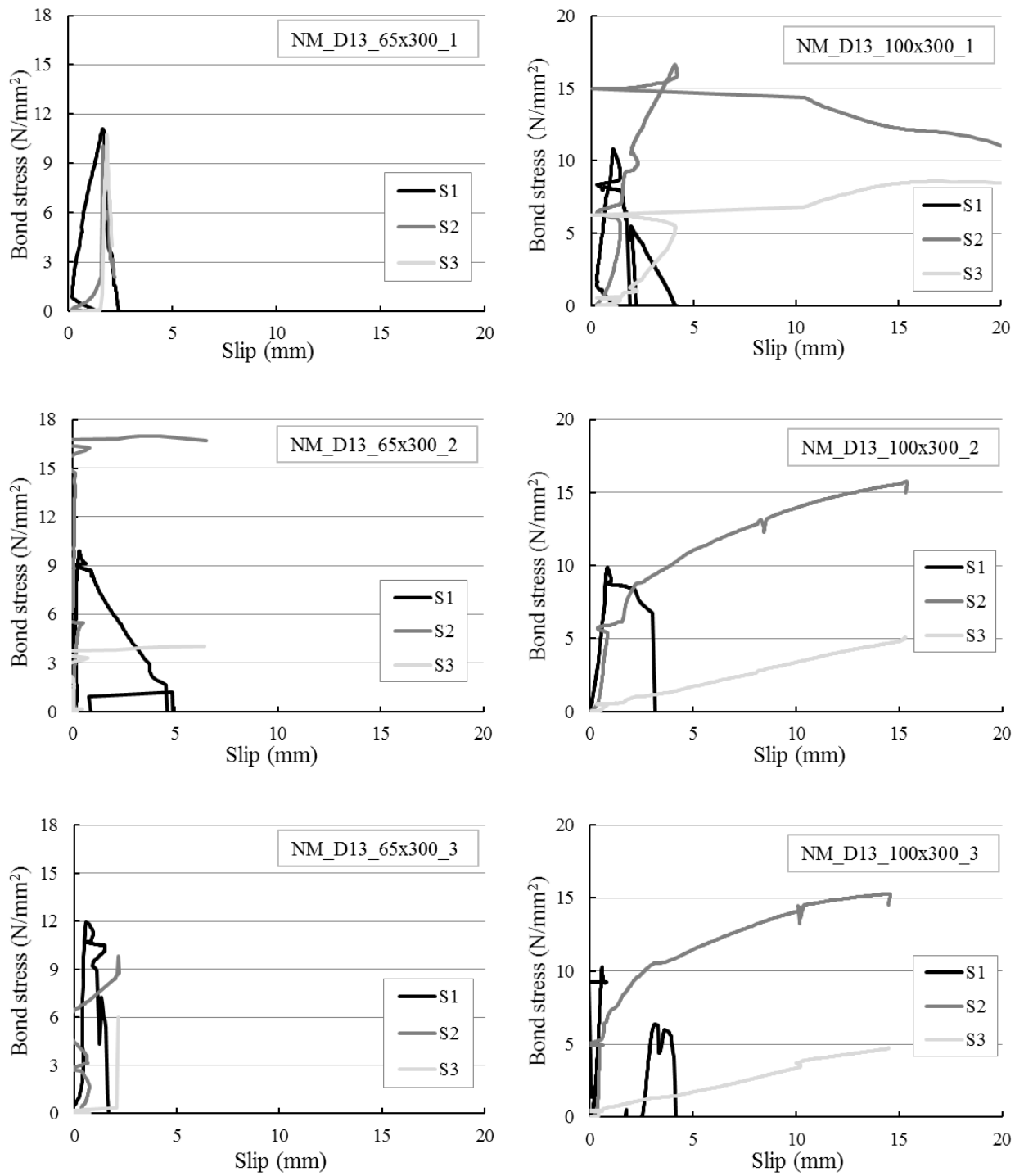
Figure 5.14 Bond stress-slip relationships (NM_D6)

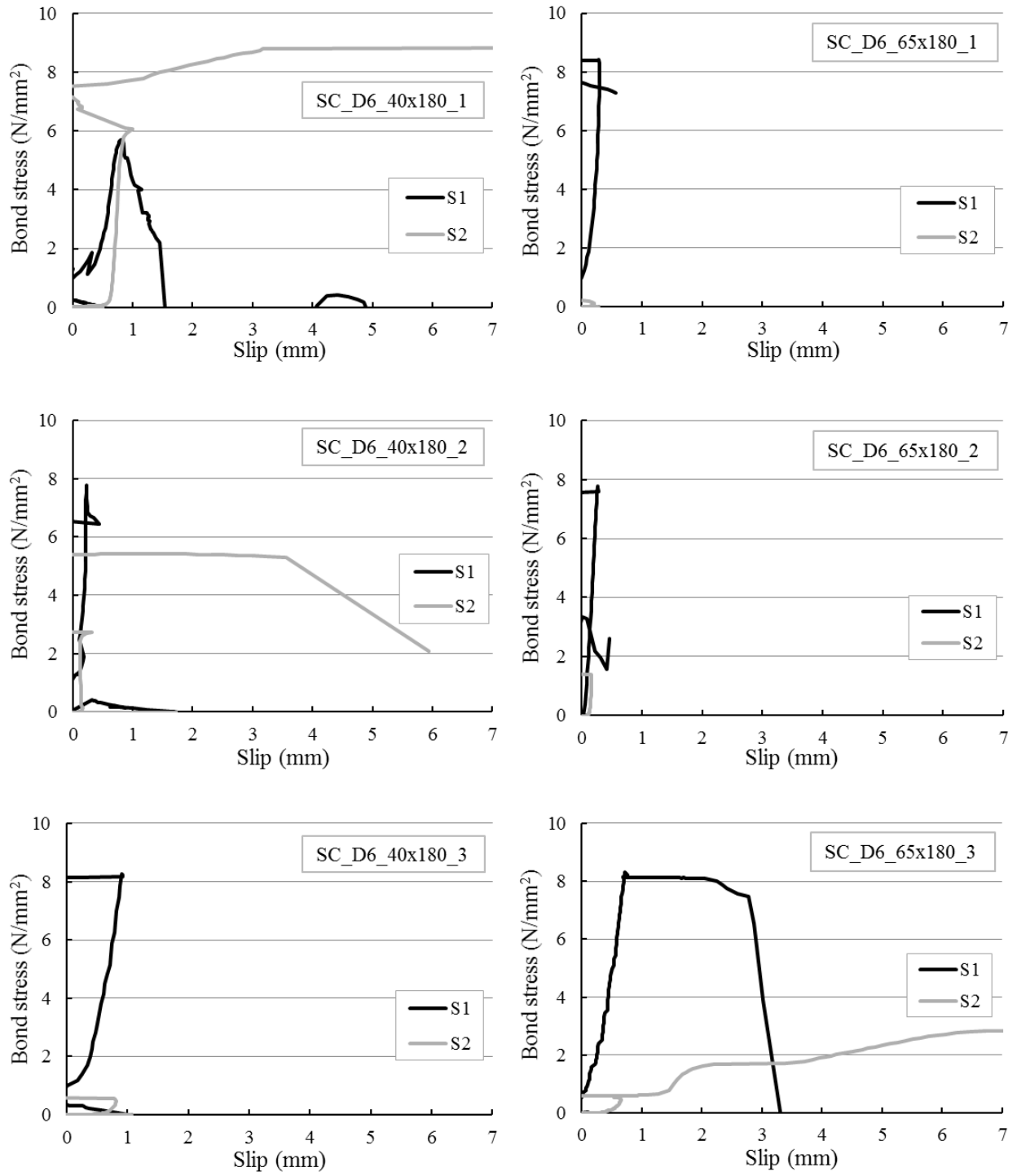Figure 5.15 Bond stress-slip relationships (NM_D13)

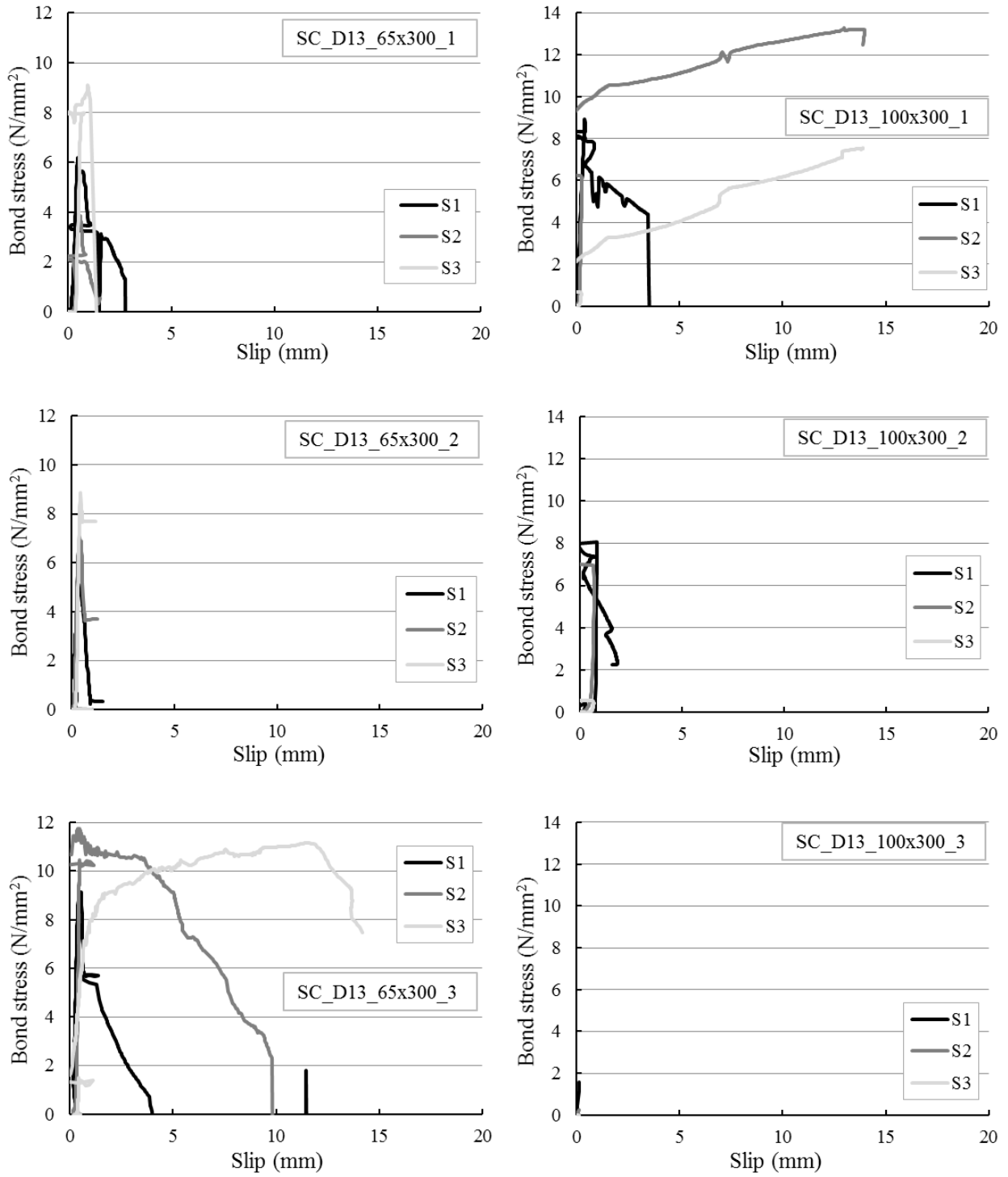Figure 5.16 Bond stress-slip relationships (SCRCC_D6)

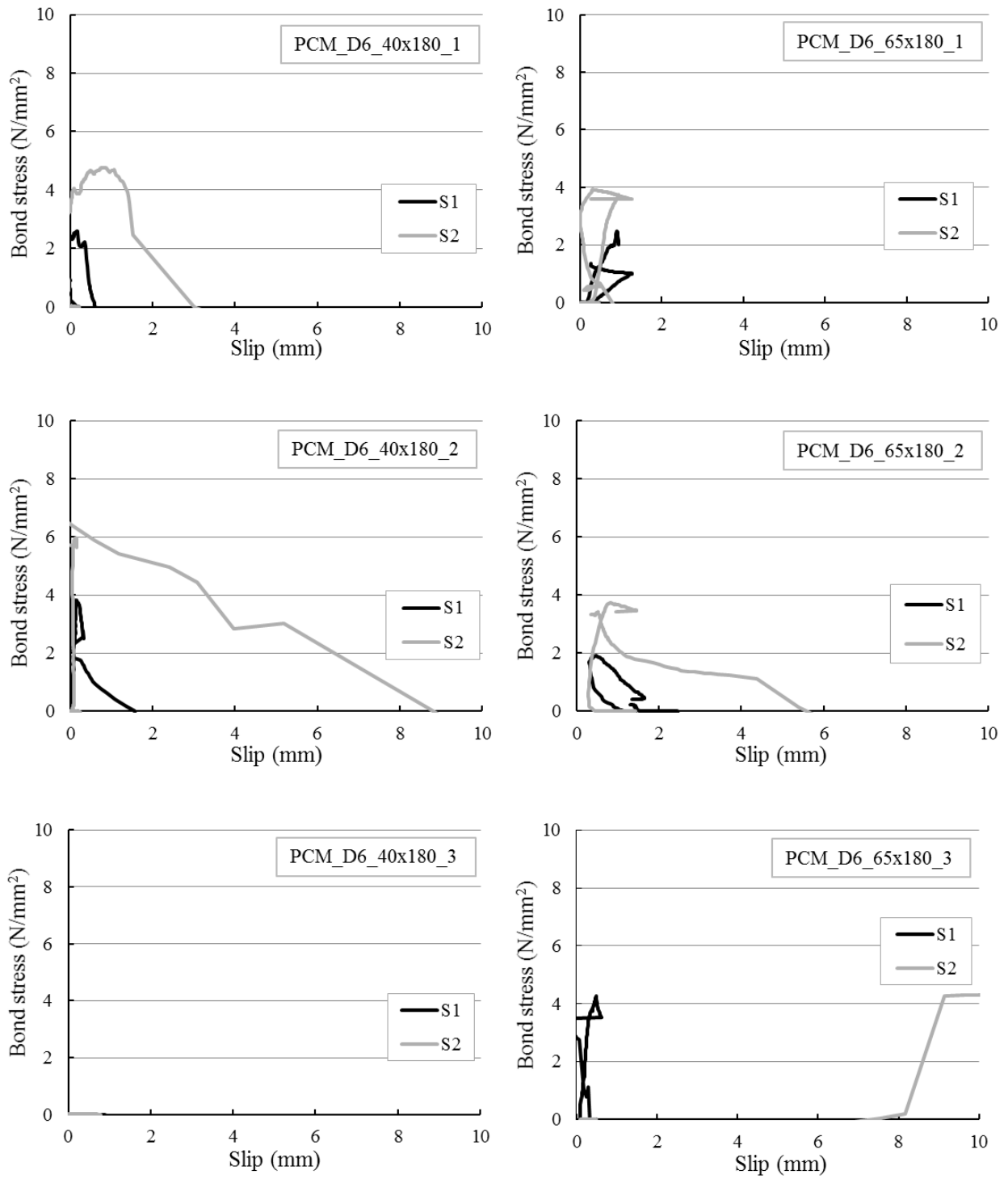Figure 5.17 Bond stress-slip relationships (SCRCC_D13)

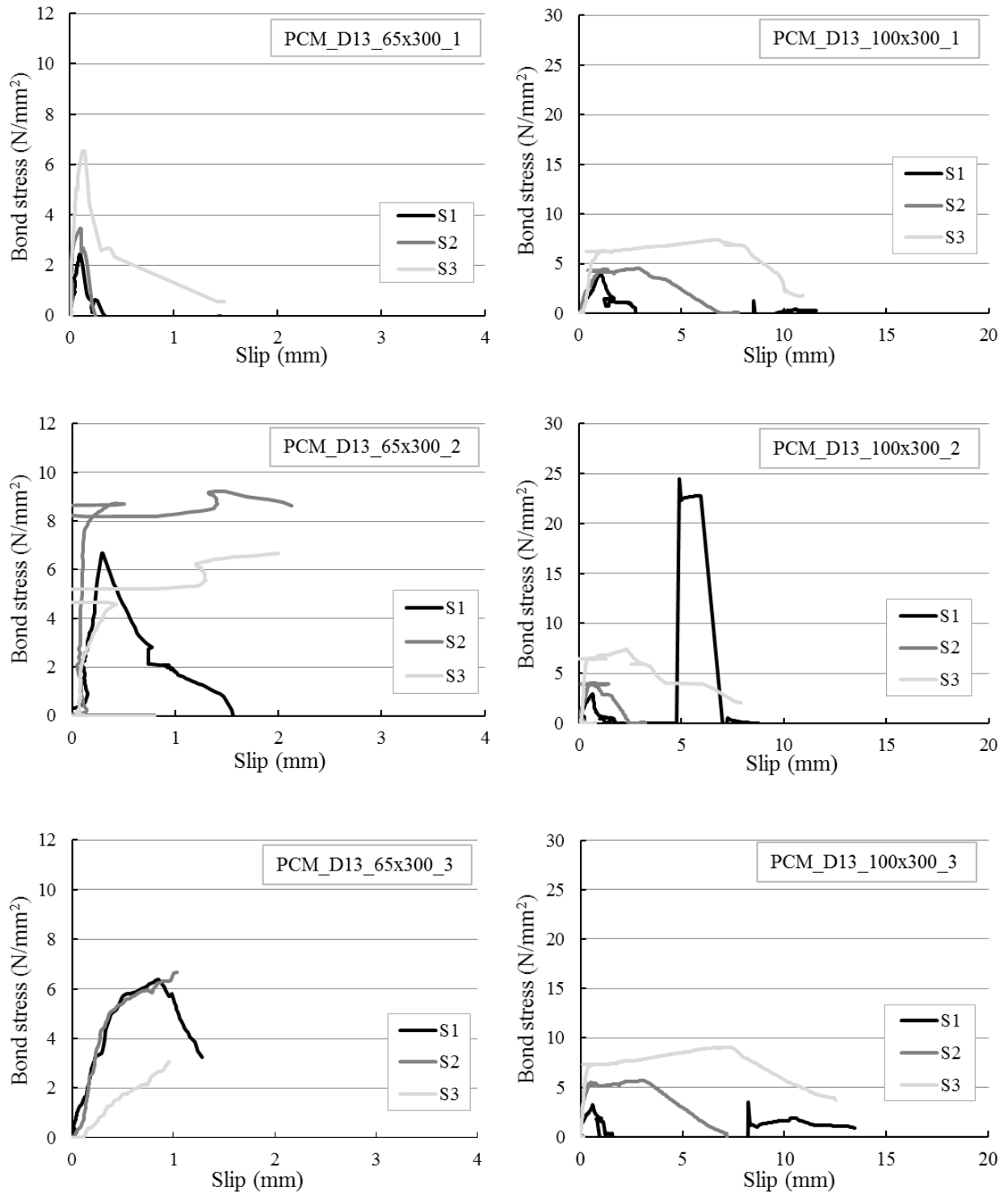Figure 5.18 Bond stress-slip relationships (PCM_D6)

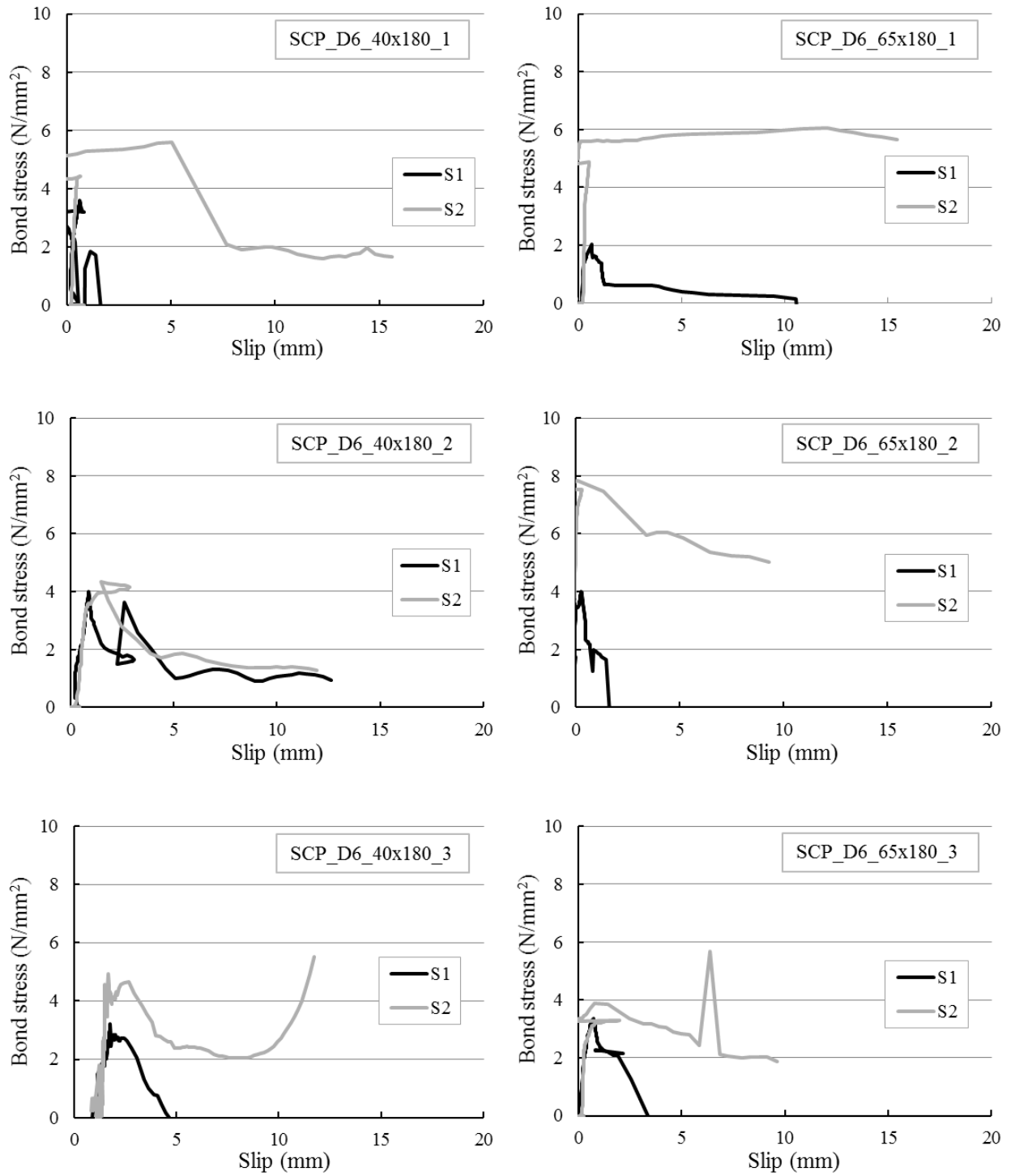Figure 5.19 Bond stress-slip relationships (PCM_D13)

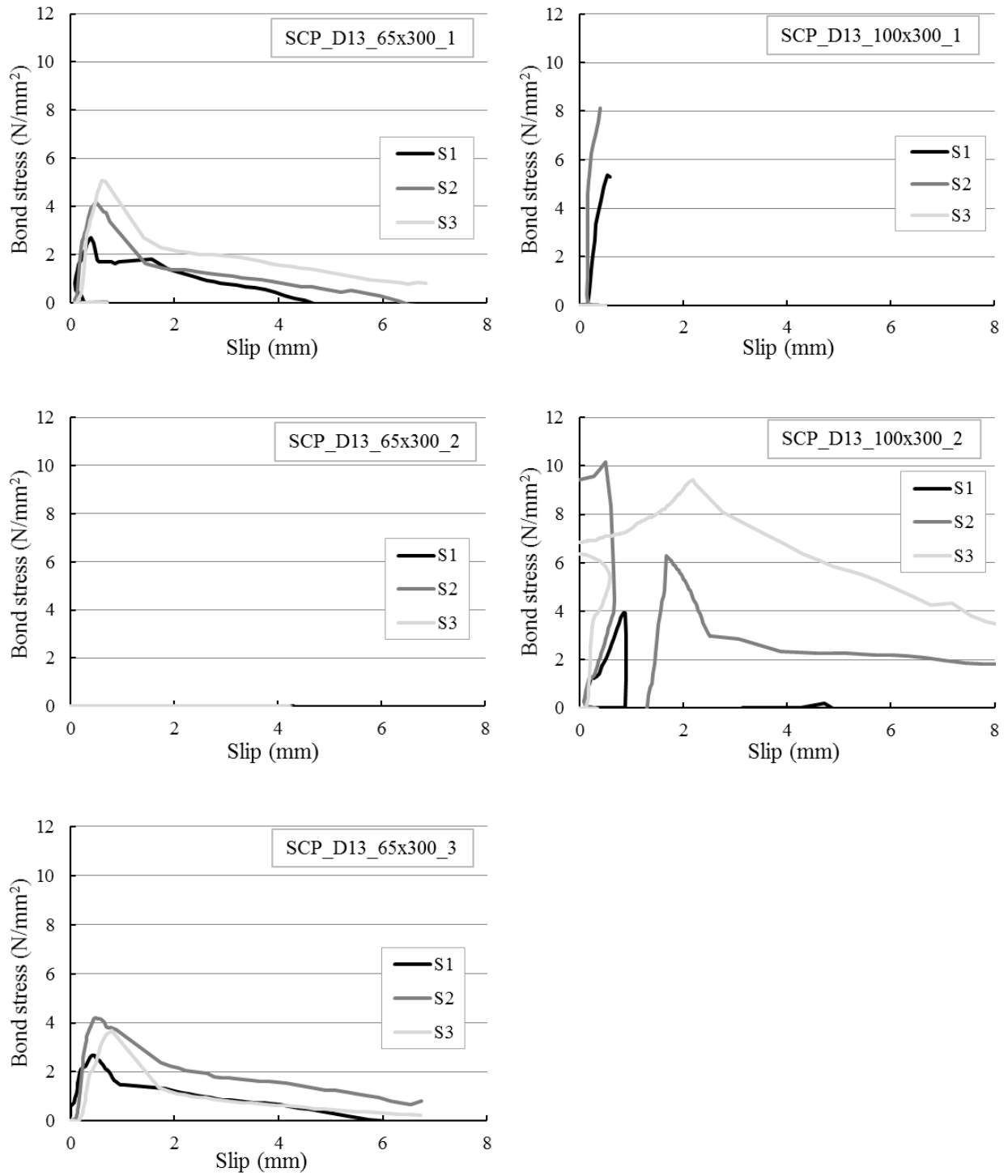Figure 5.20 Bond stress-slip relationships (SCRPCC_D6)

Figure 5.21 Bond stress-slip relationships (SCRPCC_D13)

It should be noted that, SCP_D13_100x300_3 couldn't be presented in the graph because of data error.

Maximum bond stress distribution

Bond stress of NM and PCM showed a tendancy to decrease by reinforcing with steel chip except for some specimens as shown in Figure 5.22. It is considered that the reason is that steel chip reduces the bond strength between mortar and steel bar.
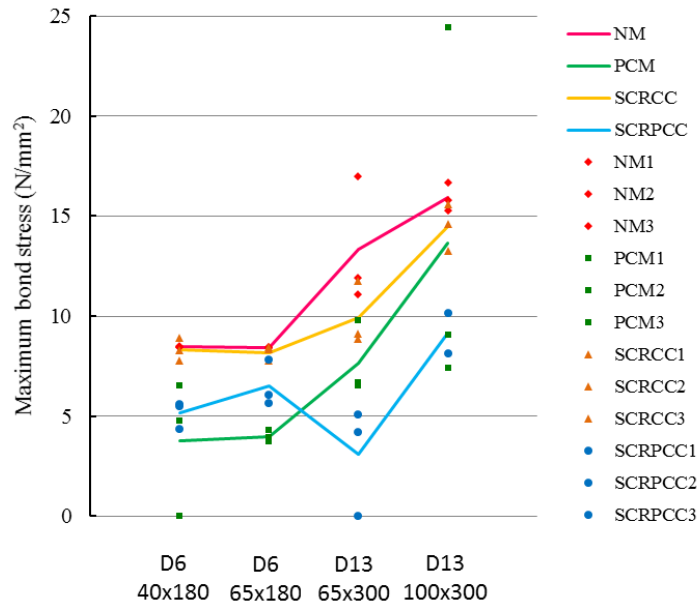
(A marker means each value, and a line means average of three values .)

Figure 5.22 Maximum bond stress distribution

The number of cracks of NM and PCM was increased with increasing of diameter of steel bar, however, it was reduced by reinforcing with steel chip and increasing of cover thickness (i.e. radius of the mortar part minus radius of the steel bar) as shown in Figure 5.23.
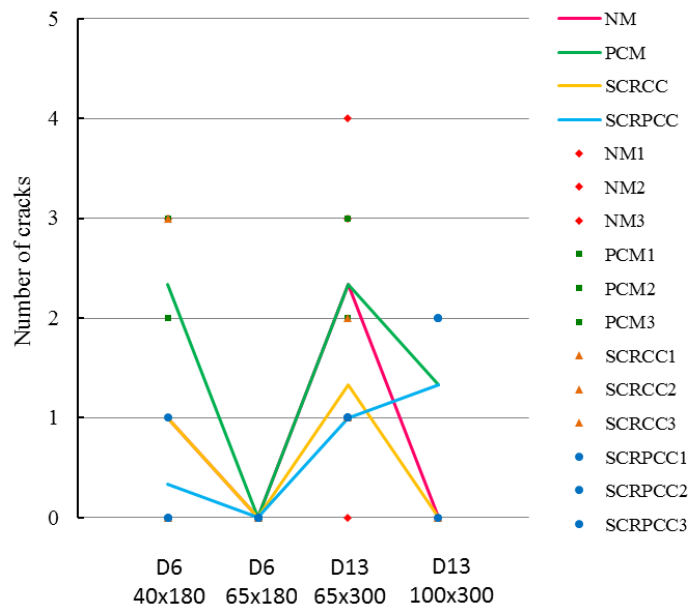
(A marker means each value, and a line means average of three values.)

Figure 5.23 Number of cracks

5.2.3 Concluding remarks of pull-out tests

In this section, it was examined about fundamental properties of relationships between steel bar and bond stress-displacement of SCRCC and SCRPCC by pull-out tests. The following remarks are obtained.

1) Some of NM specimens which have small cross sectional area were that test was finished by splitting failure, and except for these, all the others were finished by tensile fracture of steel bars.

2) In the most of PCM specimens, splitting was observed. This is attributed to the relatively low strength of PCM.

3) In the case of SCRPCC, the loading of all the specimens were stopped because of over-ranged measurement, where steel bar was pulled out from mortar in the most of these cases. The reason for this is considered to be that SCRPCC has relatively low bond stress.

4) Radially oriented cracks around the steel bar was observed in the most of specimen having splitting failure, these specimens showed bond splitting failure by ring tension (JCI 2011).

5) Some of D13 specimens were that bond stress at the inner measuring point S2 was increased than that of near-surface measuring point S1. It is considered that the reason is that a bearing failure occurred on the mortar surface corresponding to the transverse rib part of the steel bar when a steel bar is pulled out.

5.3 Uniaxial tension tests of small diameter steel bar

Uniaxial tension tests were conducted to examine the cracking characteristics of SCRCC and SCRPCC considered walls same as Section 5.2.

5.3.1 Experimental programs

Materials

Same materials and mix proportions as Section 5.2 were used in this section.

Specimens

Specimens were prepared with two types of steel bars, three types of specimen diameter and two types of specimen length as shown in Figure 5.24. In total, 56 specimens were prepared as listed in Table 5.6. NM and PCM were casted in the shape of cylinder type with PVC pipe molds as shown in Photo 5.6. And SCRCC and SCRPCC were casted in the shape of beam type (same surface area as cylinder type specimens) with wooden molds because of difficulty of casting into the narrow and long PVC pipe molds considering distribution of steel chips in the cementitious composites as shown in Photo 5.7. All the specimens were demolded after 3 days and cured in the air.
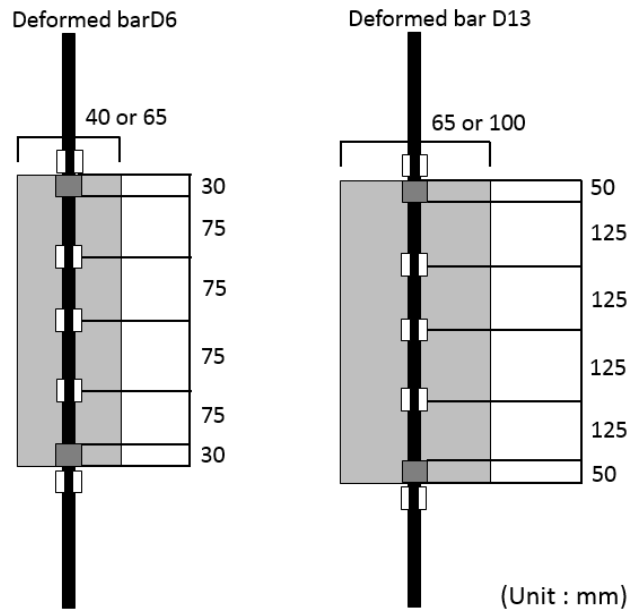
Figure 5.24 Geometry of specimens for uniaxial tension test

Table 5.6 List of specimens

Binder	Diameter of bar (mm)	Length of bar (mm)	Diameter of specimen (mm)	Length of specimen (mm)	Loading method	Number of specimens
NM	6.4	980	40	360	Monotonic	2
			40	360	Cyclic	2
			65	360	Monotonic	3
	13	1400	65	600	Monotonic	2
			65	600	Cyclic	2
			100	600	Monotonic	3
SCRCC (SCP)	6.4	980	40	360	Monotonic	2
			40	360	Cyclic	2
			65	360	Monotonic	3
	13	1400	65	600	Monotonic	2
			65	600	Cyclic	2
			100	600	Monotonic	3
PCM	6.4	980	40	360	Monotonic	2
			40	360	Cyclic	2
			65	360	Monotonic	3
	13	1400	65	600	Monotonic	2
			65	600	Cyclic	2
			100	600	Monotonic	3
SCRPCC (SCP)	6.4	980	40	360	Monotonic	2
			40	360	Cyclic	2
			65	360	Monotonic	3
	13	1400	65	600	Monotonic	2
			65	600	Cyclic	2
			100	600	Monotonic	3

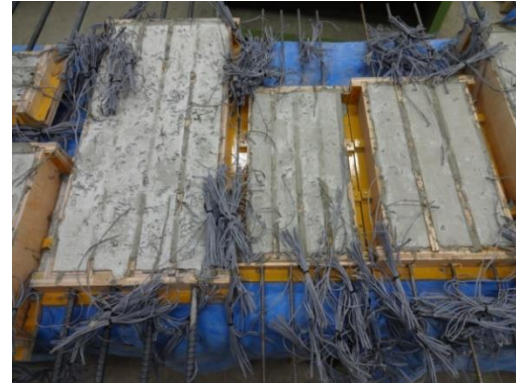| Photo 5.6 NM and PCM specimens for uniaxial tension test | Photo 5.7 SCRCC and SCRPCC specimens |

Test procedure

   Uniaxial tension test was performed using a 500kN universal testing machine. First, the upper and lower parts of a steel bar were fixed. And a tensile loading was applied to the steel bar by pulling the lower part downward. Figure 5.25 shows the uniaxial tension test method. The test was conducted with two loading methods: monotonic loading and cyclic loading. In the case of cyclic loading, loading was applied until the displacement of steel bar reached every 1mm. After reaching displacement 50mm, monotonic load was applied until the steel bar was fractured. And two specimens were tested for cyclic loading and three specimens were tested for monotonic loading. Besides pulling-out loading, displacement was measured using a displacement transducer set on the universal testing machine. A vice was fixed on the steel bar while the displacement transducer was set up to touch the vice as shown in Photos 5.8.
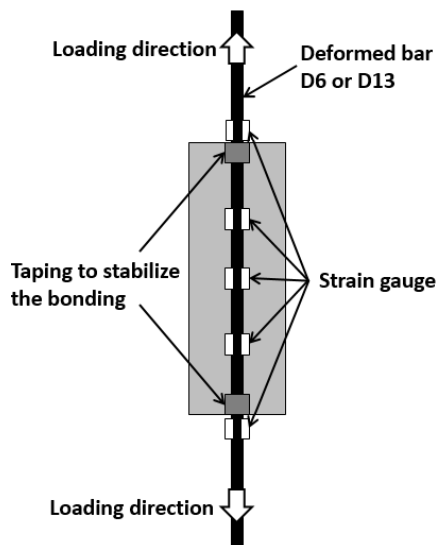

| Figure 5.25 Uniaxial tension test method | Photo 5.8 Set up of uniaxial tension test |

5.3.2 Test results and discussion

Maximum load ·Maximum bond stress ·Fracture mode and tensile load-displacement relationships

Uniaxial tension test results are listed in Tables 5.4 and 5.5. And tensile load-displacement relationships are presented in Figures 5.26 to 5.33. "C" means cyclic loaded specimen in the name of specimens.

Cracking was observed in all the specimens. Not only transverse cracks but also longitudinal cracks were observed in the specimens. Several specimens have a few cracks as shown in Photo 5.4 while the other specimens have many cracks as shown in Photo 5.5. Some of specimens were broken by impact of steel bar fracture.

Photo 5.9 Specimen having a few cracks   Photo 5.10 Specimen having many cracks

Table 5.4 Results of uniaxial tension test (Part 1)

Specimens	Cross sectional area (mm²)	Max. bar stress (N/mm²)	Max. bond stress (N/mm²)	Equivalent number of cracks	Average crack width (mm)
NM_D6_40x360_1	1590	486.7	9.05	9.1	29.9
NM_D6_40x360_2	1590	501.2	8.46	10.5	26.2
NM_D6_40x360_1C	1590	483.6	9.09	10.0	27.4
NM_D6_40x360_2C	1590	493.7	9.09	10.9	25.2
NM_D6_65x360_1	3318	485.8	5.45	3.2	71.4
NM_D6_65x360_2	3318	561.1	5.22	1.1	141.2
NM_D6_65x360_3	3318	505.5	5.45	3.1	73.6
NM_D13_65x600_1	3318	473.9	2.54	16.5	28.5
NM_D13_65x600_2	3318	582.1	11	18	26.3
NM_D13_65x360_1C	3318	587.3	11.0	12.2	37.9
NM_D13_65x360_2C	3318	590.7	10.95	12.6	36.7
NM_D13_100x600_1	7853	586.5	11	6	71.9
NM_D13_100x600_2	7853	587.1	8.71	7.4	59.8
NM_D13_100x600_3	7853	587.1	11	11.8	39.1
SC_D6_40x360_1	1590	517.6	8.11	8.6	31.2
SC_D6_40x360_2	1590	498.4	2.41	7.2	36.8
SC_D6_40x360_1C	1590	497.5	9.09	7.2	36.6
SC_D6_40x360_2C	1590	482.2	2.55	6.0	43.0
SC_D6_65x360_1	3318	483.8	9.09	2.7	81.6
SC_D6_65x360_2	3318	495.9	5.06	2.9	77.4
SC_D6_65x360_3	3318	515.7	7.54	3.2	72.3
SC_D13_65x600_1	3318	592.5	2.4	14.3	32.8
SC_D13_65x600_2	3318	587.6	3.61	10.6	43.3
SC_D13_65x600_1C	3318	593	10.97	16.5	28.6
SC_D13_65x600_2C	3318	592.7	4.13	15.7	29.9
SC_D13_100x600_1	7853	592.7	4.05	8.2	54.3
SC_D13_100x600_2	7853	579.2	10.47	7.6	58
SC_D13_100x600_3	7853	591.2	5.65	7.3	60
PCM_D6_40x360_1	1590	516.8	9.09	3.4	69
PCM_D6_40x360_2	1590	522.3	2.42	1.9	105.3
PCM_D6_40x360_1C	1590	498.3	9.09	2.6	84.5
PCM_D6_40x360_2C	1590	519.8	4.85	2.8	78.9
PCM_D6_65x360_1	3318	499	5.24	1.1	146.3
PCM_D6_65x360_2	3318	489.2	4.93	1	150
PCM_D6_65x360_3	3318	491.8	4.45	1	150
PCM_D13_65x600_1	3318	586.3	1.31	4.2	96.6
PCM_D13_65x600_2	3318	586.6	1.34	7.3	60.1
PCM_D13_65x600_1C	3318	582.4	7.56	8.5	52.9
PCM_D13_65x600_2C	3318	590.4	7.8	6.6	66
PCM_D13_100x600_1	7853	582.7	6.21	1	250
PCM_D13_100x600_2	7853	588	11	3.3	115.3
PCM_D13_100x600_3	7853	579.5	4.67	4.2	96.4
SCP_D6_40x360_1	1590	480.6	8.9	6.2	41.7
SCP_D6_40x360_2	1590	522.5	1.94	5.1	49.2
SCP_D6_40x360_1C	1590	495.1	9.01	5.6	45.5
SCP_D6_40x360_2C	1590	507.6	9.09	6.2	41.7
SCP_D6_65x360_1	3318	490.9	4.17	1.1	144.6
SCP_D6_65x360_2	3318	501.5	7.68	1	150
SCP_D6_65x360_3	3318	520.9	9.01	1.4	127.7
SCP_D13_65x600_1	3318	591.8	9.16	14.9	31.5
SCP_D13_65x600_2	3318	599.4	7.69	12.7	36.6
SCP_D13_65x600_1C	3318	615.2	1.51	11.1	41.2
SCP_D13_65x600_2C	3318	589.3	11	15.2	31
SCP_D13_100x600_1	7853	584.8	3.28	6.1	70.2
SCP_D13_100x600_2	7853	589.9	7.8	5.3	79.7
SCP_D13_100x600_3	7853	612.7	10.34	4.7	87.5

Table 5.5 Results of uniaxial tension test (Part 2)

| Specimens	Max. bond stress right before yield (N/mm^2)	Average crack width when yield (mm)
NM_D6_40x360_1	4.48	50.42
NM_D6_40x360_2	6.03	43.48
NM_D6_40x360_1C	4.73	53.57
NM_D6_40x360_2C	5.24	48.39
NM_D6_65x360_1	5.21	300.00
NM_D6_65x360_2	5.22	300.00
NM_D6_65x360_3	5.21	300.00
NM_D13_65x600_1	2.54	58.65
NM_D13_65x600_2	5.33	67.34
NM_D13_65x360_1C	4.16	66.45
NM_D13_65x360_2C	10.95	58.65
NM_D13_100x600_1	10.96	121.95
NM_D13_100x600_2	8.71	115.27
NM_D13_100x600_3	11.0	93.24
SC_D6_40x360_1	2.07	71.86
SC_D6_40x360_2	2.41	75.95
SC_D6_40x360_1C	2.63	66.30
SC_D6_40x360_2C	2.55	72.73
SC_D6_65x360_1	4.59	109.09
SC_D6_65x360_2	5.06	93.02
SC_D6_65x360_3	5.23	82.76
SC_D13_65x600_1	2.40	72.46
SC_D13_65x600_2	3.34	113.64
SC_D13_65x600_1C	2.30	65.79
SC_D13_65x600_2C	3.35	97.56
SC_D13_100x600_1	4.05	138.41
SC_D13_100x600_2	2.33	124.61
SC_D13_100x600_3	5.65	147.60
PCM_D6_40x360_1	4.33	81.08
PCM_D6_40x360_2	1.43	105.26
PCM_D6_40x360_1C	4.23	139.53
PCM_D6_40x360_2C	3.89	122.45
PCM_D6_65x360_1	3.92	300.00
PCM_D6_65x360_2	4.93	150.00
PCM_D6_65x360_3	4.45	150.00
PCM_D13_65x600_1	1.31	162.60
PCM_D13_65x600_2	1.34	235.29
PCM_D13_65x600_1C	5.03	119.76
PCM_D13_65x600_2C	3.44	111.11
PCM_D13_100x600_1	6.21	250.00
PCM_D13_100x600_2	5.33	167.36
PCM_D13_100x600_3	4.67	150.38
SCP_D6_40x360_1	1.07	68.97
SCP_D6_40x360_2	1.94	86.96
SCP_D6_40x360_1C	1.26	97.56
SCP_D6_40x360_2C	5.03	96.00
SCP_D6_65x360_1	4.17	144.58
SCP_D6_65x360_2	4.30	150.00
SCP_D6_65x360_3	8.19	176.47
SCP_D13_65x600_1	0.71	96.62
SCP_D13_65x600_2	1.13	109.29
SCP_D13_65x600_1C	1.24	114.29
SCP_D13_65x600_2C	1.49	100.50
SCP_D13_100x600_1	2.18	185.19
SCP_D13_100x600_2	2.58	170.94
SCP_D13_100x600_3	3.20	141.84
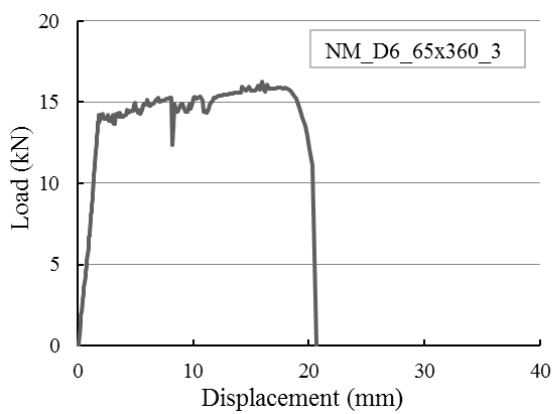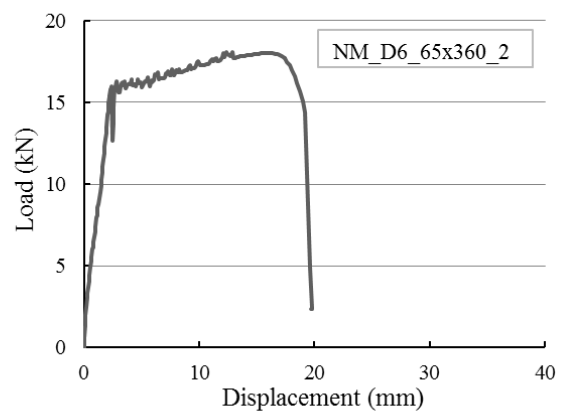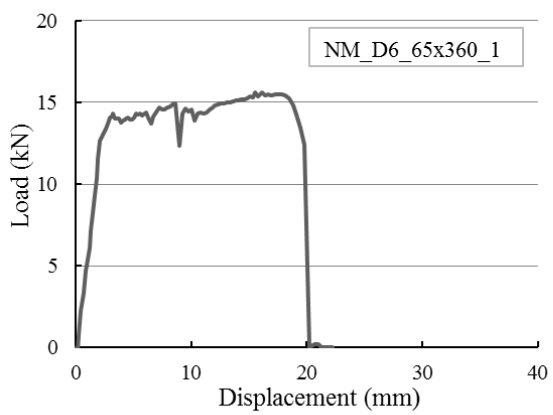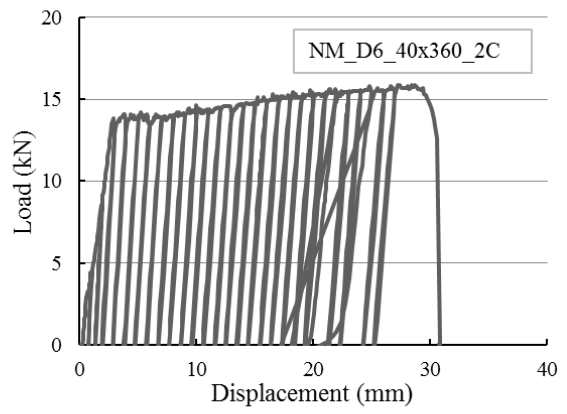
Figure 5.26 Tensile load-displacement relationships (NM_D6)

It should be noted that, NM_D13_100x600_1 couldn't be presented in the graph because of measuring error.

Figure 5.27 Tensile load-displacement relationships (NM_D13)
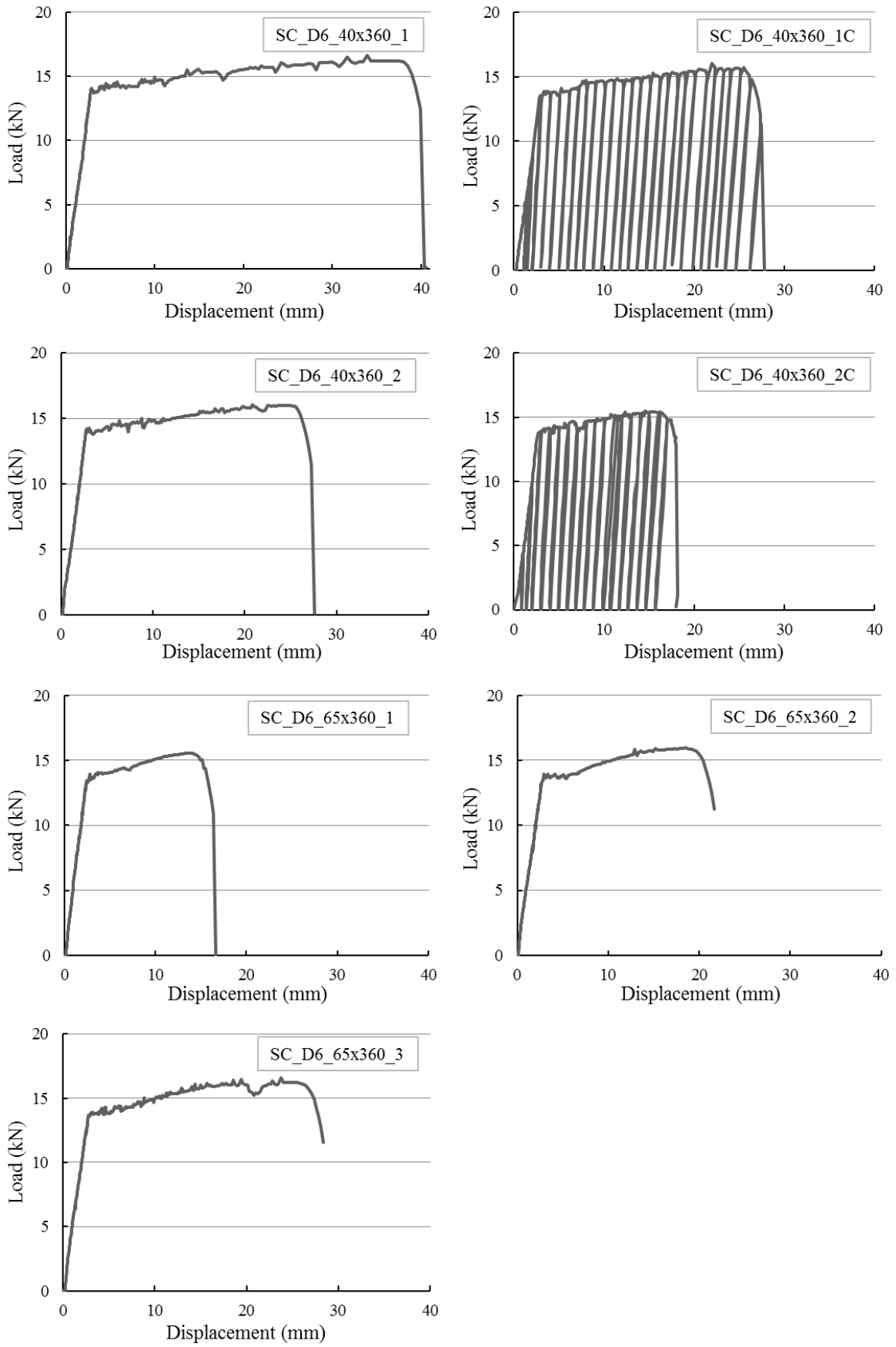
Figure 5.28 Tensile load-displacement relationships (SCRCC_D6)
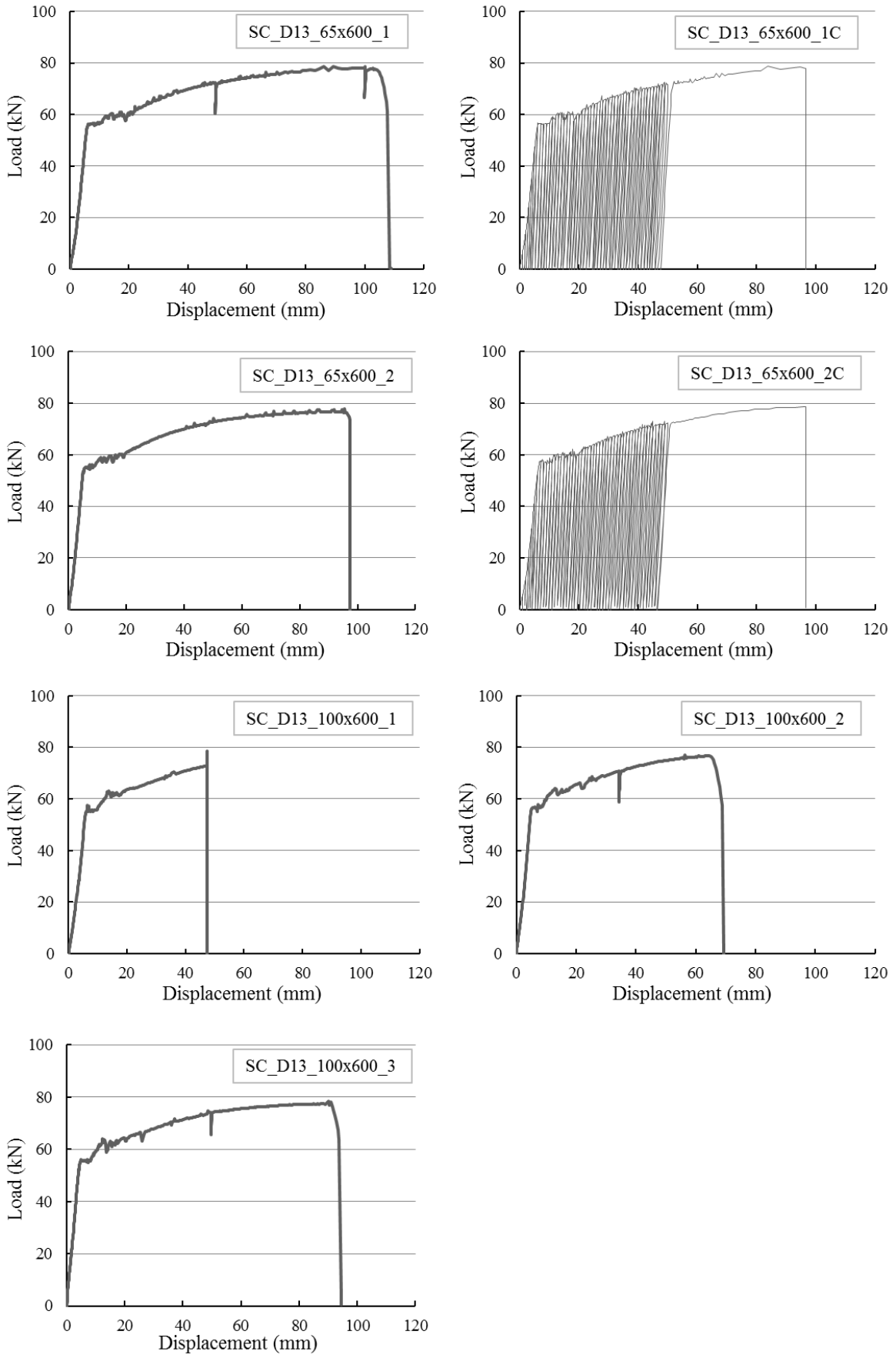
Figure 5.29 Tensile load-displacement relationships (SCRCC_D13)
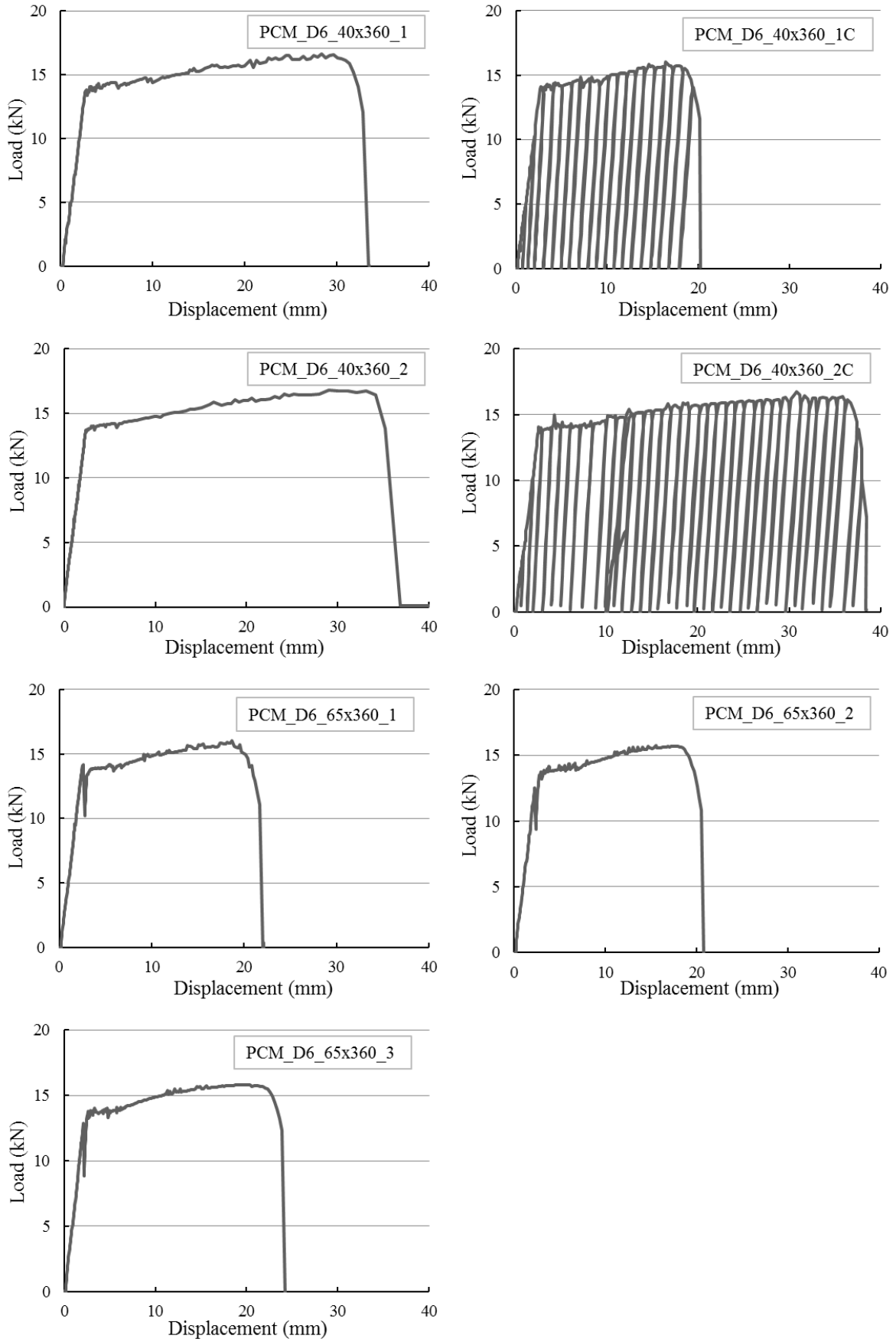
Figure 5.30 Tensile load-displacement relationships (PCM_D6)

Figure 5.31 Tensile load-displacement relationships (PCM_D13)
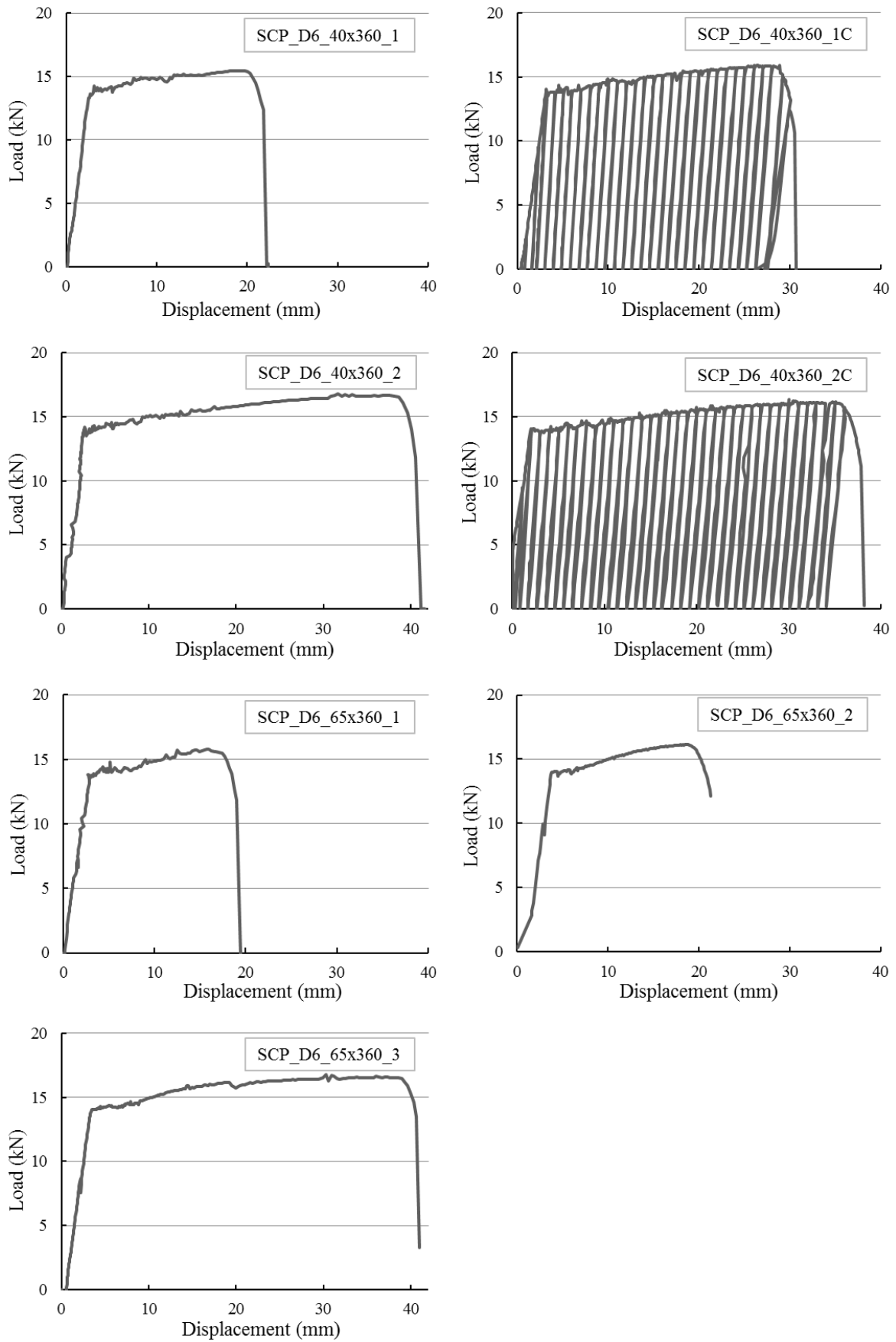
Figure 5.32 Tensile load-displacement relationships (SCRPCC_D6)
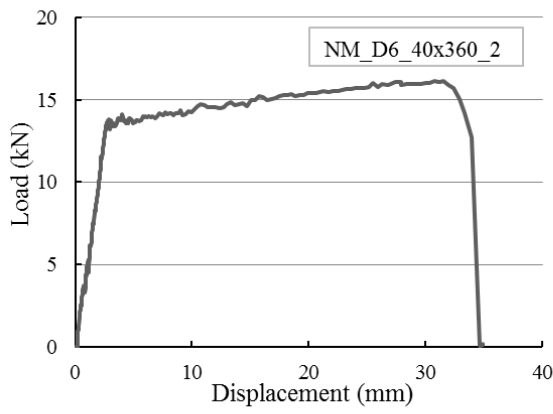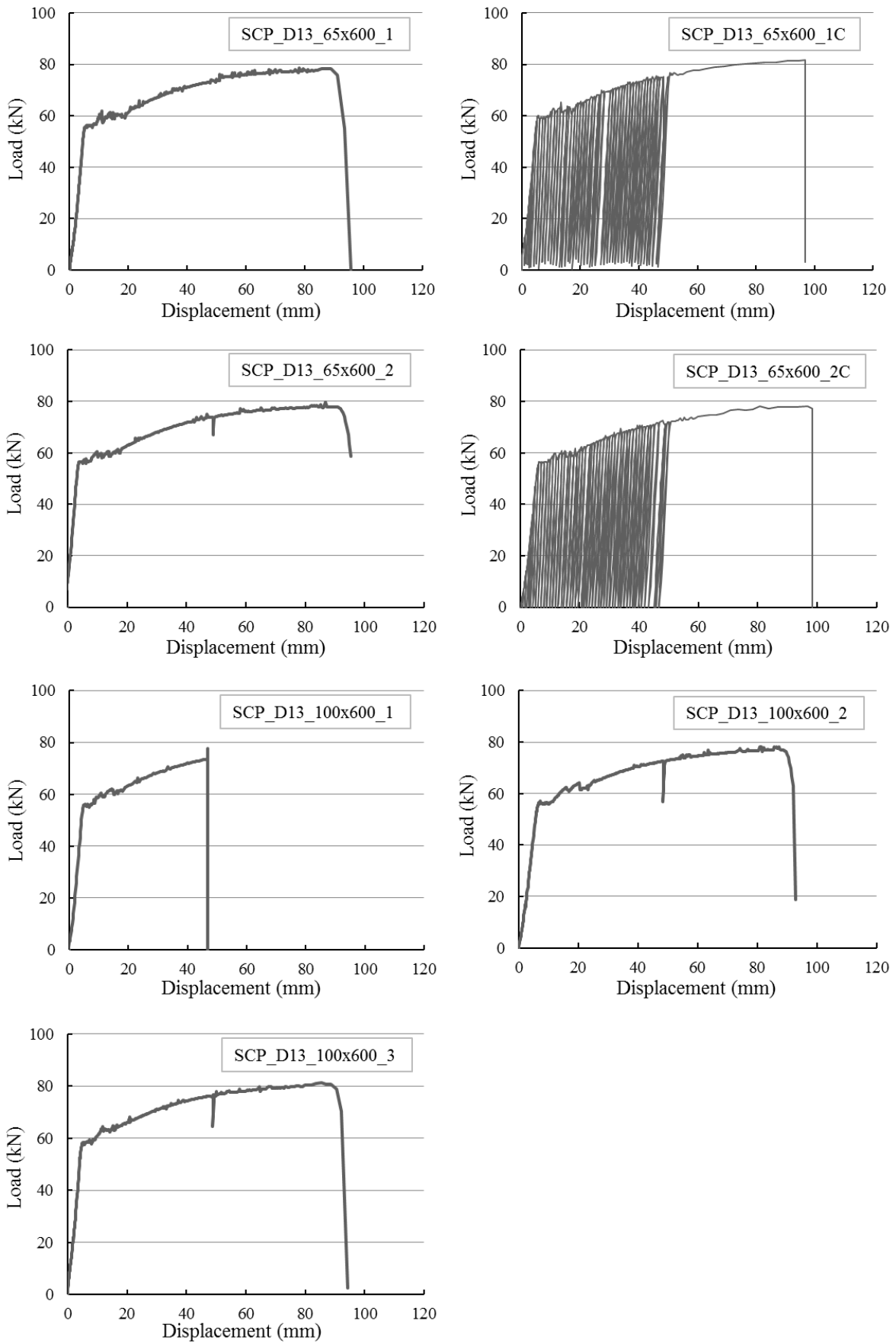
Figure 5.33 Tensile load-displacement relationships (SCRPCC_D13)

Bond stress-slip relationships

Figure 5.34 indicates the calculation method of bond stress. And bond stress-displacement relationships of specimens are shown in Figures 5.35 to 5.42. Bond stress was calculated by average stress of steel bar in each measuring point obtained considering *Bauschinger effect* (Vecchio, F.J 1999) when cyclic load of steel bar.
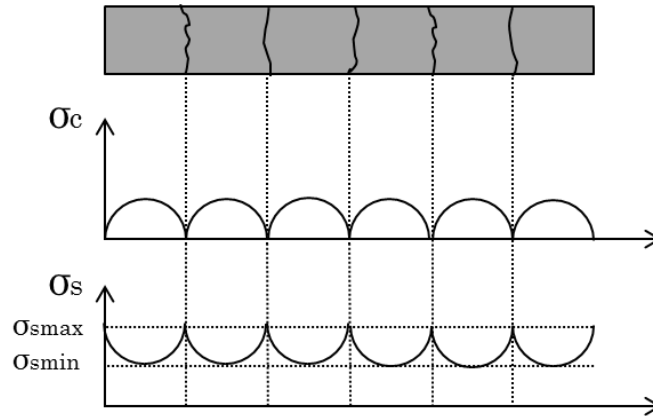
$$\Delta\sigma_s = \sigma_{smax} - \sigma_{smin} \qquad\qquad\qquad Eq(5.1)$$

$$F = \Delta\sigma_s \times A_s = \tau_b \times A \quad \text{(Balance of force)} \qquad Eq(5.2)$$

$$A = S \times d \times \pi \qquad\qquad\qquad Eq(5.3)$$

$$A_s = \pi \times d^2 \div 4 \qquad\qquad\qquad Eq(5.4)$$

$$L_s = S \times \pi \times d \qquad\qquad\qquad Eq(5.5)$$

By Eqs(5.1〜5.5), $\Delta\sigma_s \times A_s = \tau_b \times A$

$$\tau_b = \Delta\sigma_s \times A_s \div A$$
$$= (\sigma_{smax} - \sigma_{smin}) \times \pi \times d^2 \div 4 \div (S \times d \times \pi)$$
$$= (\sigma_{smax} - \sigma_{smin}) \times d \div 4\ S$$

σ_c : Stress of mortar
σ_s : Stress of steel bar
σ_{smax} : Maximum stress of steel bar
σ_{smin} : Minimum stress of steel bar
$\Delta\sigma_s$: Difference between σ_{smax} and σ_{smin}
F : Bond force
τ_b : Bond stress
A : Surface area of steel bar of section of σ_{smax} and σ_{smin}
A_s : Cross sectional area of steel bar
S : Length of the section of σ_{smax} and σ_{smin}
d : Diameter of steel bar
L_s : Circumference of steel bar
π : The circular constant

Figure 5.34 Calculation method of bond stress
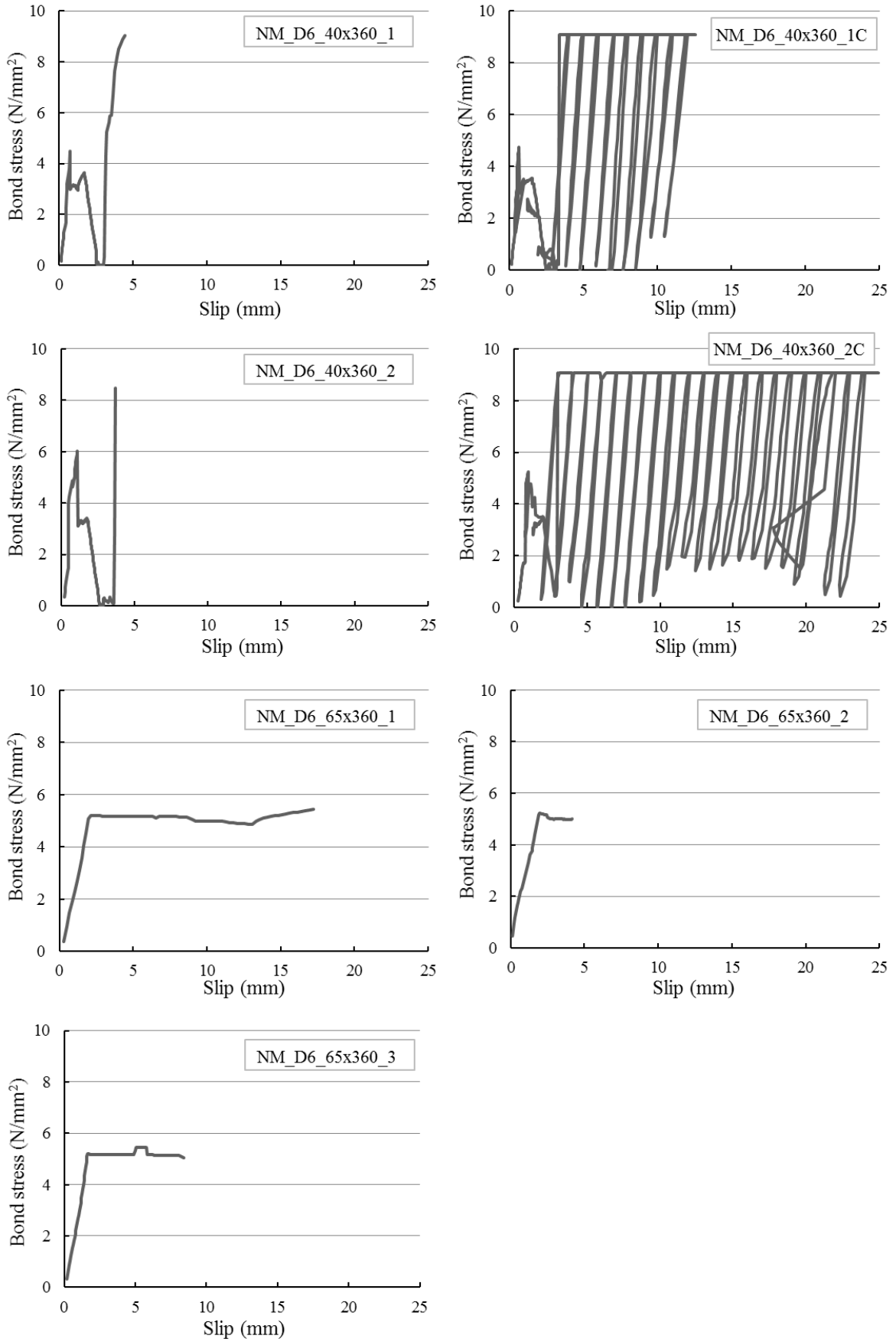
Figure 5.35 Bond stress-slip relationships (NM_D6)
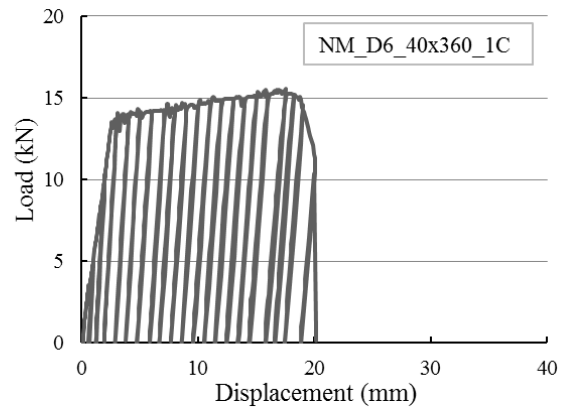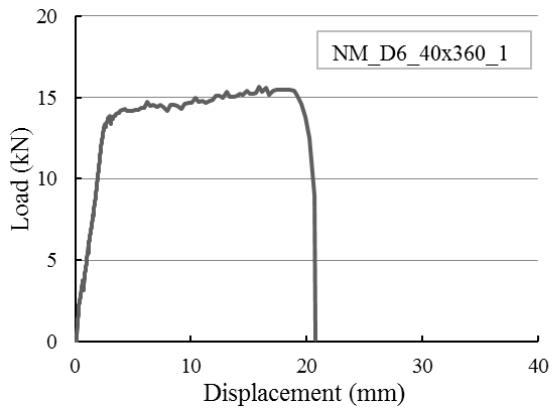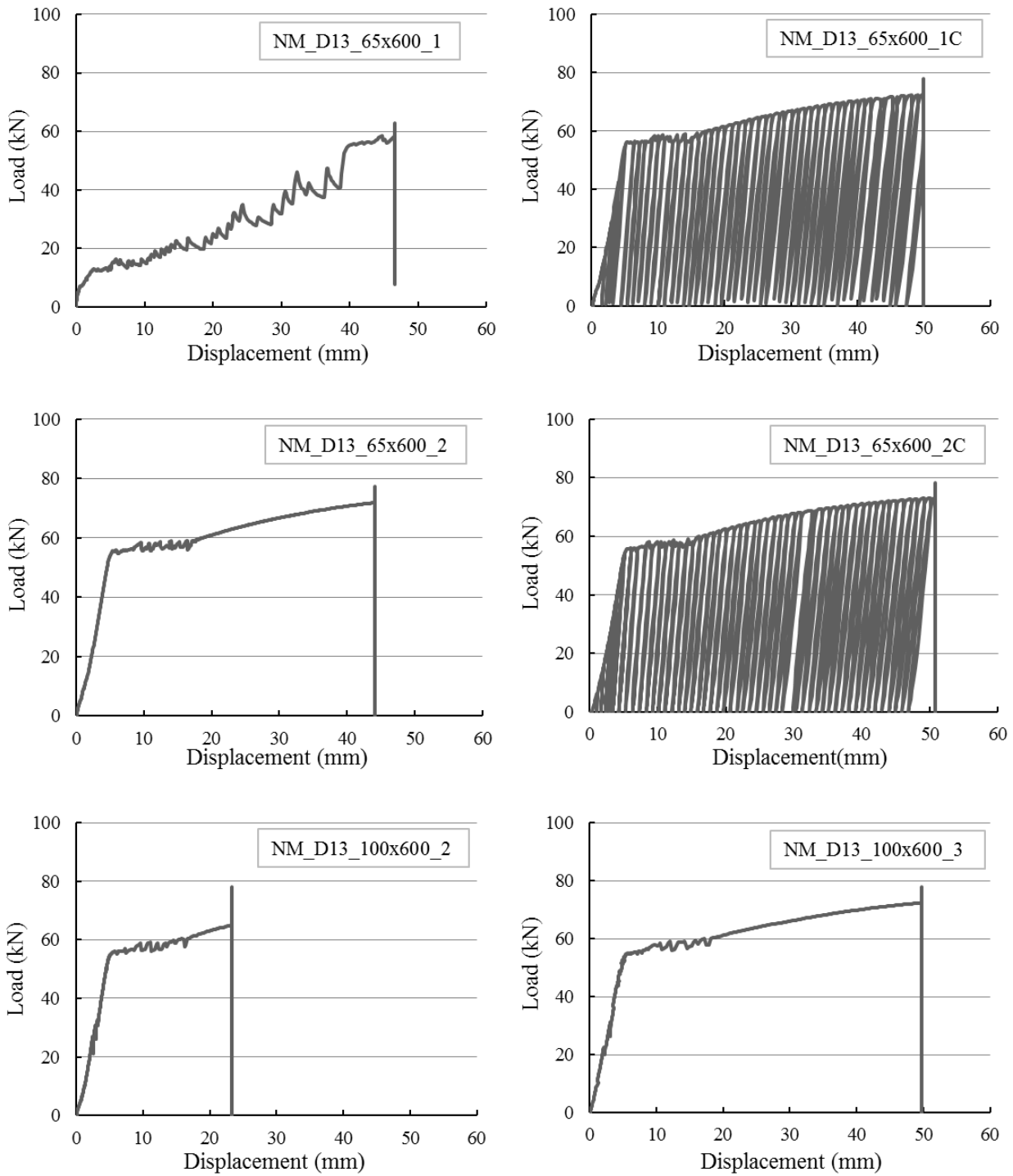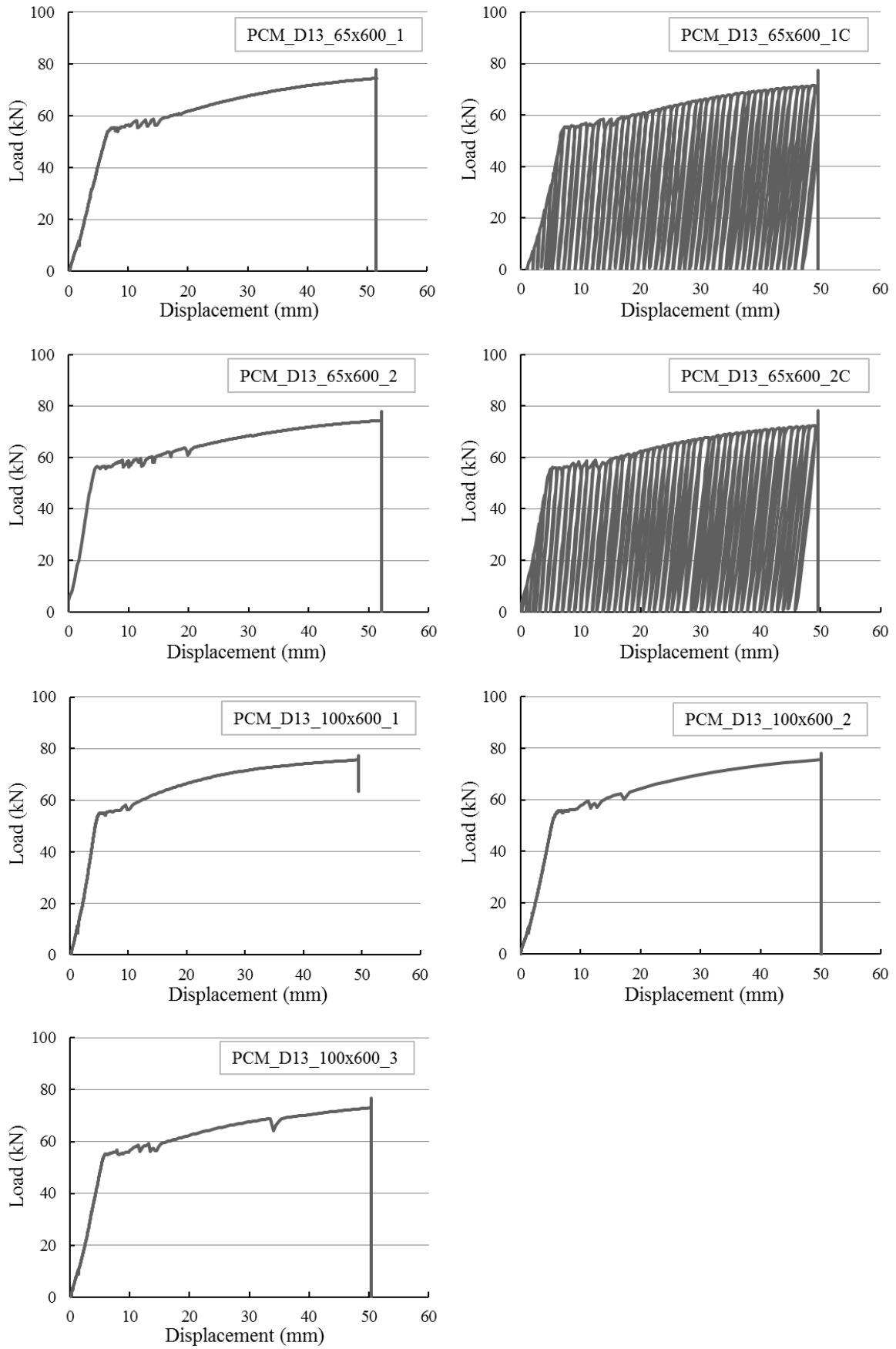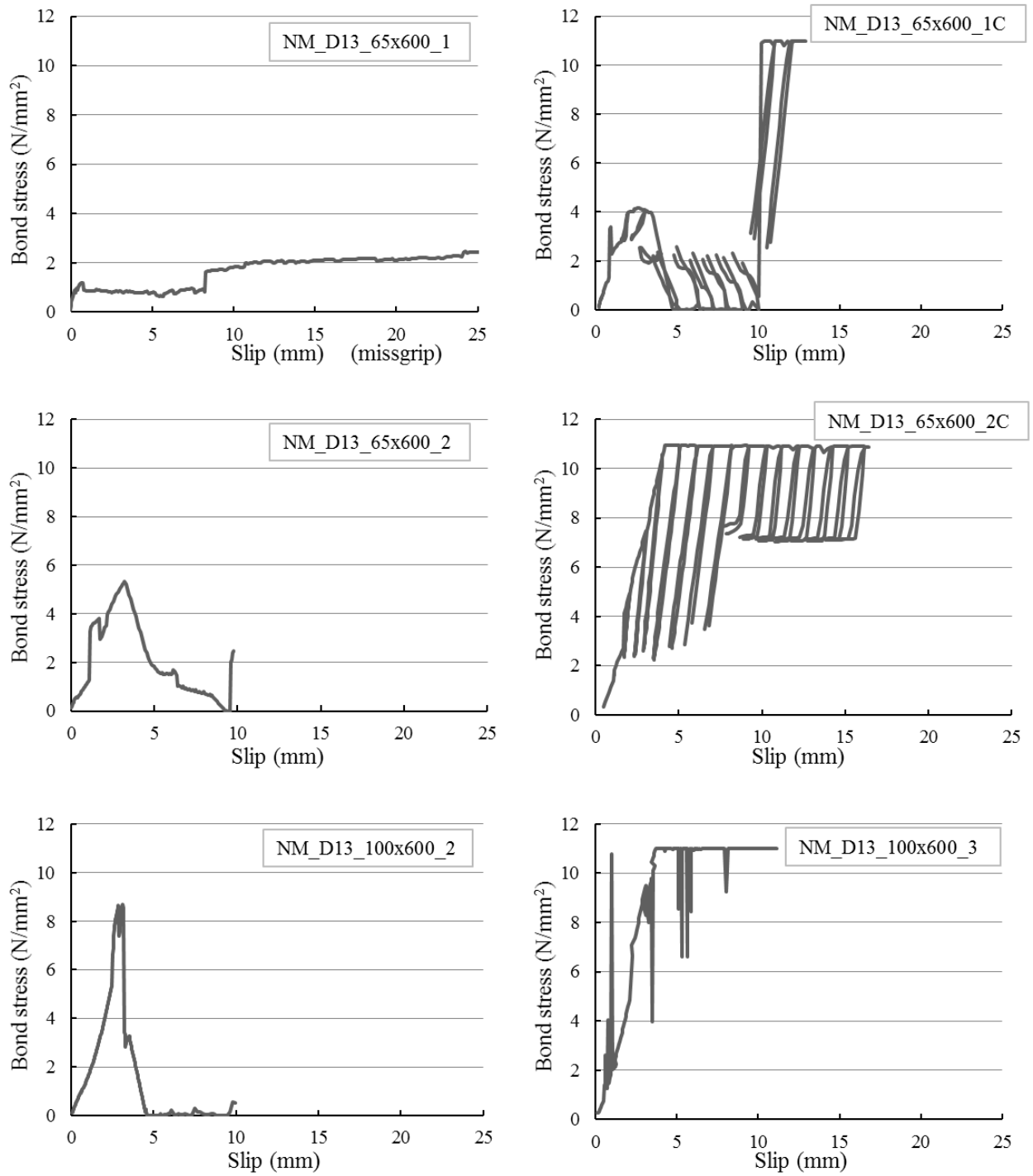
Figure 5.36 Bond stress-slip relationships (NM_D13)

It should be noted that, NM_D13_100x600_1 couldn't be presented in the graph because of measuring error.
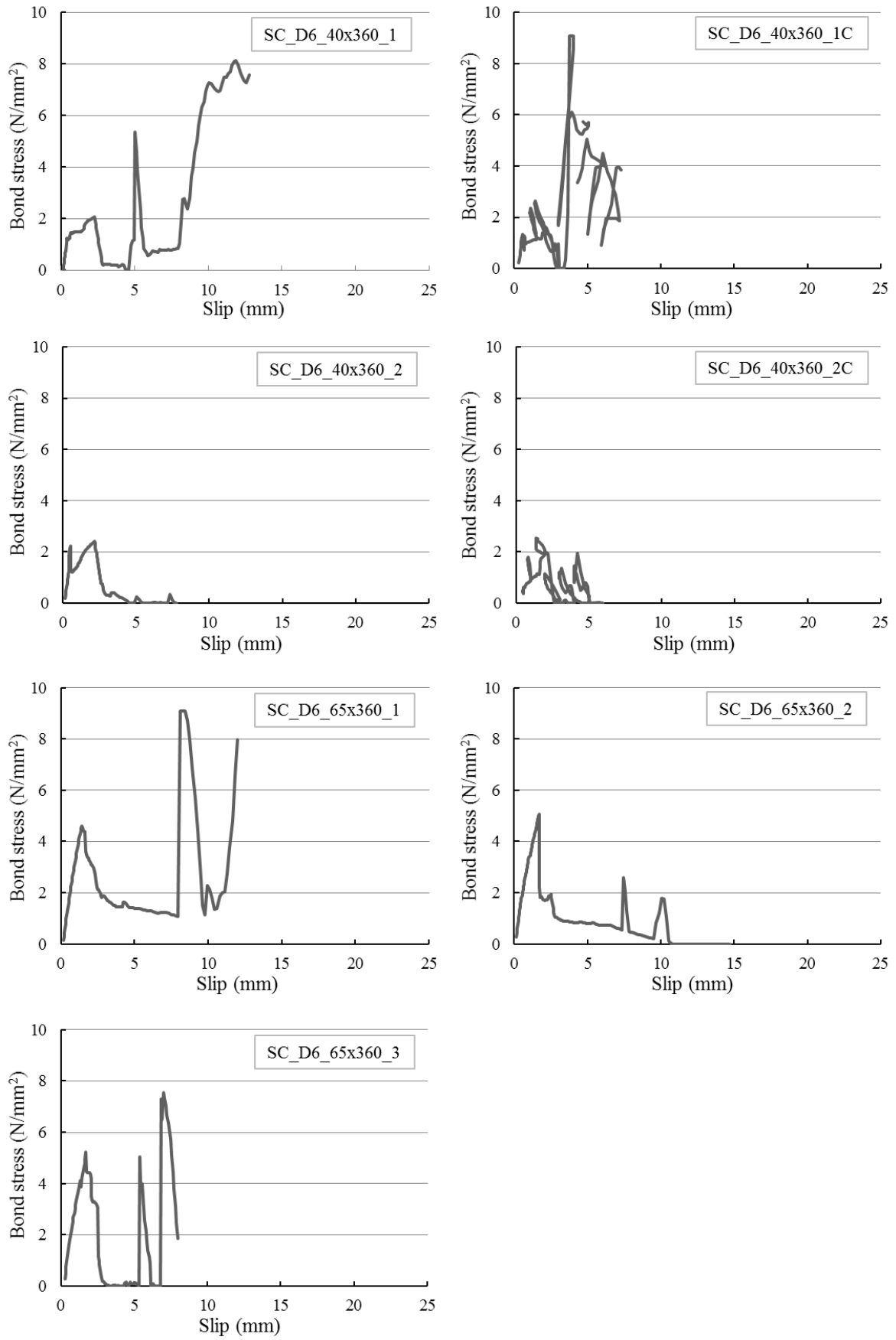
Figure 5.37 Bond stress-slip relationships (SCRCC_D6)
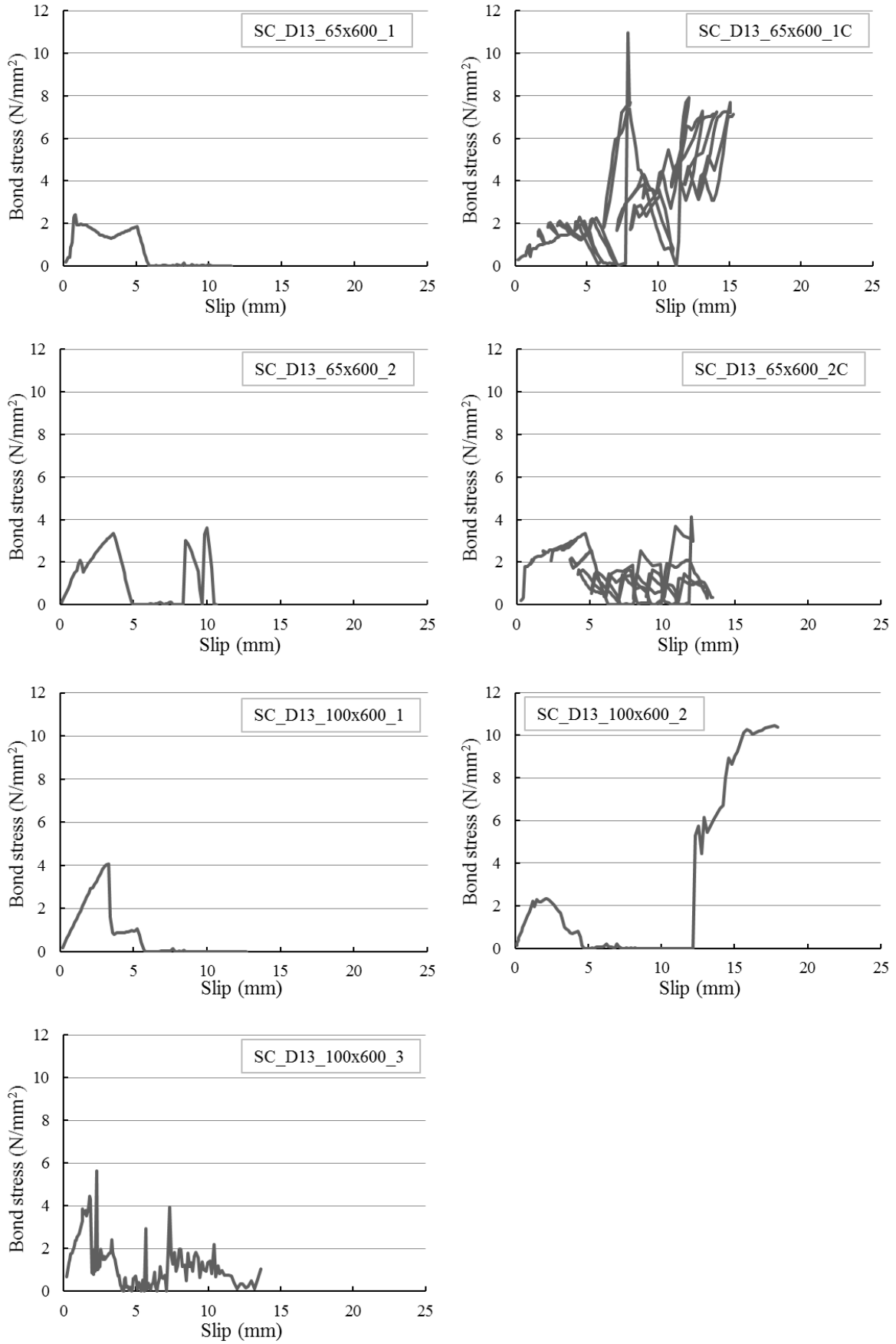
Figure 5.38 Bond stress-slip relationships (SCRCC_D13)
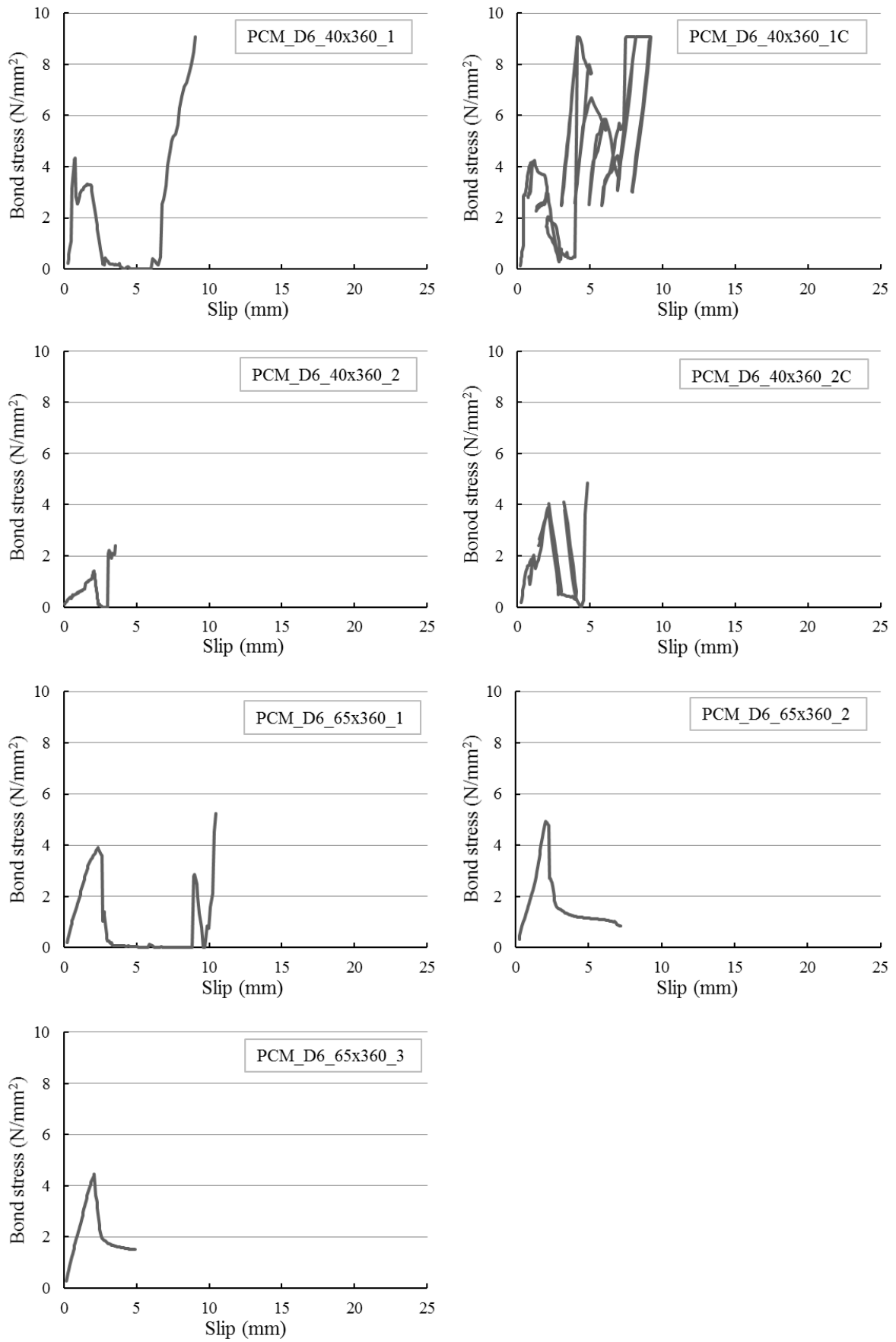
Figure 5.39 Bond stress-slip relationships (PCM_D6)
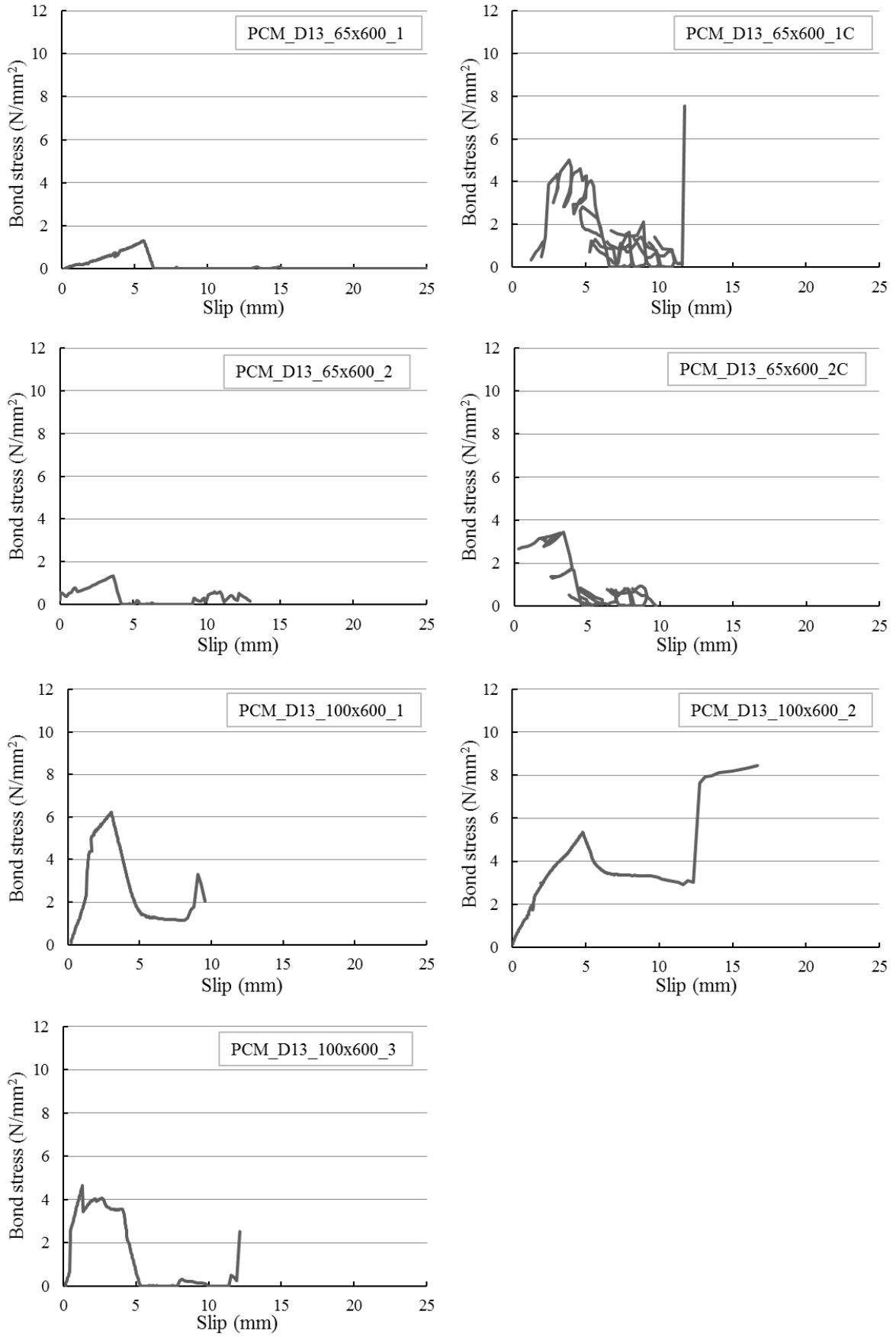
Figure 5.40 Bond stress-slip relationships (PCM_D13)
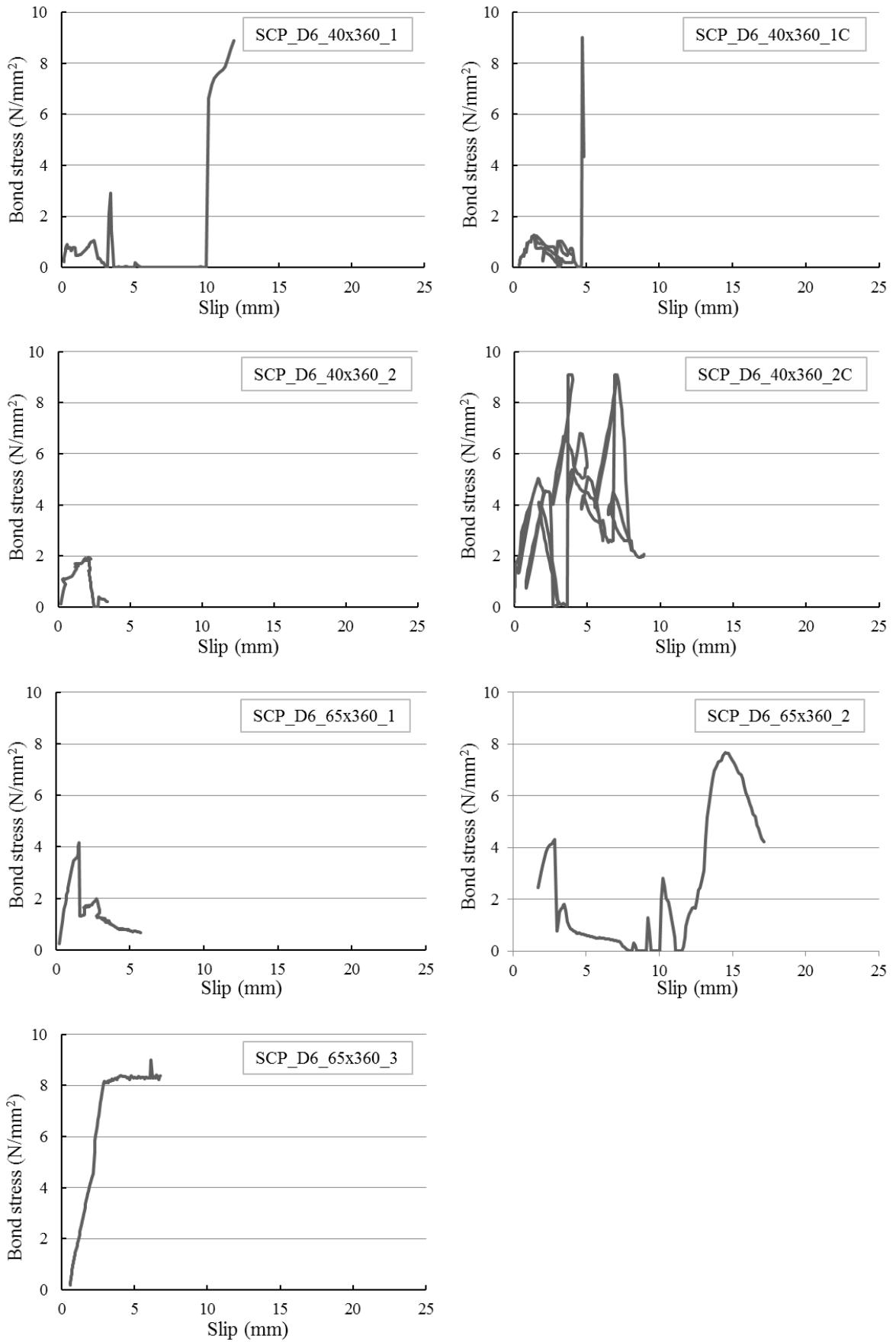
Figure 5.41 Bond stress-slip relationships (SCRPCC_D6)
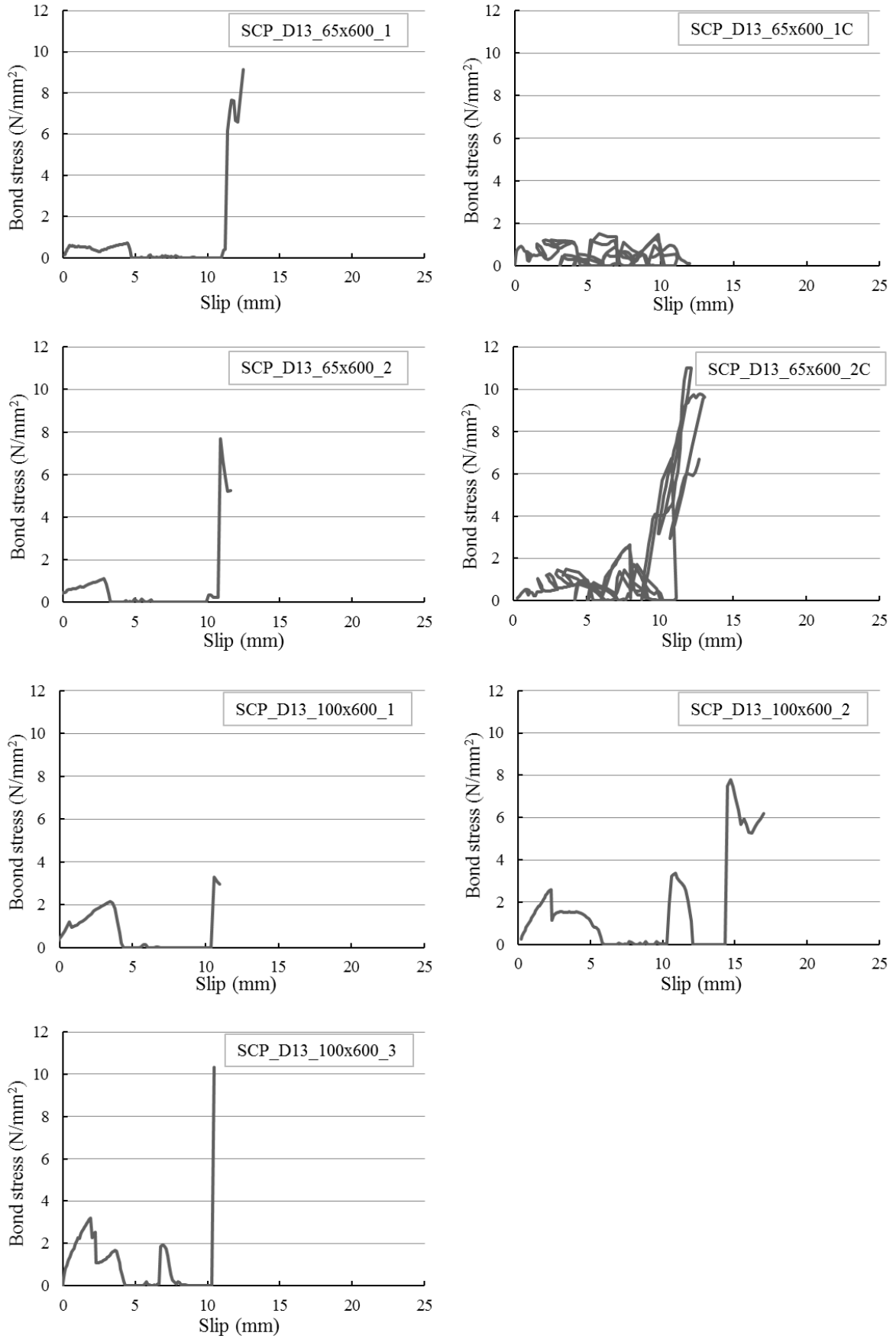
Figure 5.42 Bond stress-slip relationships (SCRPCC_D13)

Maximum bond stress distribution

All specimens were failed by tensile fracture of steel bar. Maximum bond stresses of all the specimens are shown in Figure 5.43. According to the Figure 5.43, maximum bond stress of NM shows a tendency to be higher than that of SCRCC at failure and before yielding of steel bars. And the distribution of PCM is also inclined to be higher than that of SCRPCC before yielding of steel bars.

(A marker means each value, and a line means average of the values .)
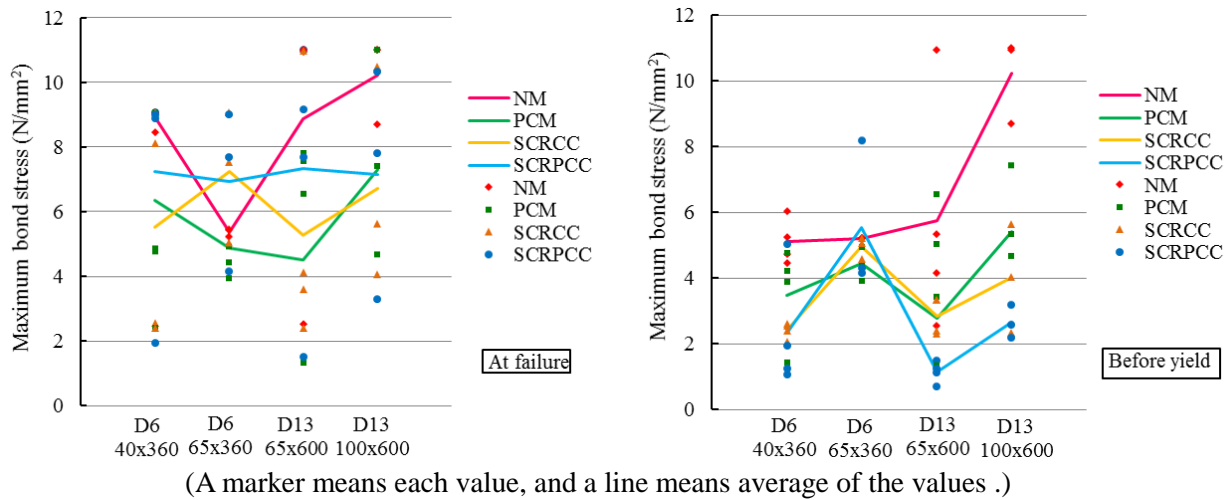
Figure 5.43 Maximum bond stress distribution

Figure 5.44 shows the average crack widths of all the specimens. The average crack widths of NM and PCM tended to decrease by reinforcing with steel chip at failure. In the same diameter of steel bar and length of specimen, the increase of diameter of specimen made the average crack widths increase.

(A marker means each value, and a line means average of the values.)
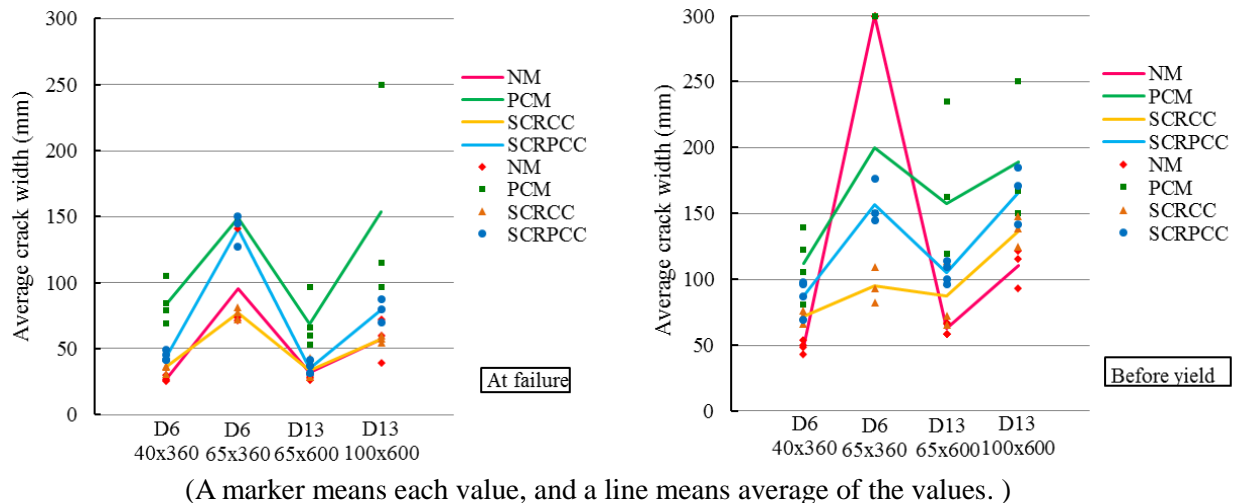
Figure 5.44 Average crack widths

5.3.3 Concluding remarks of uniaxial tension tests

In this section, cracking characteristics and bond behaviors between steel bars and SCRCC or SCRPCC by uniaxial tension test. The following remarks are obtained.

1) Maximum bond stresses before yielding of steel bars of non-reinforced NM and PCM were higher

than that of SCRCC and SCRPCC.

2) Average crack widths at failure of NM and PCM tended to decrease by reinforcing with steel chip.

3) No significant difference was observed between specimens subjected to monotonic and cyclic loading methods.

5.4 Conclusions

In this chapter, the stress-slip relationships between steel bar and steel chip reinforced cementitious composite (SCRCC) and steel chip reinforced polymer cementitious composite (SCRPCC) were investigated by conducting the pull-out tests. Also, uniaxial tension tests were conducted to examine the cracking characteristics of SCRCC and SCRPCC. The following conclusions were obtained from the results.

1) Maximum bond stresses at failure of non-reinforced NM showed a tendency to be higher than that of SCRCC. It was also higher than that of SCRCC before yielding of steel bars.

2) Maximum bond stresses before yielding of steel bars of PCM showed a tendency to be higher than that of SCRPCC.

3) Average crack width of PCM was decreased by reinforcing with steel chip at failure and before yielding of steel bars. And average crack width of NM showed a tendency to be lower than that of SCRCC.

Chapter 6   Creep characteristics of SCRPCC

6.1   Background and objective

In the Chapter 4, it was discussed about drying shrinkage of SCRCC and SCRPCC with restrained wall specimens. And the drying shrinkage behavior seems to be affected by creep influence by restraint stress. Thus it needs to evaluate the influence of creep more accurately for accurate prediction of shrinkage cracking by restraint shrinkage. For this reason, creep tests of SCRCC and SCRPCC were performed to ascertain the creep characteristics.

In this chapter, flexural creep tests of SCRCC and SCRPCC were conducted with varying loading period in order to clarify how the reinforcing with steel chip impacts on the creep behavior.

6.2   Experimental programs

6.2.1 Materials

Cementitious composites were prepared with four different types of binder. Among these binders, normal mortar (NM) and SCRCC contain silica fume and superplasticizer for high strength development, but polymer cement mortar (PCM) and SCRPCC don't contain silica fume and superplasticizer for high durability considering the general use of PCM and an economical efficiency. The mix proportions of cementitious composites used in this study are given in Table 6.1.

For the mix proportions of SCRCC, Ordinary Portland cement and silica fume were used as a binder. River sand of saturated surface dry condition was used as a fine aggregate. And superplasticizer was used to reduce the unit water content of cementitious composites. Steel chip content of 3% by volume were used in this test.

Table 6.1 Mix proportions of cementitious composites

	Normal Mortar (NM)	SCRCC	Polymer Cement Mortar (PCM)	SCRPCC
W/B (%)	23.30	23.30	30.00	30.00
Water (kg/m^3)	222.35	222.35	205.92	205.92
Cement (kg/m^3)	754.40	754.40	686.40	686.40
Fine aggregate (kg/m^3)	1152.35	1044.07	1372.80	1220.08
Silica fume (kg/m^3)	199.90	199.90	0.00	0.00
Polymer (kg/m^3)	0.00	0.00	68.64	68.64
Steel chip (Vol. %)	0.00	3.00	0.00	3.00
Antifoaming Agent (kg/m^3)	0.00	0.00	0.69	0.69
Chemical admixture (kg/m^3)	20.79	20.79	0.00	0.00

For the mix proportions of SCRPCC, Ordinary Portland cement was used. And ethylene vinyl acetate emulsion was used as a polymeric admixture. This is a fluid milk-white solution with a solid content of 45% and the density $1.07g/cm^3$. River sand of saturated surface dry condition was used as a fine aggregate. Steel chip content of 3% by volume was used in this test.

6.2.2 Specimens

Specimens for the creep tests were made into beam specimens of size $100 \times 100 \times 500$ mm. The specimens were demolded after 3 days. And then, all the specimens were notched to a depth of 20 mm and width of 5 mm with an electric cutting machine. Three specimens were prepared with four types of cementitious composites for each test. Two specimens of them were used for flexural creep test, the other specimen was cured without loading and its strain was measured for comparison. All the specimens were subjected to a constant temperature and humidity condition of 20℃ and =60%R.H.

6.2.3 Test procedures

The specimens are listed in Table 6.2. Three types of loading were conducted on the creep specimens in a 42-day cycle. The first type of loading was that when a load was applied for 28 days after which creep was observed for 14 days. The second type of loading was that when a load was applied for 14 days after which creep was observed for 28 days. The third type of loading was that when a load was applied for 7 days after which creep was observed for 35 days. Loading was applied to only two of the three specimens. And the third was compared to the other two. One of the third term NM specimens couldn't bear the loading on 7-day, and was broken. Because NM specimens didn't develop enough strength to bear the loading. So third term NM specimen was loaded on 21-day.

In the fourth term, not notched specimens were prepared to examine the impact of whether the specimens were notched or not (PCM, SCRPCC).

The loading conditions consisted of a 48-kg steel block hanging from the end of a loading arm, so three-point loading was applied to each specimen, as shown in Figure 6.1.

The load and flexural stress of the center part of each specimen were respectively 2.97 kN, and 2.78 N/mm² for NM and SCRCC, 1.77 N/mm² and 1.66 N/mm² for PCM and SCRPCC. The creep test was conducted under a constant temperature and humidity (20 ℃, 60% R.H.).
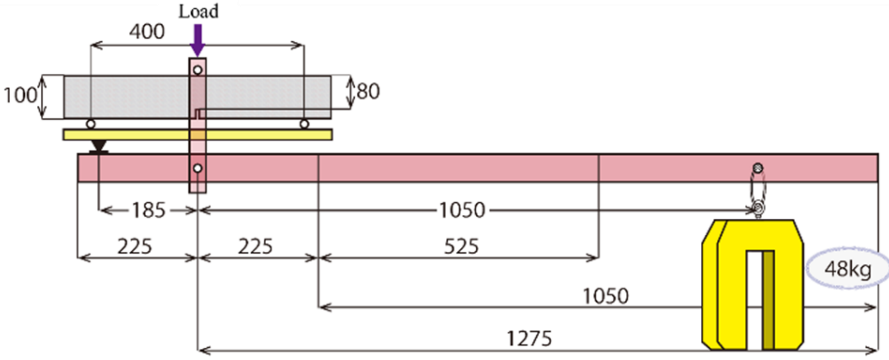
Figure 6.1 Creep test

Table 6.2 Creep test

Initial loading day	Cementitious composite	Specimen	Load (kN)	Tensile stress (N/mm²)
Day 28 (First term)	NM	1NM-1	-	-
		1NM-2	2.97	2.78
		1NM-3	2.97	2.78
	SCRCC (SC)	1SC-1	-	-
		1SC-2	2.97	2.78
		1SC-3	2.96	2.78
	PCM	1PC-1	-	-
		1PC-2	1.77	1.66
		1PC-3	1.75	1.64
	SCRPCC (SCP)	1SCP-1	-	-
		1SCP-2	1.77	1.66
		1SCP-3	1.73	1.62
Day 14 (Second term)	NM	2NM-1	-	-
		2NM-2	2.97	2.78
		2NM-3	2.97	2.78
	SCRCC (SC)	2SC-1	-	-
		2SC-2	2.97	2.78
		2SC-3	2.96	2.78
	PCM	2PC-1	-	-
		2PC-2	1.77	1.66
		2PC-3	1.75	1.64
	SCRPCC (SCP)	2SCP-1	-	-
		2SCP-2	1.77	1.66
		2SCP-3	1.73	1.62
Day 7 (Third term)	NM	3NM-1	-	-
		3NM-2	2.97	2.21
	SCRCC (SC)	3SC-1	-	-
		3SC-2	2.97	2.78
		3SC-3	2.96	2.78
	PCM	3PC-1	-	-
		3PC-2	1.77	1.66
		3PC-3	1.75	1.64
	SCRPCC (SCP)	3SCP-1	-	-
		3SCP-2	1.77	1.62
		3SCP-3	1.73	1.66
Day 14 (Fourth term)	PCM	4PC-1	-	-
		4PC-2	1.77	1.06
		4PC-3	1.75	1.05
	SCRPCC (SCP)	4SCP-1	-	-
		4SCP-2	1.77	1.06
		4SCP-3	1.73	1.05

As shown in Figure 6.2, the measuring point of 100 mm was fixed on the center of the top and bottom of each specimen, and the change in the length was measured with a contact gauge. The state of measurement is shown in Photo 6.1. Finally, the creep strain could be obtained by deducting the drying shrinkage strain of a specimen with no loading from the strain of a specimen with loading.
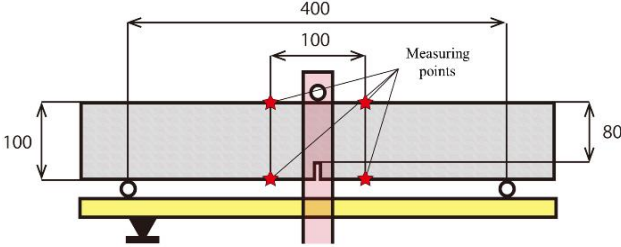
Figure 6.2 Measuring points of creep specimen

Photo 6.1 Strain measurement with a contact gauge

Also, the strain was calculated by following formula.

$$\varepsilon = \frac{\left[(100 + X_n - 0.5) \times \frac{100 + A_n - 0.5}{100}\right] - \left[(100 + X_3 - 0.5) \times \frac{100 + A_3 - 0.5}{100}\right]}{100}$$

ε : Strain

X_3 : Distance between measuring points of a specimen on 3-day (mm)

A_3 : Distance between measuring points of standard bar on 3-day (mm)

X_n : Distance between measuring points of a specimen on n-day (mm)

A_n : Distance between measuring points of standard bar on n-day (mm)

6.3.1 Steel Chip Reinforced Cementitious Composites

Test results of first term

Strain-drying period relationships of first term (shrinkage + creep) are shown in Figure6.3. In the name of specimen, C and T means flexural compressive and tensile (upper and lower of specimen). Strain of NM showed a tendency to decrease by reinforcing with steel chip except for 1SC-3 specimen.
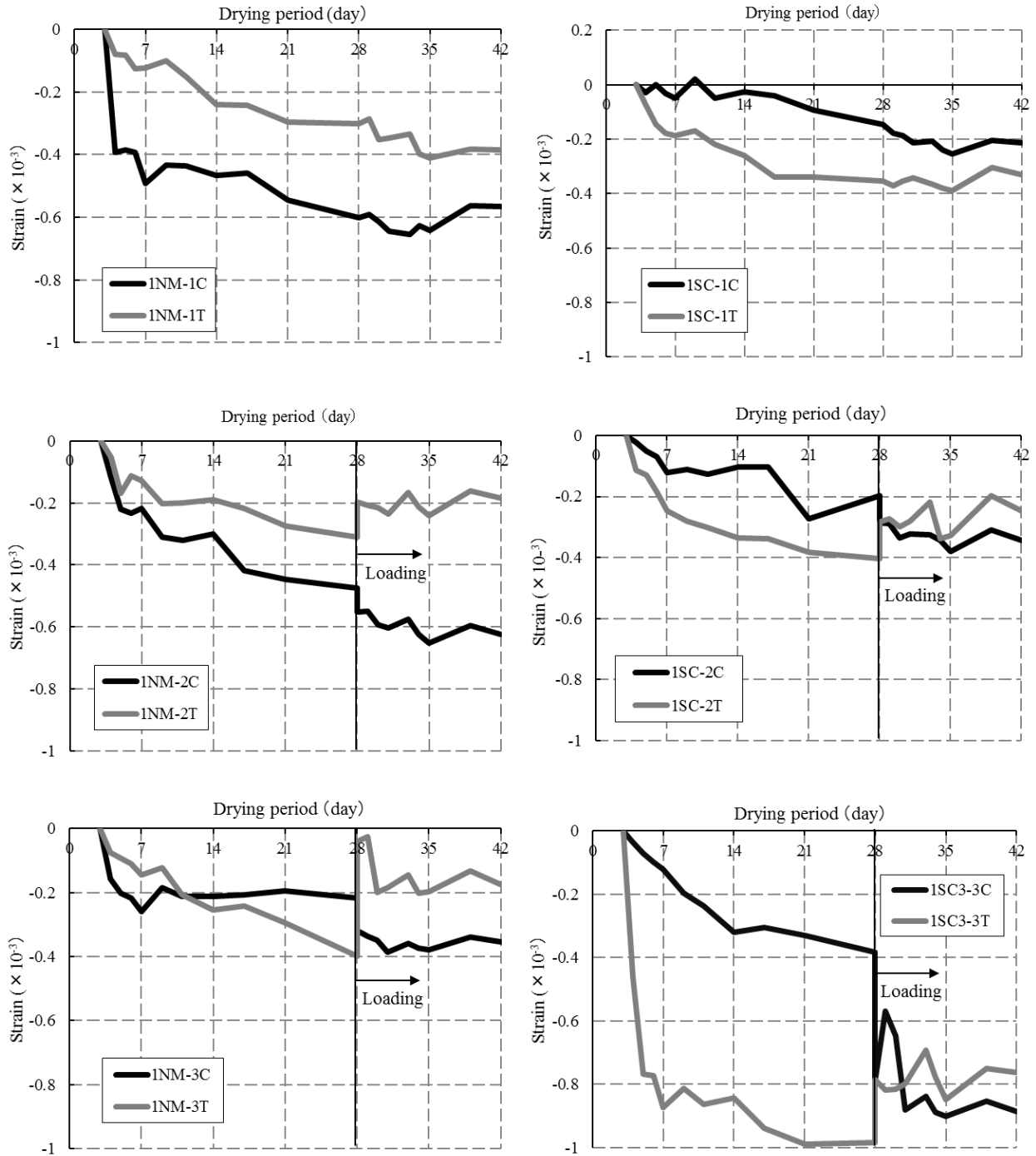
Figure 6.3 Strain-drying period relationships (SCRCC, First term)

Creep strain produced by sustained loading was calculated by following equation.

$$\varepsilon_{creep} = (X_n - X_a) - (Y_n - Y_a) \qquad \qquad Eq\ (6.1)$$

X_n: n-day strain of loaded specimen

X_a: Strain before loading of loaded specimen

Y_n: Average of n-day upper and lower strain of same type of specimen No.1 as X

Y_a: Average of loading day upper and lower strain of same type of specimen No.1 as X

Creep strains produced by loading (first term) are shown in Figure 6.4. In the name of specimen, C and T means flexural compressive and tensile (upper and lower of specimen).

Figure 6.4 Creep strain-time under load relationships (SCRCC, First term)

Creep coefficient was calculated by following equation.

$$\Phi = \frac{\varepsilon_{n\ creep}}{Z_{a2} - Z_{a1}} - 1$$

$\varepsilon_{n\ creep}$: n-day creep strain

Z_{a1}: Loading day strain of right before loading

Z_{a2}: Loading day strain of right after loading

Creep coefficient of first term are shown in figure 6.5. In the name of specimen, C and T means flexural compressive and tensile (upper and lower of specimen).

Figure 6.5 Creep coefficient-time under load relationships (SCRCC, First term)

Test results of second term

Strain-drying period relationships of second term (shrinkage + creep) are shown in Figure6.6. In the name of specimen, C and T means flexural compressive and tensile (upper and lower of specimen). Strain of NM showed a tendency to decrease by reinforcing with steel chip except for 2SC-2 specimen.

Figure 6.6 Strain-drying period relationships (SCRCC, Second term)

Creep strains produced by loading (second term) are shown in Figure 6.7. In the name of specimen, C and T means flexural compressive and tensile (upper and lower of specimen).

Figure 6.7 Creep strain-drying period relationships (SCRCC, Second term)

Creep coefficients of second term are shown in figure 6.8. In the name of specimen, C and T means flexural compressive and tensile (upper and lower of specimen).

Figure 6.8 Creep coefficient-time under load relationships (SCRCC, Second term)

Test results of third term

Strain-drying period relationships of third term (shrinkage + creep) are shown in Figure6.9. In the name of specimen, C and T means flexural compressive and tensile (upper and lower of specimen).

Figure 6.9 Strain-drying period relationships (SCRCC, Third term)

Creep strains produced by loading (third term) are shown in Figure 6.10. In the name of specimen, C and T means flexural compressive and tensile (upper and lower of specimen).

Figure 6.10 Creep strain-drying period relationships (SCRCC, Third term)

Creep coefficients of third term are shown in figure 6.11. In the name of specimen, C and T means flexural compressive and tensile (upper and lower of specimen).

Figure 6.11 Creep coefficient-time under load relationships (SCRCC, Third term)

6.3.2 Steel Chip Reinforced Polymer Cementitious Composites

Test results of SCRPCC are as in the following.

Test results of first term

Strain-drying period relationships of first term (shrinkage + creep) are shown in Figure 6.12. In the name of specimen, C and T means flexural compressive and tensile (upper and lower of specimen). In the first term, strain of PCM and SCP was increased with drying period. However, the increment of stain of PCM was reduced by reinforcing with steel chip.

Figure 6.12 Strain-drying period relationships (SCRPCC, First term)

Creep strains produced by loading (first term) are shown in Figure 6.13. In the name of specimen, C and T means flexural compressive and tensile (upper and lower of specimen).
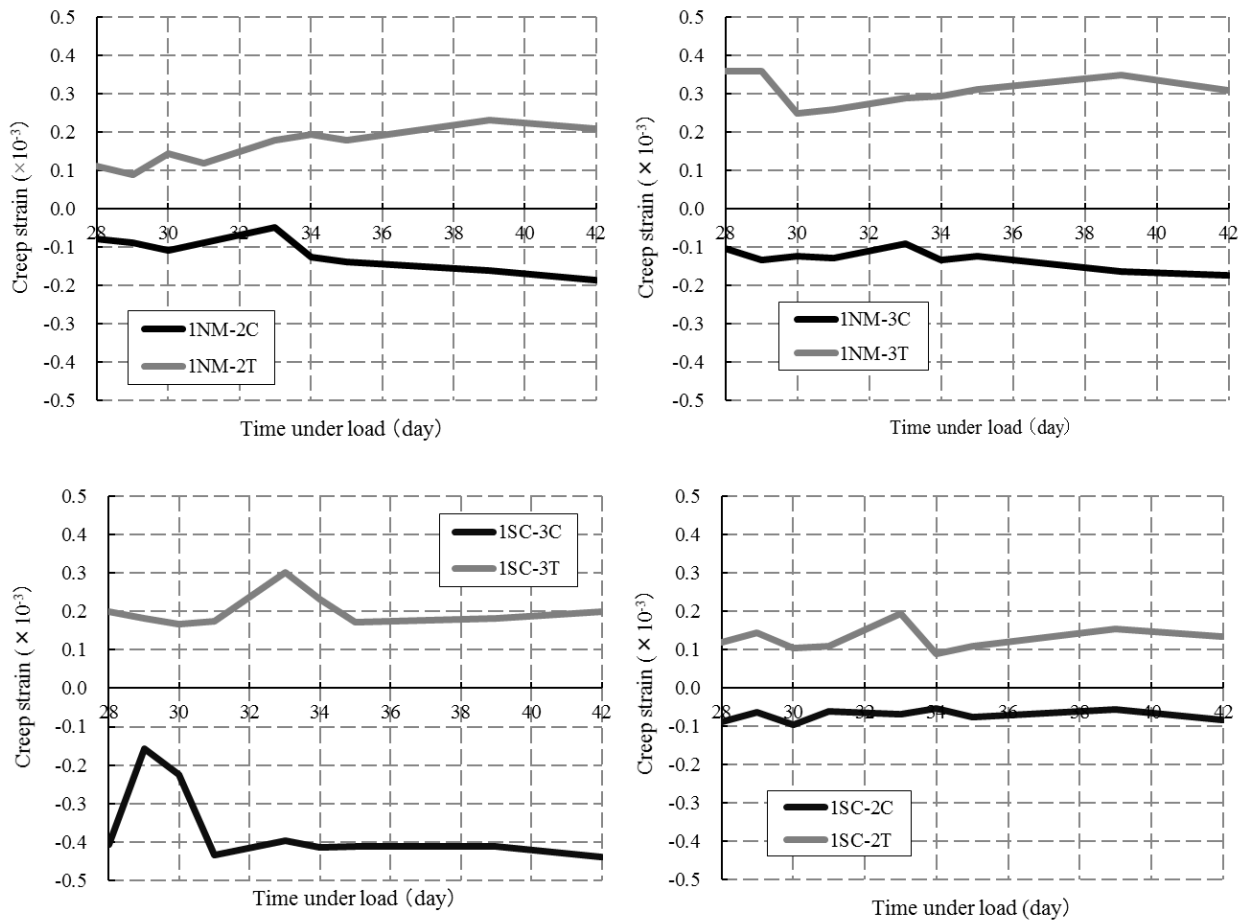

Figure 6.13 Creep strain-drying period relationships (SCRPCC, First term)

Creep coefficients of first term are shown in figure 6.14. In the name of specimen, C and T means flexural compressive and tensile (upper and lower of specimen).
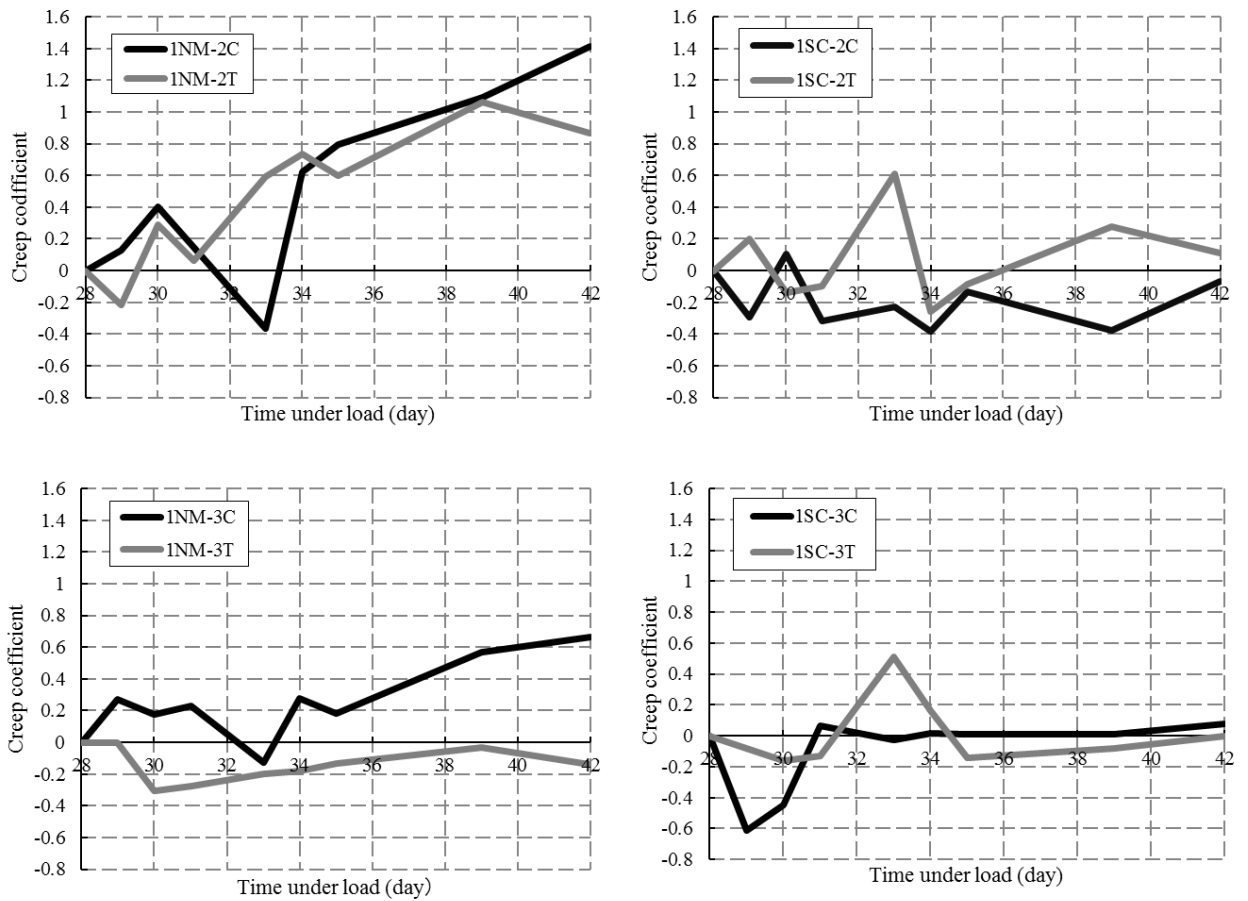

Figure 6.14 Creep coefficient-drying period relationships (SCRPCC, First term)

Test results of second term

Strain-drying period relationships of second term (shrinkage + creep) are shown in Figure 6.15. In the name of specimen, C and T means flexural compressive and tensile (upper and lower of specimen).
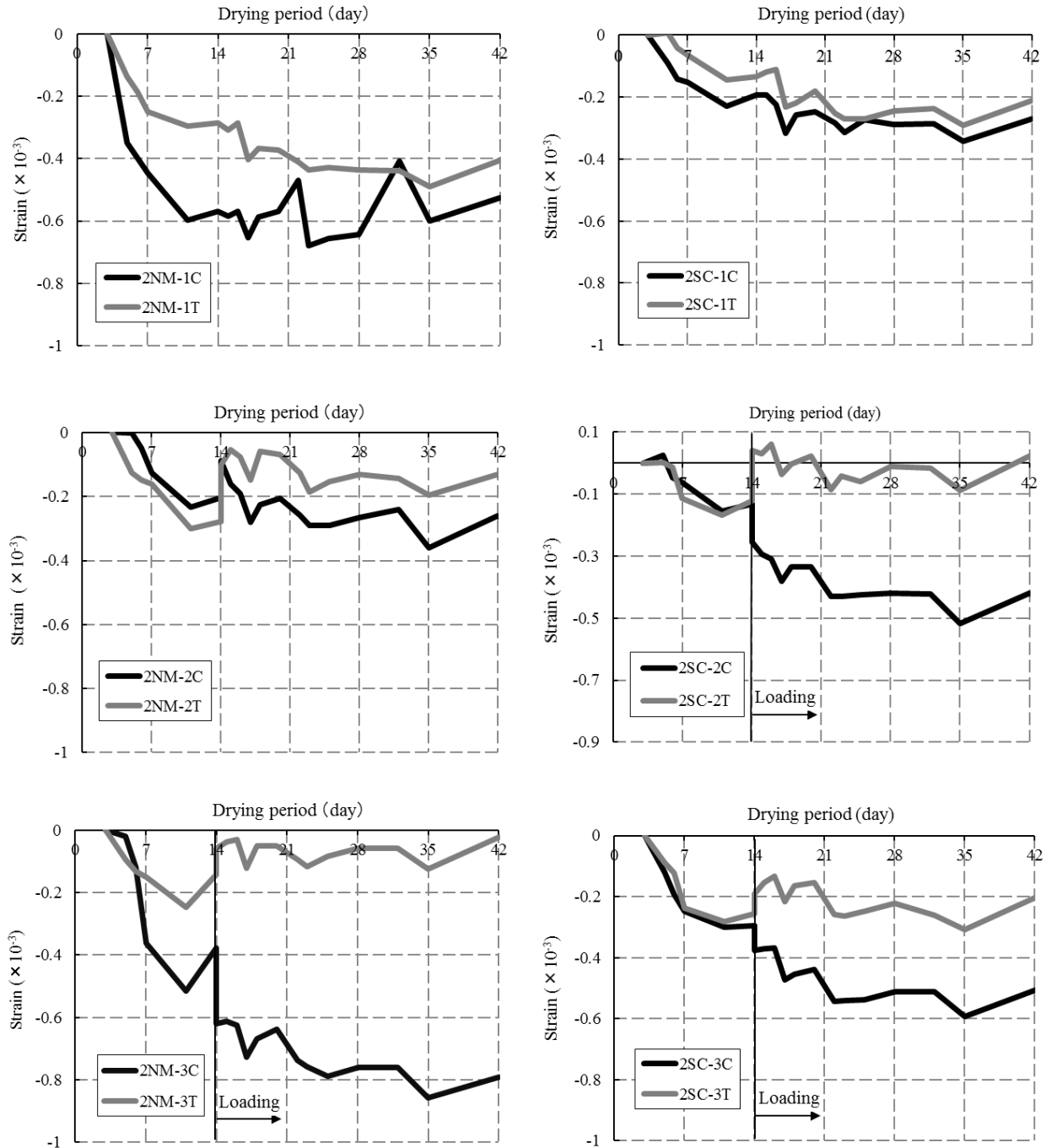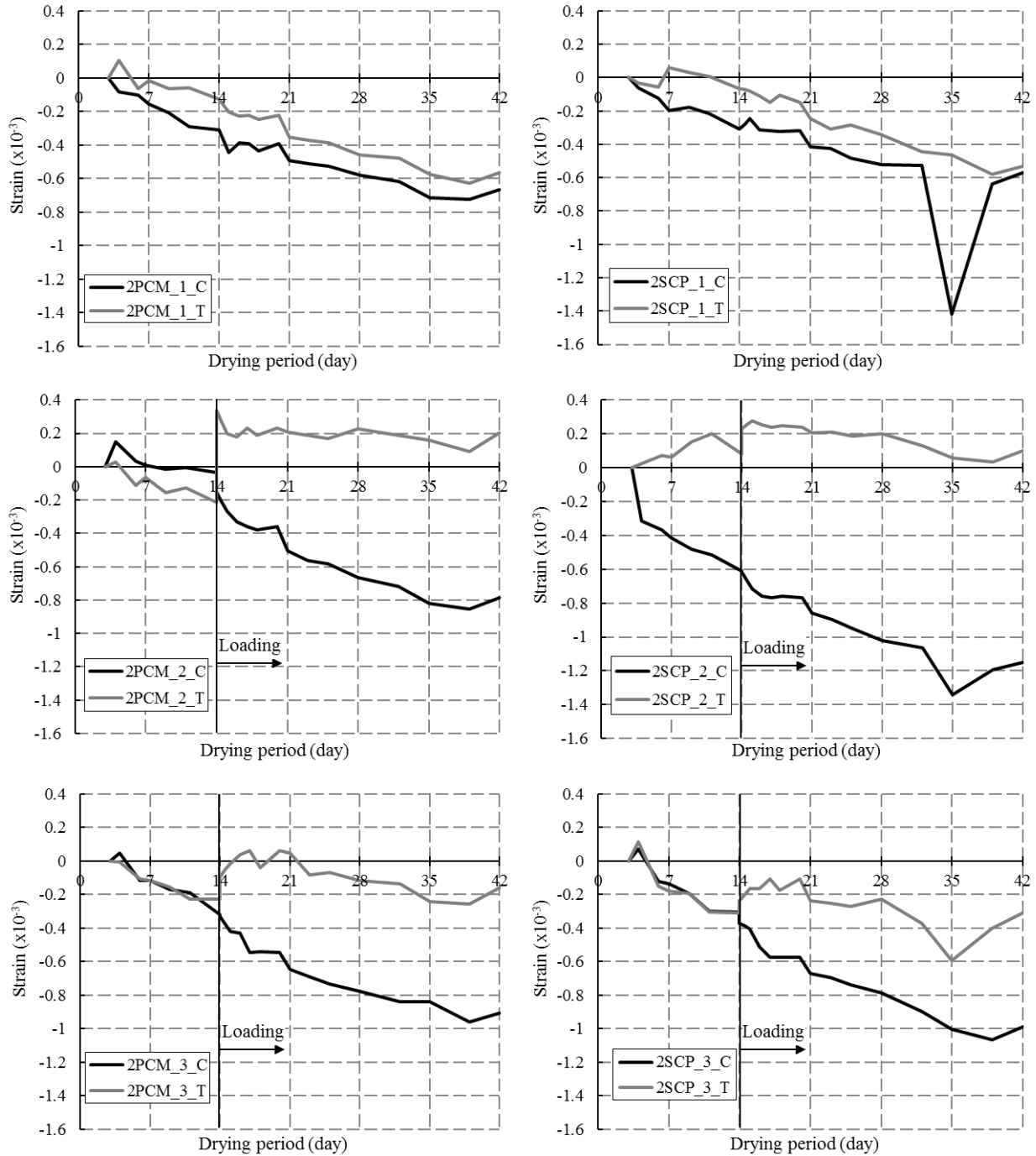

Figure 6.15 Strain-drying period relationships (SCRPCC, Second term)

Creep strains produced by loading (second term) are shown in Figure 6.16. In the name of specimen, C and T means flexural compressive and tensile (upper and lower of specimen).
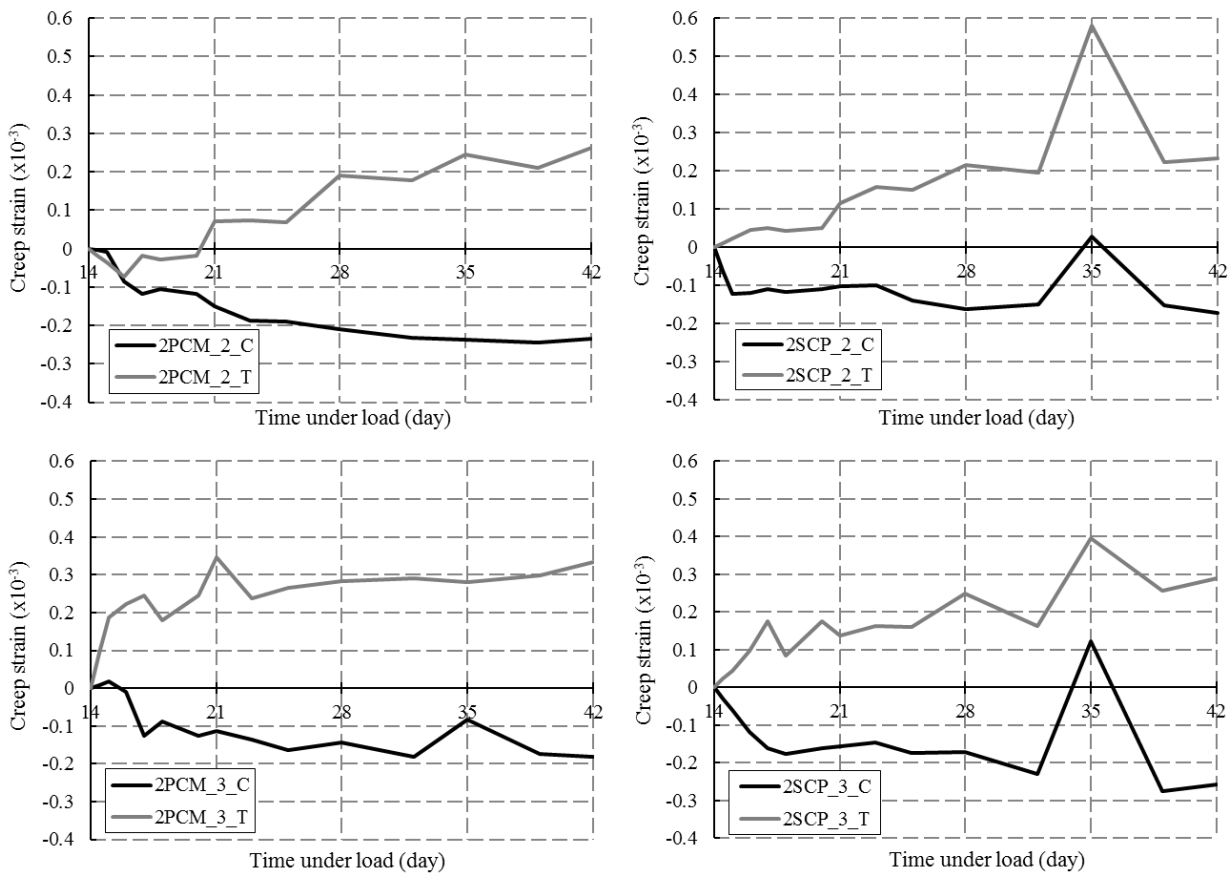
Figure 6.16 Creep strain-drying period relationships (SCRPCC, First term)

Creep coefficients of second term are shown in figure 6.17. In the name of specimen, C and T means flexural compressive and tensile (upper and lower of specimen).
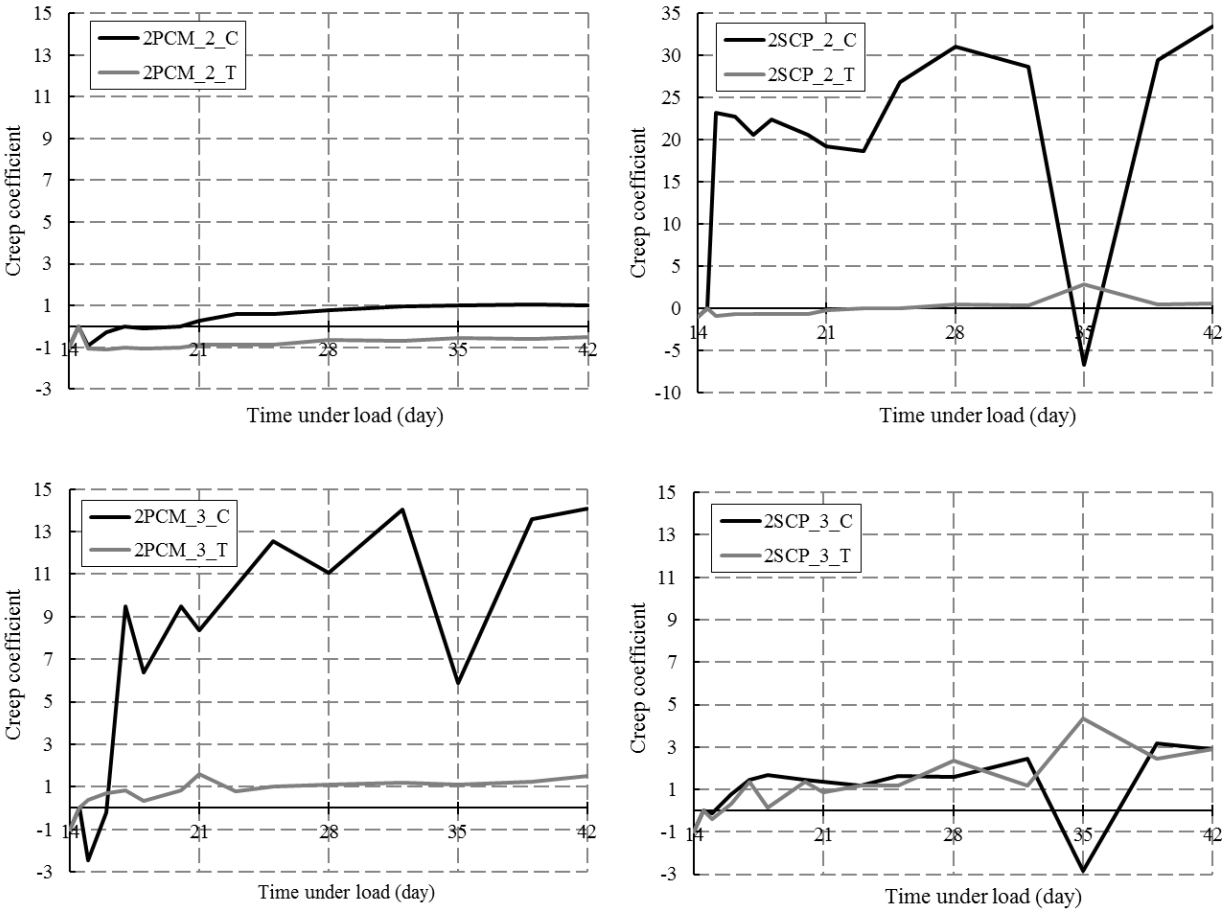
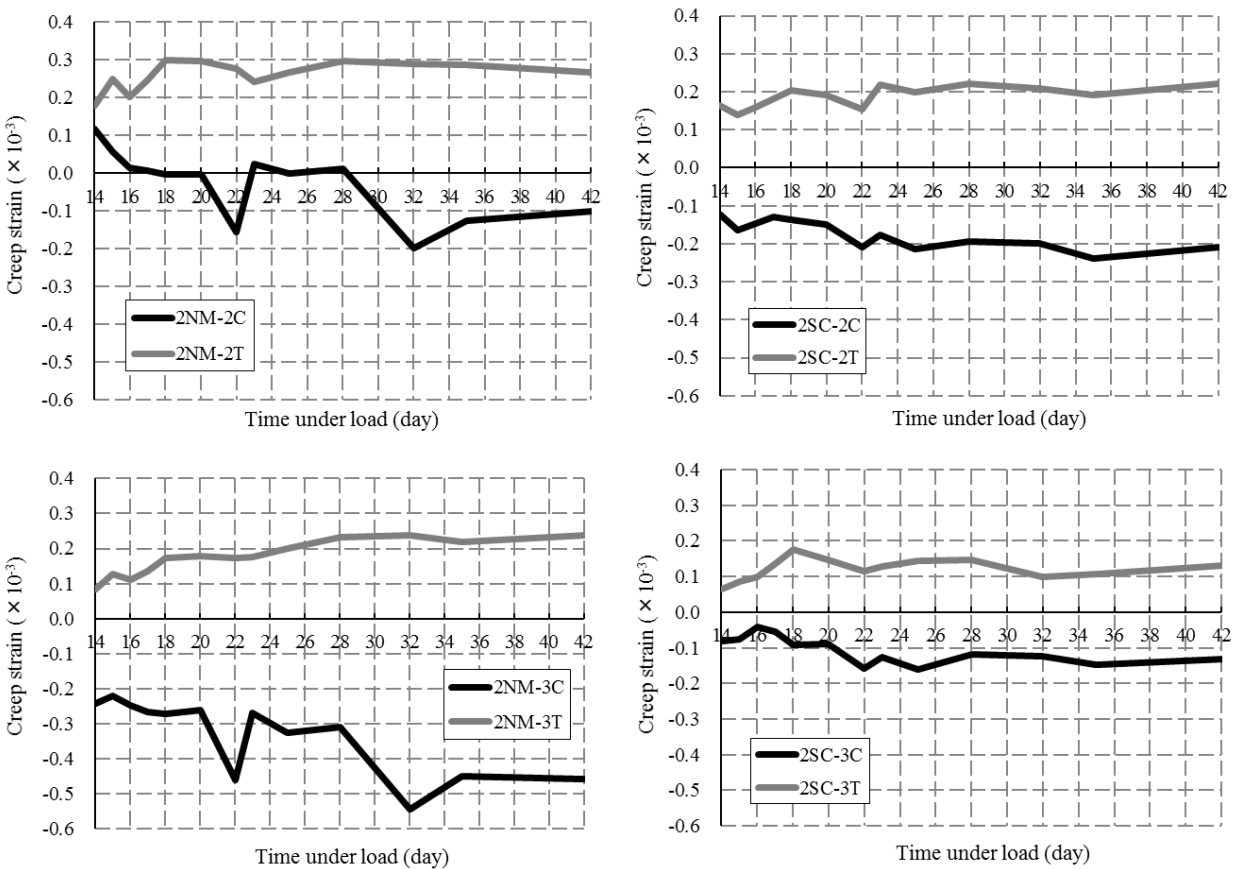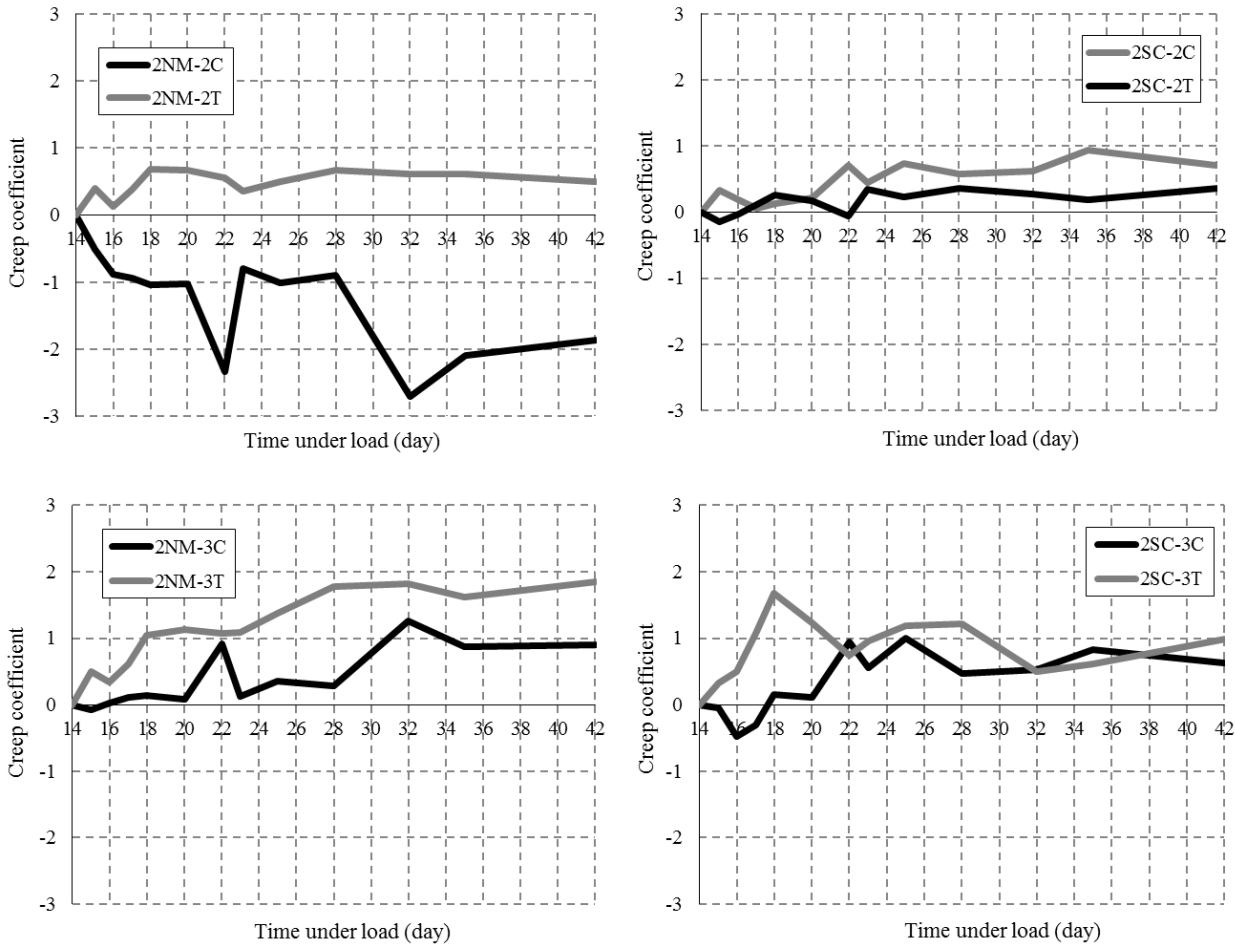Figure 6.17 Creep coefficient-drying period relationships (SCRPCC, First term)

Test results of third term

Strain-drying period relationships of third term (shrinkage + creep) are shown in Figure 6.18. In the name of specimen, C and T means flexural compressive and tensile (upper and lower of specimen). In the third term, strain of PCM and SCP was increased with drying period. However, the increment of stain of SCP was smaller than that of PCM because of reinforcing effect by steel chip.
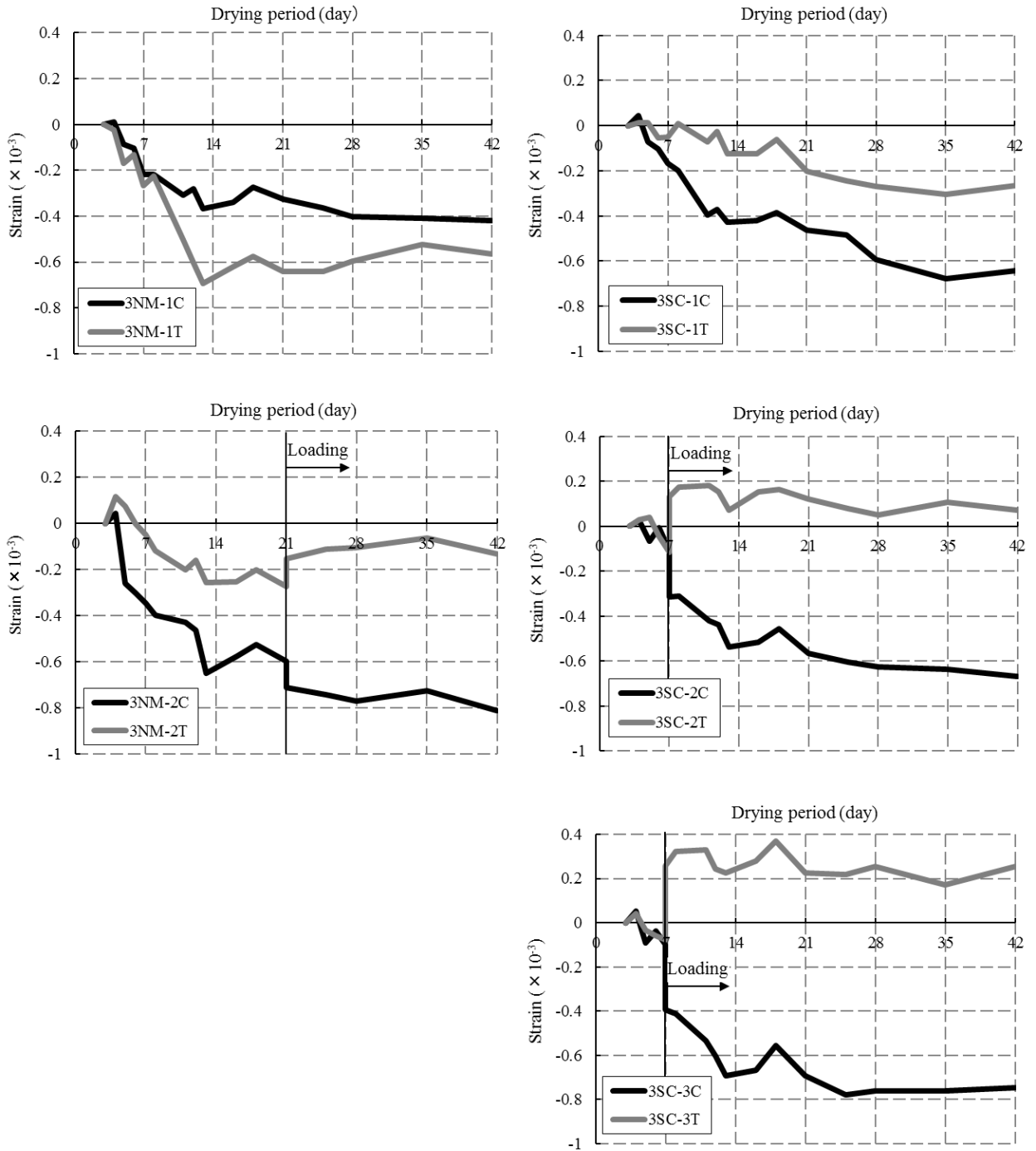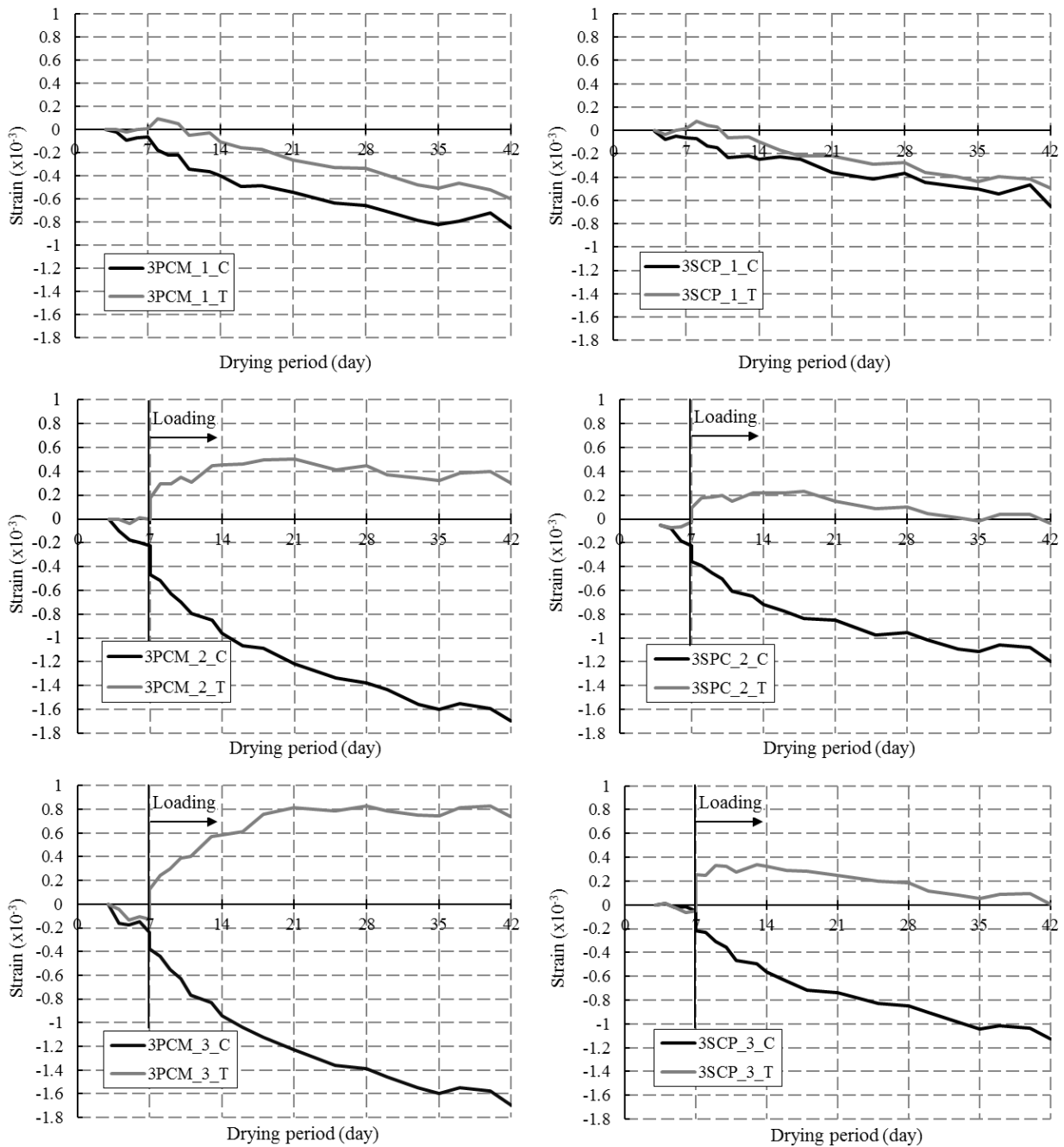

Figure 6.18 Strain-drying period relationships (SCRPCC, Third term)

Creep strains produced by loading (third term) are shown in Figure 6.19. In the name of specimen, C and T means flexural compressive and tensile (upper and lower of specimen). The increment of creep strain of SCP was also smaller than that of PCM.
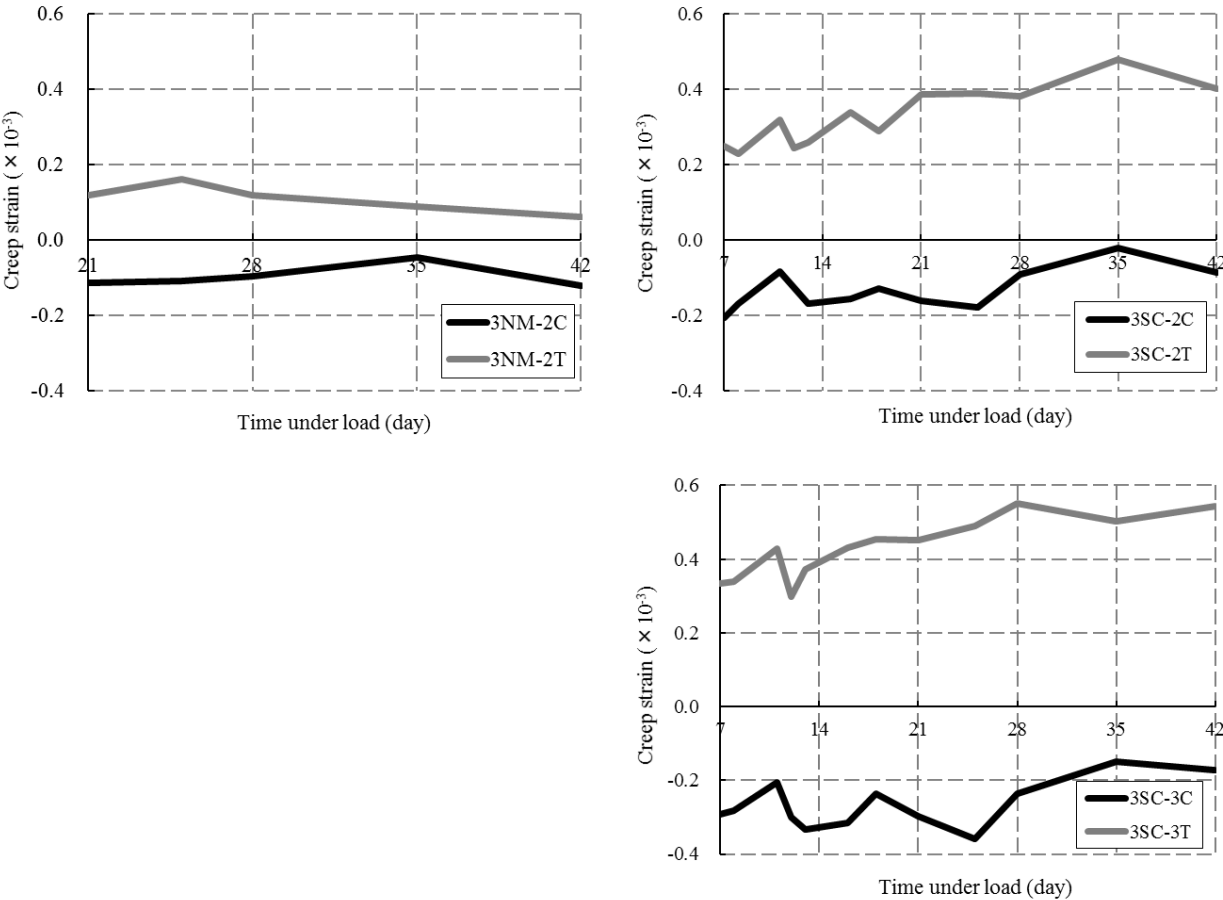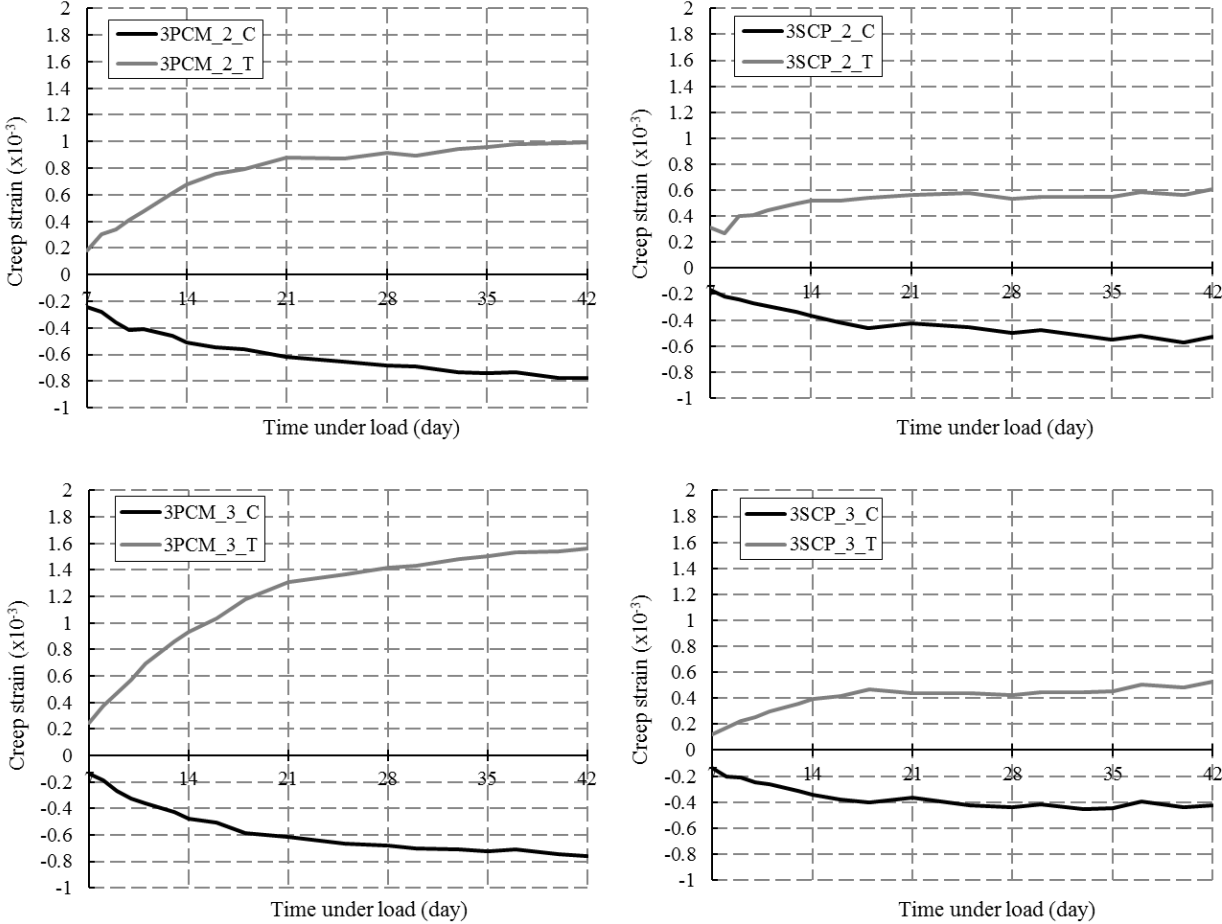
Figure 6.19 Creep strain-drying period relationships (SCRPCC, Third term)

Creep coefficients of third term are shown in figure 6.20. In the name of specimen, C and T means flexural compressive and tensile (upper and lower of specimen).
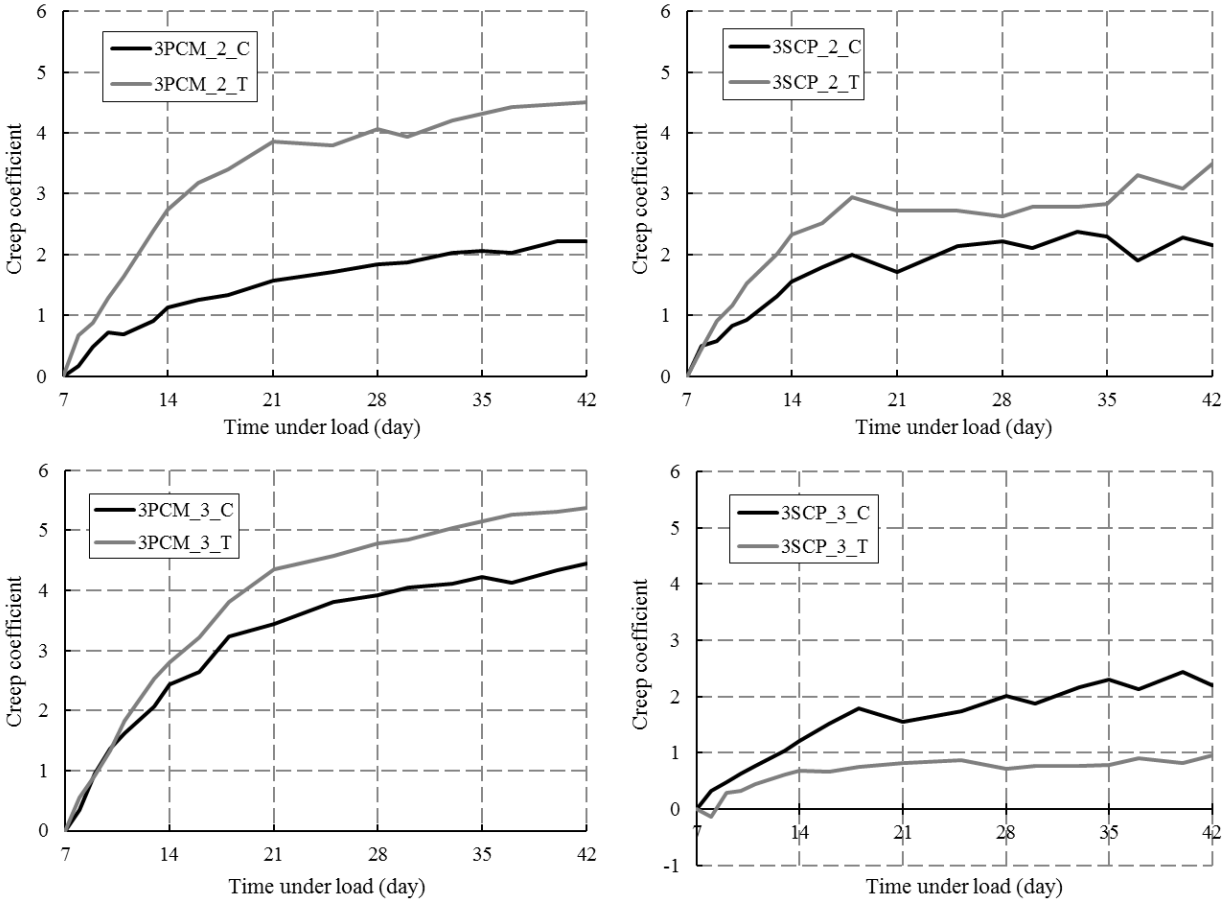
Figure 6.20 Creep coefficient-drying period relationships (SCRPCC, Third term)

Test results of fourth term

Strain-drying period relationships of fourth term (shrinkage + creep) are shown in Figure 6.21. In the name of specimen, C and T means flexural compressive and tensile (upper and lower of specimen).

In the fourth term, strain of PCM and SCP was increased with drying period. However, the strain of PCM showed a tendency to decrease by reinforcing with steel chip except for 4SCP-2 specimen. The change of strains was small compare with change of strains of other terms. The reason for this is considered that stresses were not concentrated in the middle of specimen. Also, the drying shrinkage of upper and lower sides were almost same because these specimens were not notched. (4PCM_1, 4SCP_1)
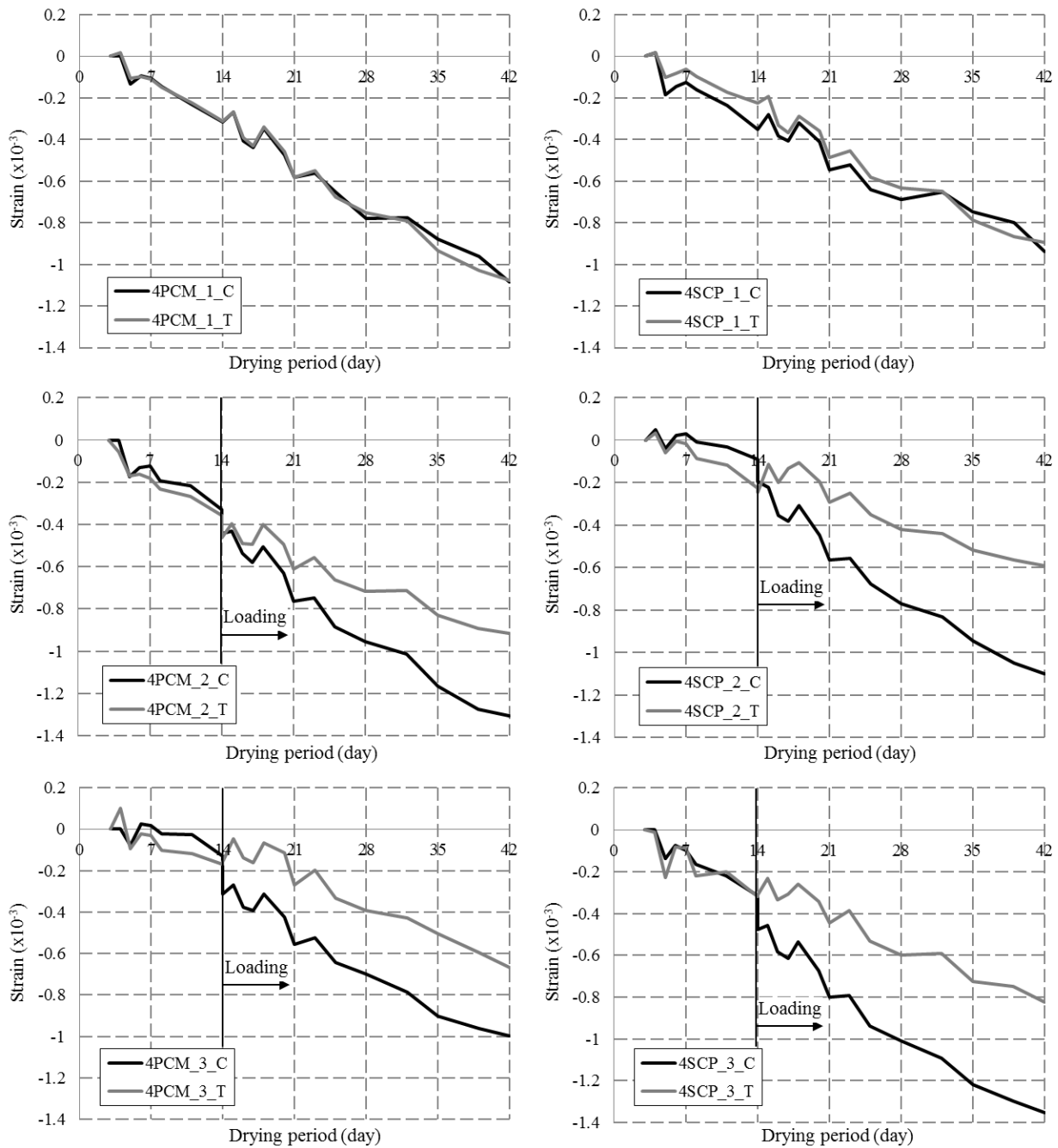
Figure 6.21 Strain-drying period relationships (SCRPCC, Fourth term)

Creep strains produced by loading (fourth term) are shown in Figure 6.22. In the name of specimen, C and T means flexural compressive and tensile (upper and lower of specimen).
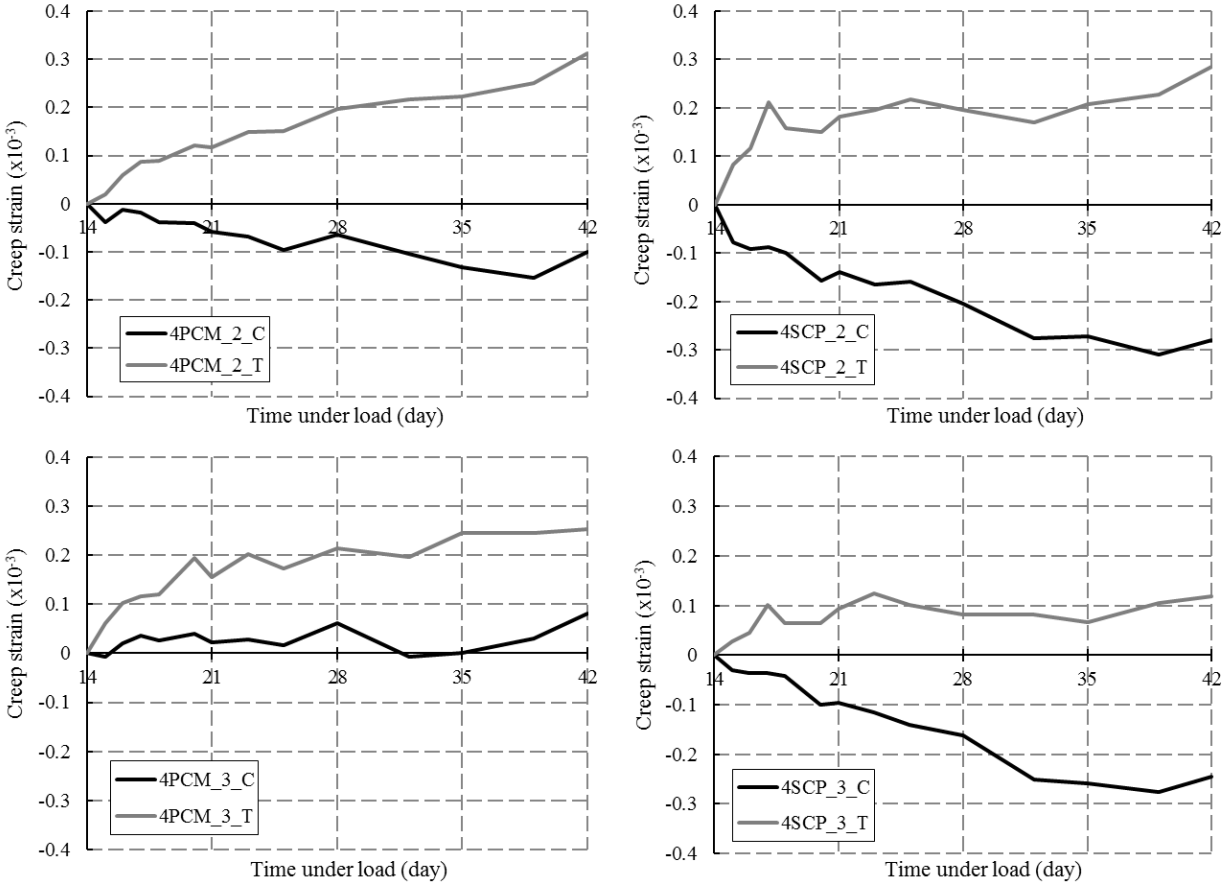
Figure 6.22 Creep strain-drying period relationships (SCRPCC, Fourth term)

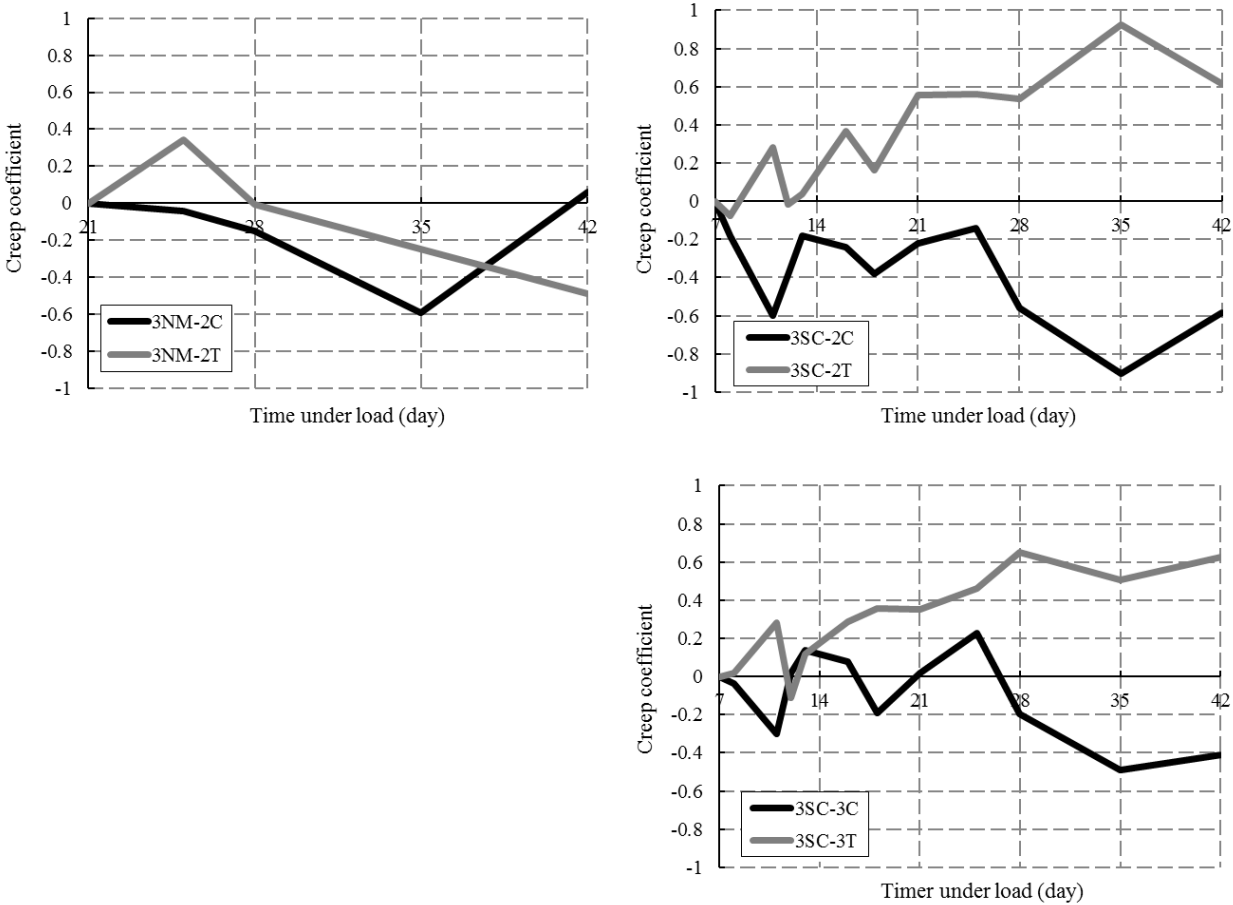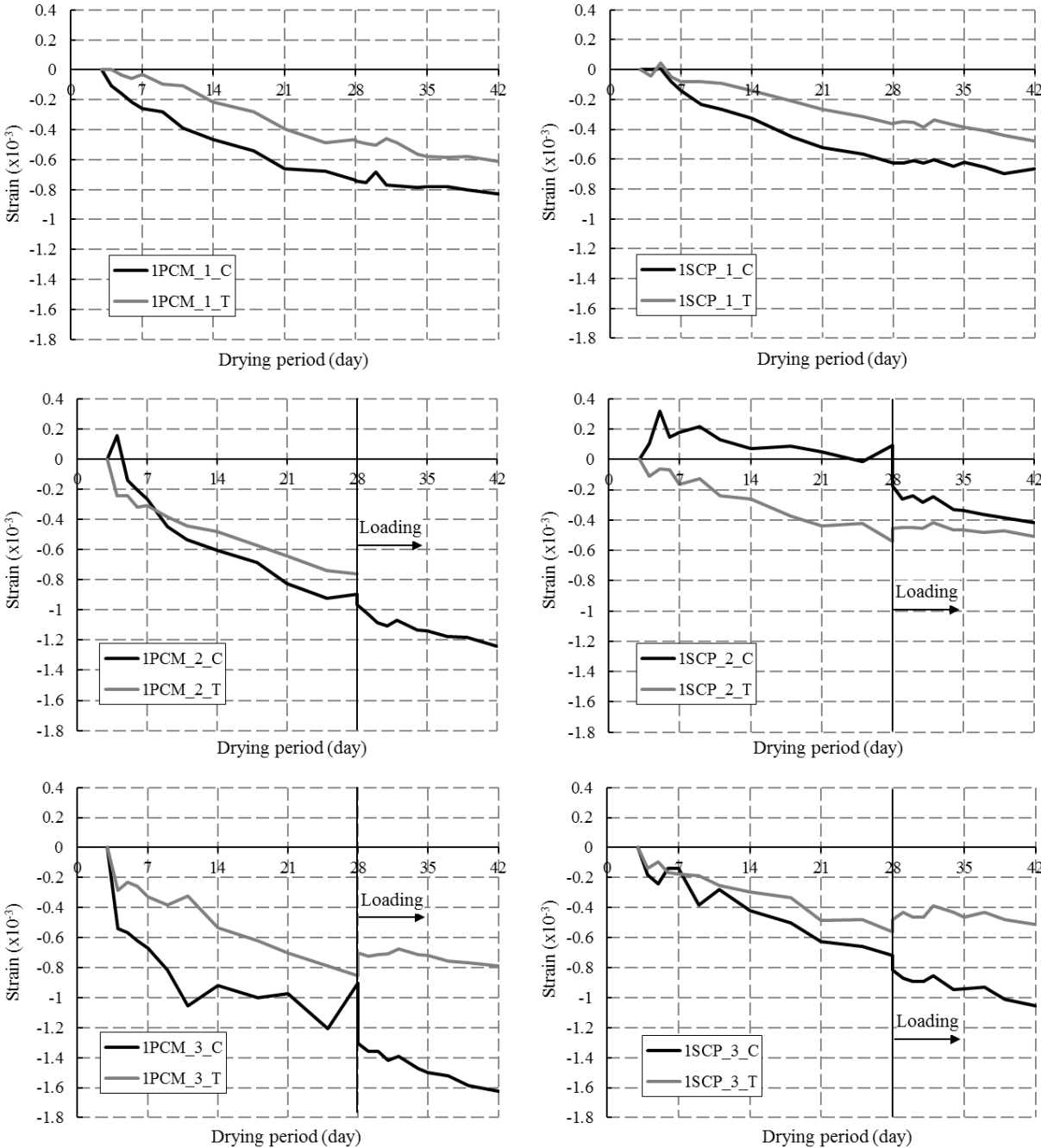Creep coefficients of fourth term are shown in figure 6.23. In the name of specimen, C and T means flexural compressive and tensile (upper and lower of specimen). The data of 4PCM_2_T and 4SCP_2_T were excluded from the graph because of some errors.
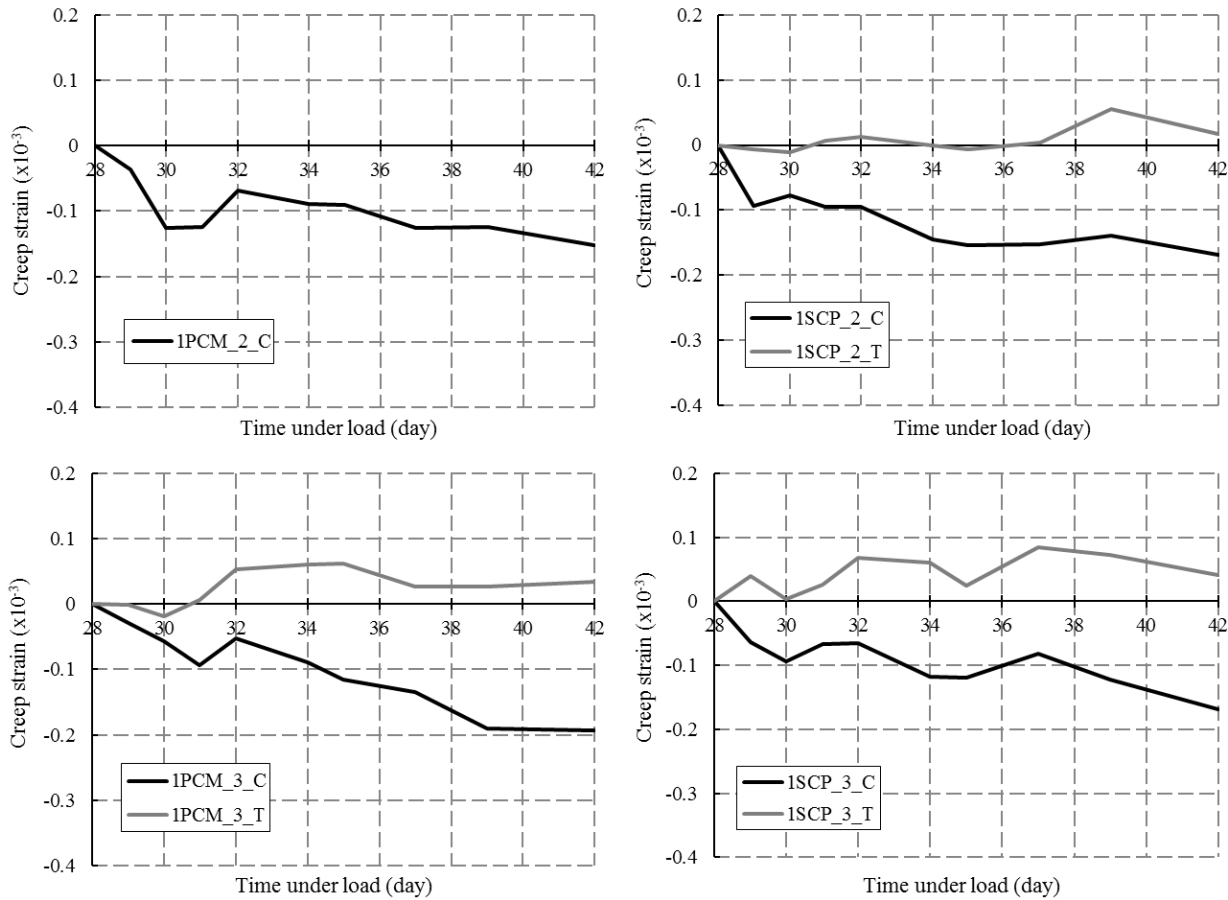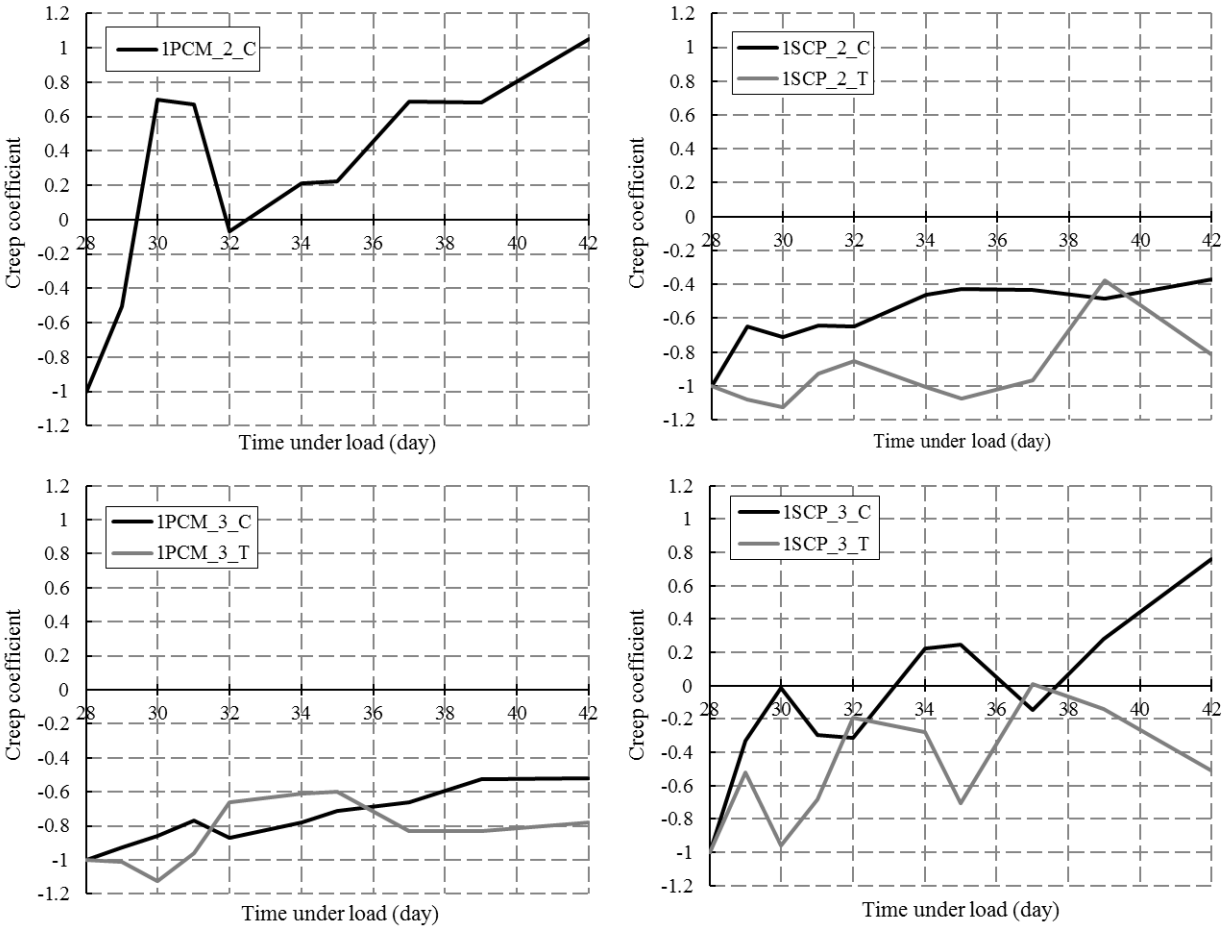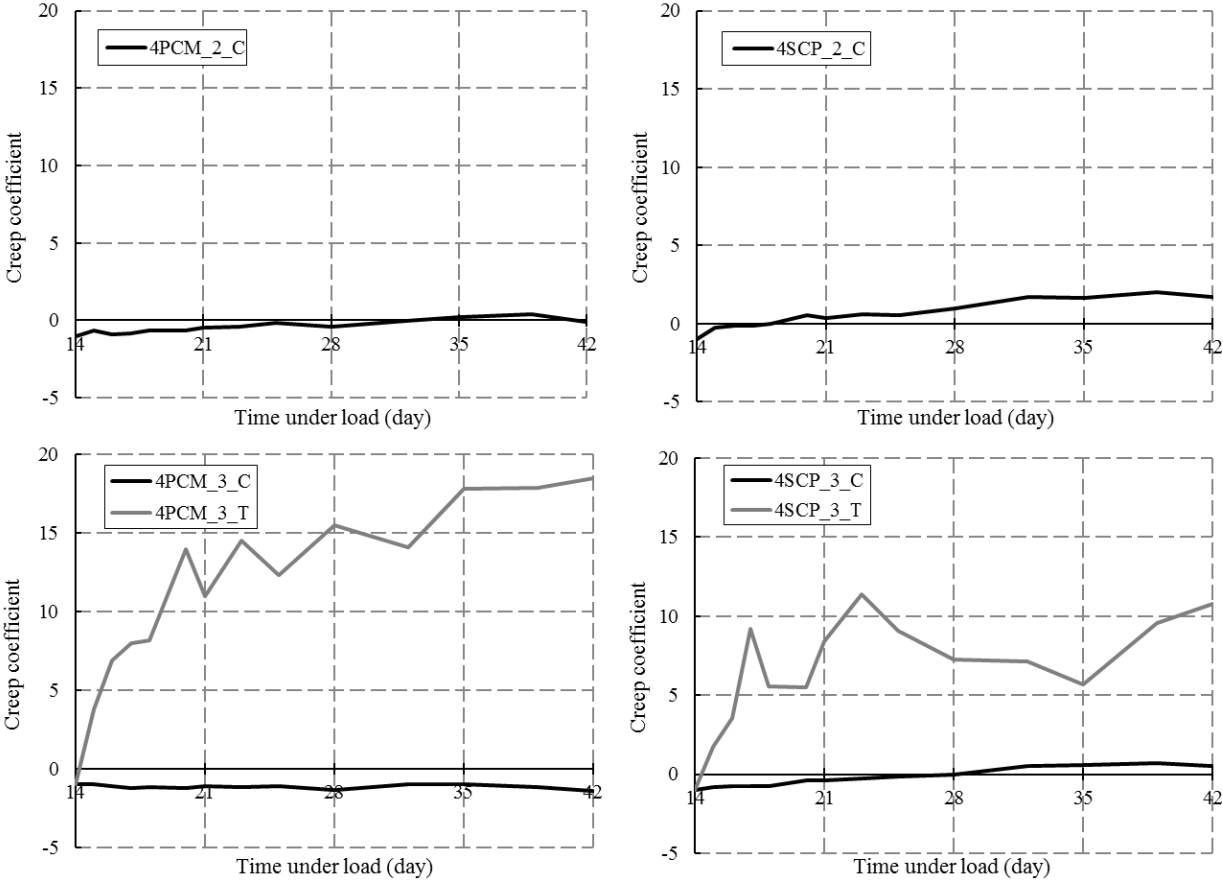

Figure 6.23 Creep coefficient-drying period relationships (SCRPCC, Fourth term)

6.4   Conclusions

In this chapter, flexural creep test was conducted to examine the creep behaviors of SCRCC under a constant temperature and humidity (20 ℃, 60% R.H.). The following conclusions were obtained from the test results.

1) Strains of NM and PCM showed a tendency to decrease by reinforcing with steel chip.
2) Creep strains of NM and PCM were reduced by reinforcing with steel chip.
3) The earlier loading start, the bigger increment of creep is. Because sufficient strength of specimen wasn't developed by loading day.
4) In the case of not notched specimens, the increments of strain were smaller than those of notched specimens
5) In the test results, some specimens showed irregular tendency. It needs to be examined additionally on this problem.

The observed specific creep is modeled by fib Model Code2010 (fib 2010) in the next chapter.

Chapter 7   Prediction of drying shrinkage crack of SCRPCC

7.1   Background and objective

In this chapter, prediction of the drying shrinkage cracking behavior of SCRCC and SCRPCC was attempted to verify the long-period durability of SCRCC and SCRPCC based on the experiment results of the previous chapters. A formula for calculating the accompanied cracking of drying shrinkage strain was worked out.

7.2   Prediction of drying shrinkage crack of SCRCC

In the previous chapters, an experiment based on the researches of Koyanagi et al (1990) and Kheder (1997) was conducted in an attempt to predict the shrinkage strain and cracking behavior of SCRCC. However, the prediction did not correspond to the experimental result (Hong et al. 2014).

It was considered that the drying shrinkage strain of SCRCC induced cracks due to the restraint of the reinforcing bars, but the net restraining strain was reduced by tensile creep. For this reason, the drying shrinkage cracking behavior was predicted analytically by considering tensile creep based on studies by Kojima et al. (2008), Kumano et al. (1999), and Ranavomanana et al. (2013).

7.2.1 Prediction of drying shrinkage cracking without tensile creep

The equivalent number of cracks of SCRCC was predicted by modeling of material properties based on the results of drying shrinkage test and creep test. In this prediction, autogenous shrinkage which affects drying shrinkage in the early days (AIJ 2013) was not considered because the measuring of drying shrinkage was started from a week after casting the specimens.

Among the results of drying shrinkage strain obtained from free shrinkage specimens, curve fitting was done on the drying shrinkage strain of NM-Out and SC-Out specimens which were placed in conditions to similar outside by regression-calculating with an equation referred CEB-FIP equation. Shrinkage strain (ε_{sc}) is formulated in *Eq(7.1)* with the modified coefficient C_1 of CEB-FIP Model Code 1990 equation (Comite Euro-International du Beton-Federation Internationale du la Precontrainte 1990).

$$\varepsilon_{sc} = \left[\left\{ 160 + 10 \cdot C_1 \cdot (9 - f_{cm}) \right\} \cdot 10^{-3} \cdot \beta_{RH} \right] \cdot \left[t / \left\{ 350 \cdot (H/100)^2 + D \right\} \right]^{0.5}$$

Eq(7.1)

$$\beta_{RH} = -1.55 \cdot \left\{ 1 - (RH/100)^3 \right\}$$

Eq(7.2)

where,

$$H = 2A_C / u$$

  t : Drying period (day)

  f_{cm} : 28day compressive strength (MPa)

  RH : Relative humidity during drying period (64.4%)

  C_1 : 6.078 (NM : Normal mortar)；4.079 (SC : SCRCC)

  D : Loading period (day)

  A_C : Cross sectional area of a member (mm^2)

  u : Circumference of a member (mm)

The experimental result of drying shrinkage strain-drying period relationships and curve fittings by *Eq(7.1)* are shown in Figure 7.1.
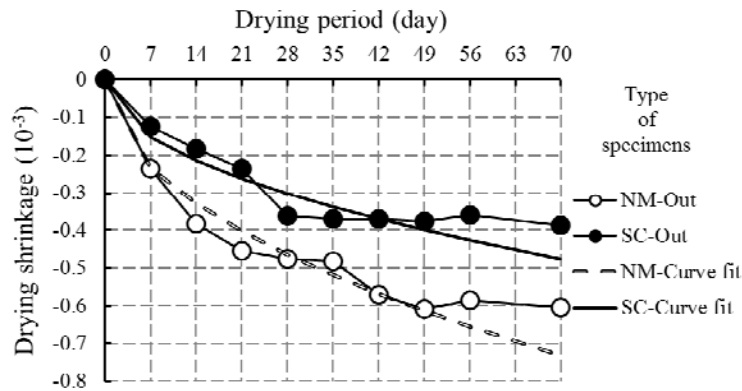
Figure 7.1 Drying shrinkage strain-drying period relationships of NM and SC specimens

Because of the drying shrinkage strain, the bond between the reinforcing bar and the cementitious composite caused a redistribution of stress in the specimen, and cracking sequentially occurred. In view of the bond stress-slip relationship between the cementitious composite and the steel bar, it is possible to predict crack width and number of cracks within each test period by calculating the compatibility of deformations and equivalence of stresses.

Using the bond stress-slip model by fib Model Code 2010 (fédération internationale du béton 2010), the calculation is performed by numerical integration of ordinary differential equations, which are shown here from the research by Rehm (1961) and Yannapouos et al (1991).

The compatibility condition is given by the following *Eq(7.3)*.

$$\frac{dS}{dx} = \varepsilon_s - \varepsilon_c - \varepsilon_{sc} - \varepsilon_{crp} \qquad\qquad Eq(7.3)$$

where,

  S : Bond Slip（mm）

x : Coordinate along bar axis （mm）

ε_c : Steel bar direction strain of cementitious composite

ε_{sc} : Drying shrinkage strain of cementitious composite

ε_{crp} : Creep strain of cementitious composite

ε_s : Strain of steel bar

The ordinary differential equation for bond problem is given by *Eq(7.4)*.

$$\frac{d^2 S}{dx^2} = \frac{4}{d_b} \cdot \left(\frac{1}{E_s} + \frac{\rho}{E_c} \right) \cdot \tau \qquad\qquad\qquad Eq(7.4)$$

Where,

d_b : Diameter of steel bar (mm)

E_c : Elastic modulus of cementitious composite (N/mm^2)

E_s : Elastic modulus of steel bar (N/mm^2)

τ : Bond stress (N/mm^2)

ρ : Reinforcement ratio

Figure 7.2 shows the assumed relationships between bond stress and the slip of the interface between the cementitious composite and the steel bar. This relationship is based on the fib Model Code 2010 (fib 2010) with slight modification.

$$S_1 = 0.1 \text{ mm} \qquad\qquad\qquad Eq(7.5)$$
$$S_2 = 1 \text{ mm} \qquad\qquad\qquad Eq(7.6)$$

$$\tau_0 = \Omega_y \cdot \tau_1 \cdot S / S_1 \quad \text{for} \ \ 0 \le S < S_1 \qquad\qquad\qquad Eq(7.7)$$

$$\tau_0 = \Omega_y \cdot \left\{ \tau_1 + (\tau_2 - \tau_1) \cdot (S_2 - S)/(S_2 - S_1) \right\} \quad \text{for} \ \ S_1 \le S < S_2 \qquad\qquad\qquad Eq(7.8)$$

$$\tau_0 = \Omega_y \cdot \tau_2 \quad \text{for} \ \ S_2 \le S \qquad\qquad\qquad Eq(7.9)$$

$$\tau_1 = 1.25\sqrt{f_{cm}} \qquad\qquad\qquad Eq\ (7.10)$$

$$\tau_2 = 2.5\sqrt{f_{cm}} \qquad\qquad\qquad Eq\ (7.11)$$

$$\Omega_y = 1 \quad \text{for} \ \ \varepsilon_s \le \varepsilon_{sy} \qquad\qquad\qquad Eq\ (7.12)$$

$$\Omega_y = 1 - 0.85 \cdot \left[1 - \exp\left[-5 \cdot \left\{ \frac{\varepsilon_s - \varepsilon_{sy}}{\varepsilon_{su} - \varepsilon_{sy}} \right\}^{\left(2 - \frac{\sigma_{su}}{\sigma_{sy}}\right)^2} \right] \right] \quad \text{for} \quad \varepsilon_{sy} < \varepsilon_s \le \varepsilon_{su} \qquad Eq(7.13)$$
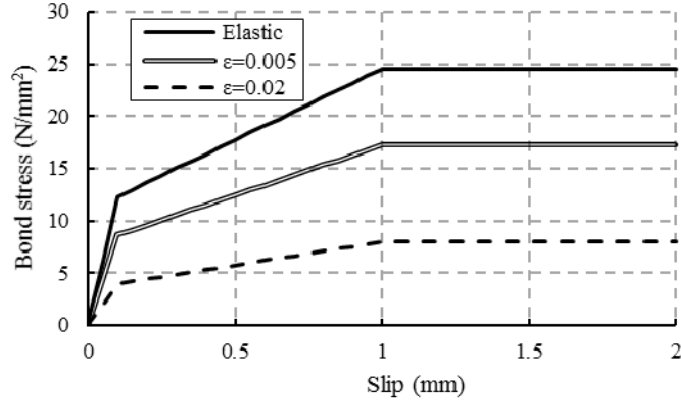
Fig. 7.2 Relationship between bond stress and slip for bond between cementitious composite and steel bar

The tensile stress increment of cementitious composite $\Delta\sigma_c$ is obtained by integrating cross sectional area A_c of the cementitious composite divided by bond stress ($n_s \times \pi \times d_b \times \tau$) in the x direction.

Thus, *Eq(7.14)* is established.

$$\sigma_c(x) = -\int_0^x \frac{n_s \, \pi \, d_b \, \tau}{A_c} dx + \sigma_c(x = 0) \qquad Eq(7.14)$$

where,

n_s : Number of steel bars

$\sigma_c(x)$: Stress of cementitious composite (N/mm^2)

$\sigma_c(x = 0)$: Stress of cementitious composite at the centers of adjacent cracks (N/mm^2)

The tensile stress of the cementitious composite becomes greatest at the center of an adjacent crack, and cracking occurs when the stress reaches the tensile strength.

The crack behaviors were analyzed based on the above method. The analyzed relationships between the equivalent number of cracks and drying periods are shown in Figure 7.3.
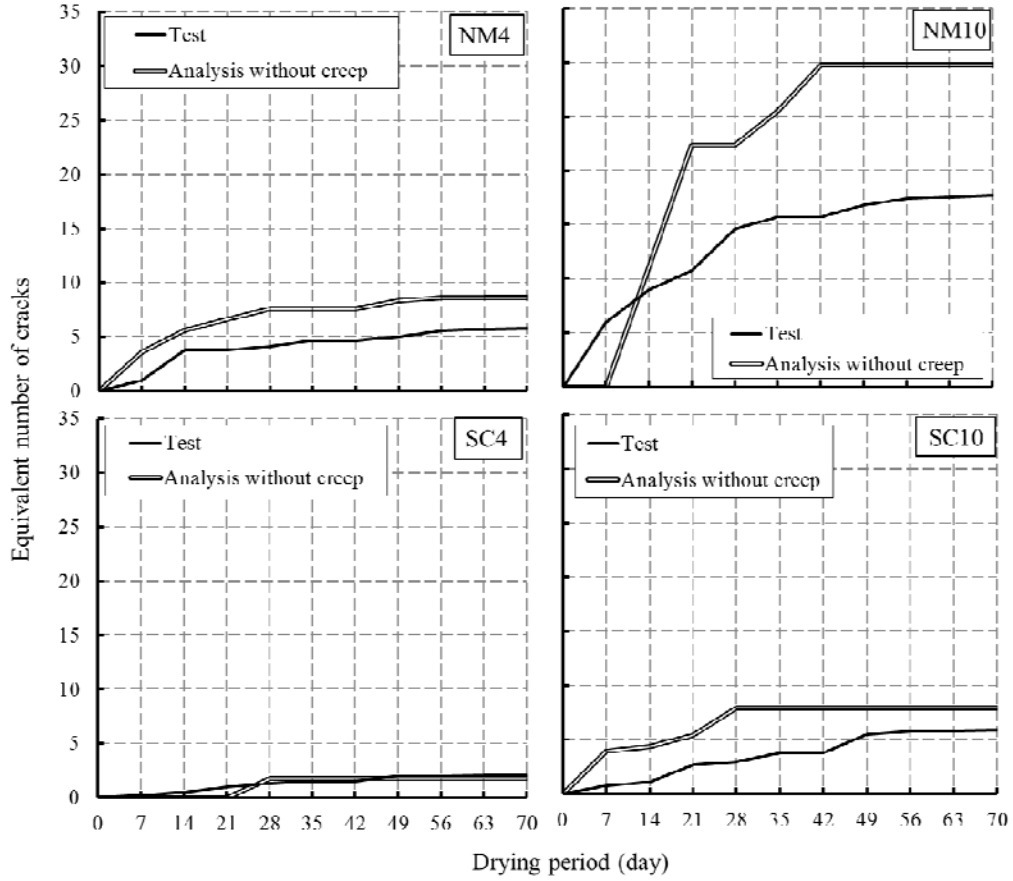
Figure 7.3 Equivalent number of cracks-drying period relationships of NM and SC (not considered creep)

As apparent from comparison with the test results, the analyses overestimated the test results. It is thought that this discrepancy is due to the neglect of creep strain. As a result, an estimation method that considers creep strain is examined in the next part.

7.2.2 Prediction of drying shrinkage cracking with tensile creep

Modeling of specific creep

As expressed in *Eq(7.3)* the real strain that causes tensile stress in the cementitious composite is the sum of drying shrinkage strain ε_{sc} (negative value) and creep strain ε_{crp} (positive value). A formula for calculating specific creep based on CEB-FIP Model Code 1990 (CEB-FIP 1990) is given here.

$$\phi_{CEB} = \left\{ 1 + \frac{1 - RH/100}{0.46 \cdot \left(\dfrac{A_c}{50 \cdot u} \right)^{1/3}} \right\} \times \frac{5.3}{\sqrt{\dfrac{f_{cm}}{11}}} \times \frac{1}{0.1 + t_0^{C_2}} \times \left(\frac{t - t_0}{\beta_H + t - t_0} \right)^{C_3} \qquad Eq(7.15)$$

where,

$$\beta_H = 150 \cdot \left\{ 1 + \left(1.2 \cdot \frac{RH}{100} \right)^{18} \right\} \cdot \frac{A_c}{50 \cdot u} + 250 \leq 1500 \qquad Eq(7.16)$$

A_c : Cross-sectional area of member （mm^2）

u : Length of part in contact with outside air (mm)

t_0 : Age when loaded （day）

Coefficients C_2 and C_3, are respectively 0.2 and 0.3 in the original equation, but the coefficients are set based on the results of the creep test, as follows.

C_2 : 0.420 （SC）; 0.303 （NM）

C_3 : 0.189 （SC）; 0.235 （NM）

Furthermore, it is necessary to model the changes caused by compressive strength f_{cm}, tensile strength f_t, and age of elastic modulus E_c in the calculation of $Eqs(7.4)$ to (7.16). Based on the experiment, compressive strength, tensile strength, and elastic modulus are respectively given by $Eqs(7.17), (7.18)$ and (7.19).

$$f_{cm} = f_{c28} \cdot \left\{ \frac{t}{28 \cdot (1 - C_5) + C_5 \cdot t} \right\} \qquad Eq(7.17)$$

$$f_t = f_{t28} \cdot \left(\frac{t}{28} \right)^{C_6} \qquad Eq(7.18)$$

$$E_c = E_{28} \cdot \exp \left[C_7 \cdot \left\{ 1 - \left(\frac{28}{t} \right)^{\frac{1}{2}} \right\} \right]^{\frac{1}{2}} \qquad Eq(7.19)$$

Where,

f_{c28} : 28-day compressive strength (N/mm^2)

f_{t28} : 28-day tensile strength (N/mm^2)

E_{28} : 28-day elastic modulus (N/mm^2)

C_5 : 0.939

C_6 : 0.047 （NM）; 0.127 （SC）

C_7 : 0.158 （NM）; 0.402 （SC）

The relationships between specific creep calculated by $Eqs(7.15)$ to $Eq(7.19)$ and creep coefficients obtained experimentally are shown in Figure 7.4. In addition, the relationships between drying shrinkage strain (negative value), creep strain (positive value), sum of both values calculated by $Eqs(7.15)$ to $Eq(7.19)$,

and drying period are represented in Figure 7.5. Creep strain was drawn by combining the creep strain of each day caused by the daily increasing tensile stress. The sum of shrinkage strain and creep strain shown in Figure 7.5 is real effective strain, which causes tensile stress in the cementitious composite. By applying this strain, the calculation of the number of cracks was retried.

Figure 7.4 Specific creep-drying period relationships of NM and SC

Figure 7.5 Relationships between drying shrinkage strain, creep strain and drying period of NM and SC

Calculation of the number of cracks

The analyzed relationships between the equivalent number of cracks considering the influence of creep and the drying period is shown in Figure 7.6 (indicated by "Analysis with creep"). There is some disjunction between the analysis findings and the test values of NM4, but the analyses values of the other specimens correspond closely with the test results.

As is apparent from a comparison of the results of the analysis without respect to creep, the number of cracks could be more accurately predicted by considering the influence of tensile creep on the cementitious composite.

Figure 7.6 Equivalent number of cracks-drying period relationships of NM and SC (considered creep)

7.2.3 Concluding remarks of prediction of drying shrinkage crack of SCRCC

In this section, the number of cracks was predicted by modeling the drying shrinkage strain of SCRCC and the specific creep coefficient based on the test results. The following remarks are obtained.

1) According to the superposition method used in this study, appropriate modeling can be achieved by changing the coefficient in the specific creep formula of CEB-FIP Model Code 1990 to a new coefficient.

2) The equivalent number of cracks was predicted by analyzing the bond behavior of the steel bars and binder in the wall using the specific creep model and drying shrinkage strain model which was proposed in this paper. The result nearly matched the number of cracks obtained by the experiments.

Same as the previous section, prediction of the drying shrinkage cracking behavior of SCRPCC was attempted based on the experiment results of the previous chapters in this section.

7.3.1 Prediction of drying shrinkage cracking without tensile creep

The drying shrinkage strains of PCM-Out and SCP-Out specimens, which were placed in conditions to similar outside, were curve-fitted in the same manner as the specimens NM-Out and SC-Out. The modified coefficient C_1 of Eq.(7.1) is given as 12.212 for the PCM, and 11.557 for the SCP.

The experimental result of drying shrinkage strain-drying period relationships and curve fitting by *Eqs(7.1)*and *(7.2)* are shown in Figure 7.7.
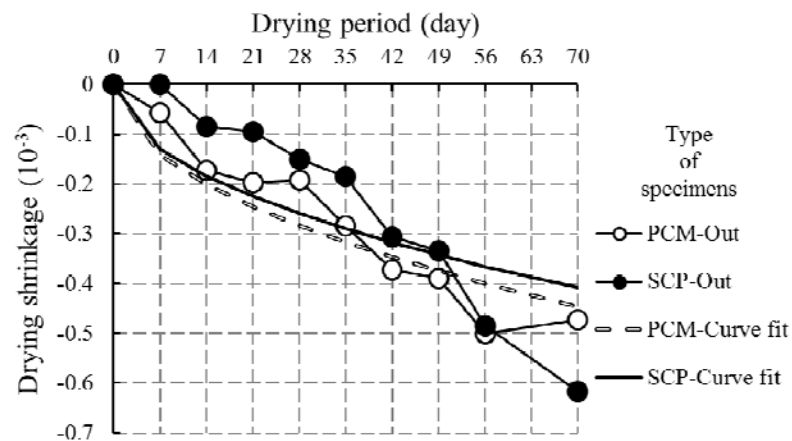
Figure 7.7 Drying shrinkage strain-drying period relationships of PCM and SPC specimens

The crack behaviors were analyzed using *Eqs.(7.1)* to *(7.14)*. The analyzed relationships between the equivalent number of cracks and drying periods are shown in Figure 7.8.

As apparent from comparison with the test results, the analyses again overestimated the test results. An estimation method that considers creep strain is examined in the next part.
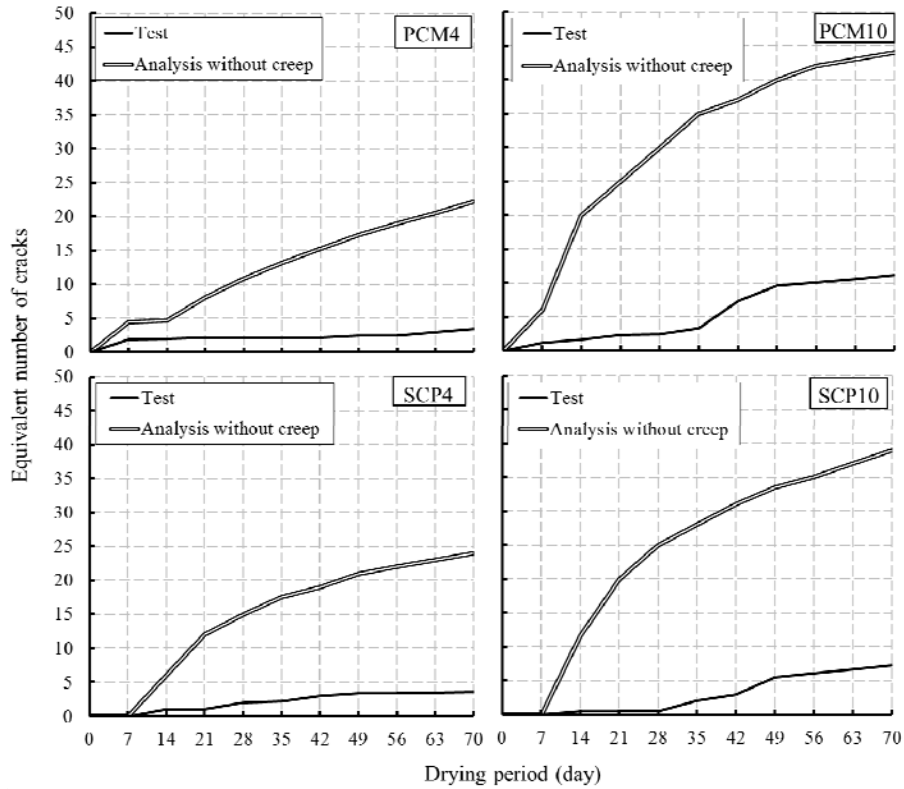
Figure 7.8 Equivalent number of cracks-drying period relationships (not considered creep)

7.3.2 Prediction of drying shrinkage cracking with tensile creep

Modeling of specific creep

The specific creep of the PCM and SCP are also modeled by *Eq(7.15)*to *(7.19)*. The coefficients C_2 to C_7 are modified as the followings based on creep tests.

C_2　　: 0.317（PCM）; 0.13（SCP）

C_3　　: 0.417（PCM）; 0.568（SCP）

C_5　 : 0.901（PCM）; 0.902（SCP）

C_6　 : 0.254（PCM）; 0.351（SCP）

C_7　 : 0.108（PCM）; 0.094（SCP）

The relationships between specific creep calculated by *Eqs(7.15)* to *Eq(7.19)* and those obtained experimentally are shown in Figure 7.9. In addition, the relationships between drying shrinkage strain (negative value), creep strain (positive value), sum of both values calculated by *Eqs(7.15)* to *Eq(7.19)*, and drying period are represented in Figure 7.10. Creep strain was drawn by combining the creep strain of each day caused by the daily increasing tensile stress. The sum of shrinkage strain and creep strain shown in Figure 7.10 is real effective strain, which causes tensile stress in the cementitious composite. By applying this strain, the calculation of the number of cracks was retried.
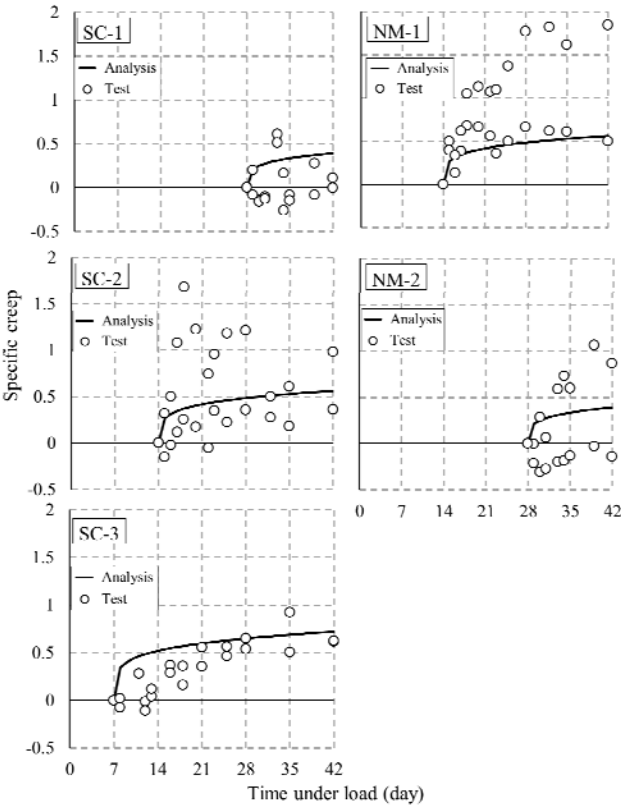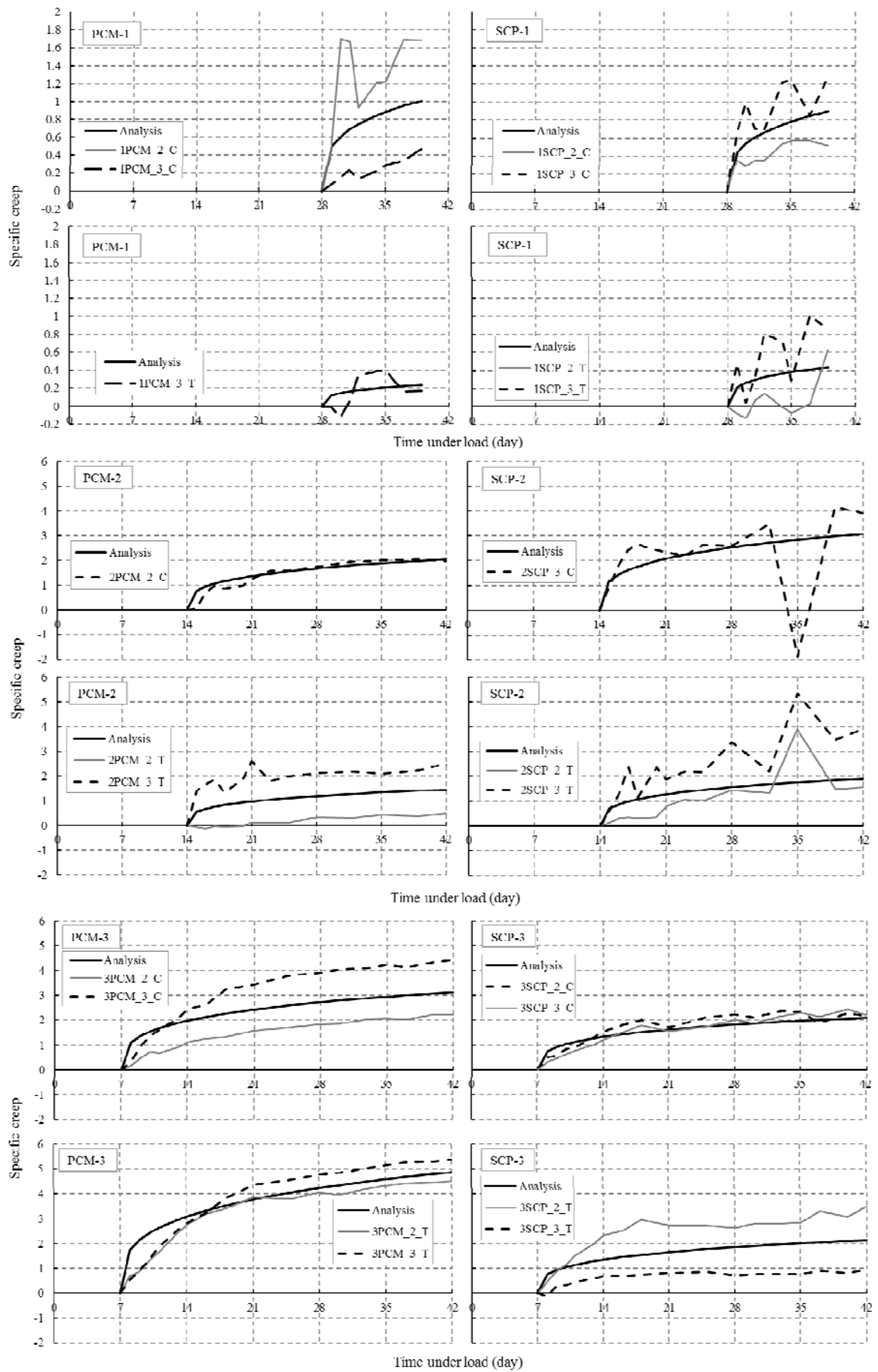
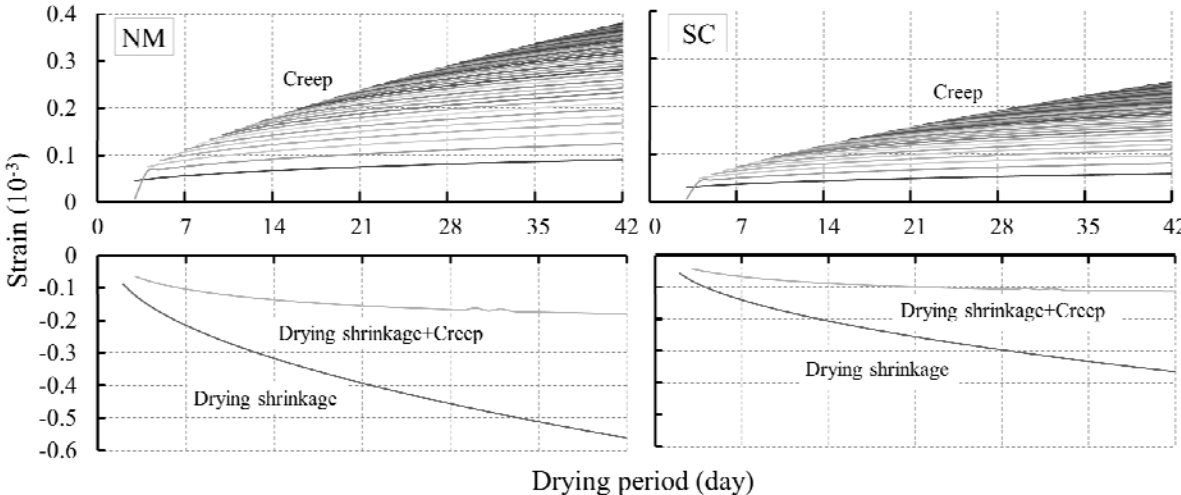Figure 7.9 Specific creep-drying period relationships of PCM and SCP
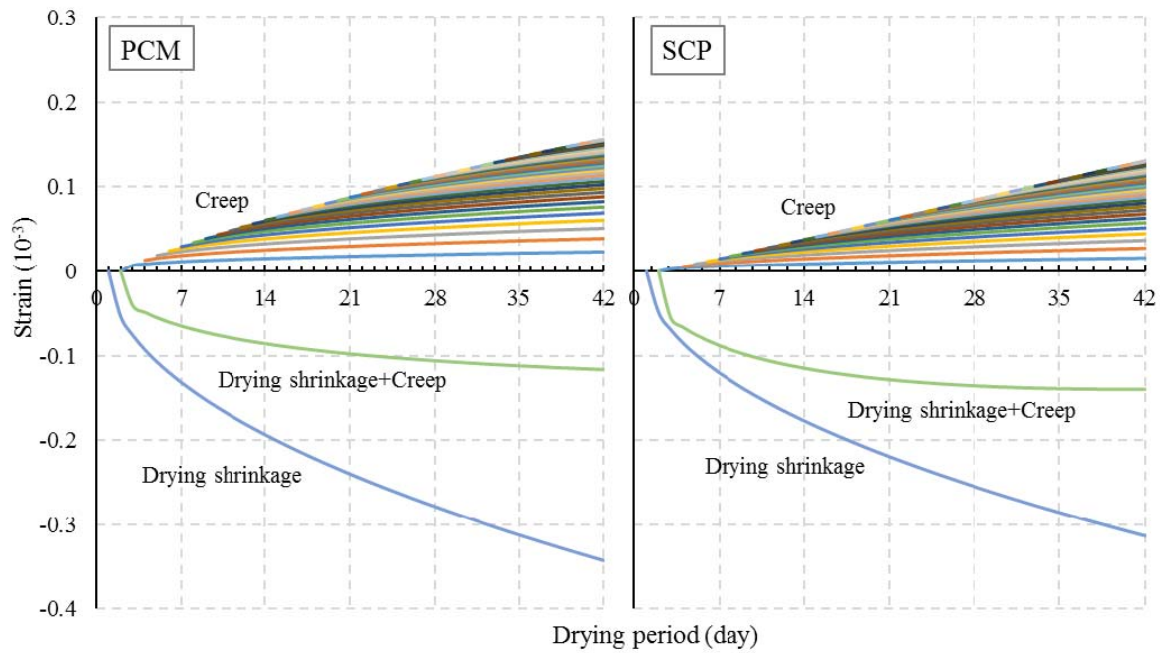
Figure 7.10 Relationships between drying shrinkage strain, creep strain and drying period of PCM and SCP

Calculation of the number of cracks

The analyzed relationships between the equivalent number of cracks considering the influence of creep and the drying period is shown in Figure 7.11 (indicated by "Analysis with creep"). There is some disjunction between the analysis findings and the test values of PCM4 and PCM10 before 35day but the analyses values after 35day correspond closely with the test results. In the case of SCP4 and SCP10, there is some disjunction between the analysis results and the test values before 28day but the analysis results simulates the later days well.

As is apparent from a comparison of the results of the analysis without respect to creep, the number of cracks could be more accurately predicted by considering the influence of tensile creep on the cementitious composite.
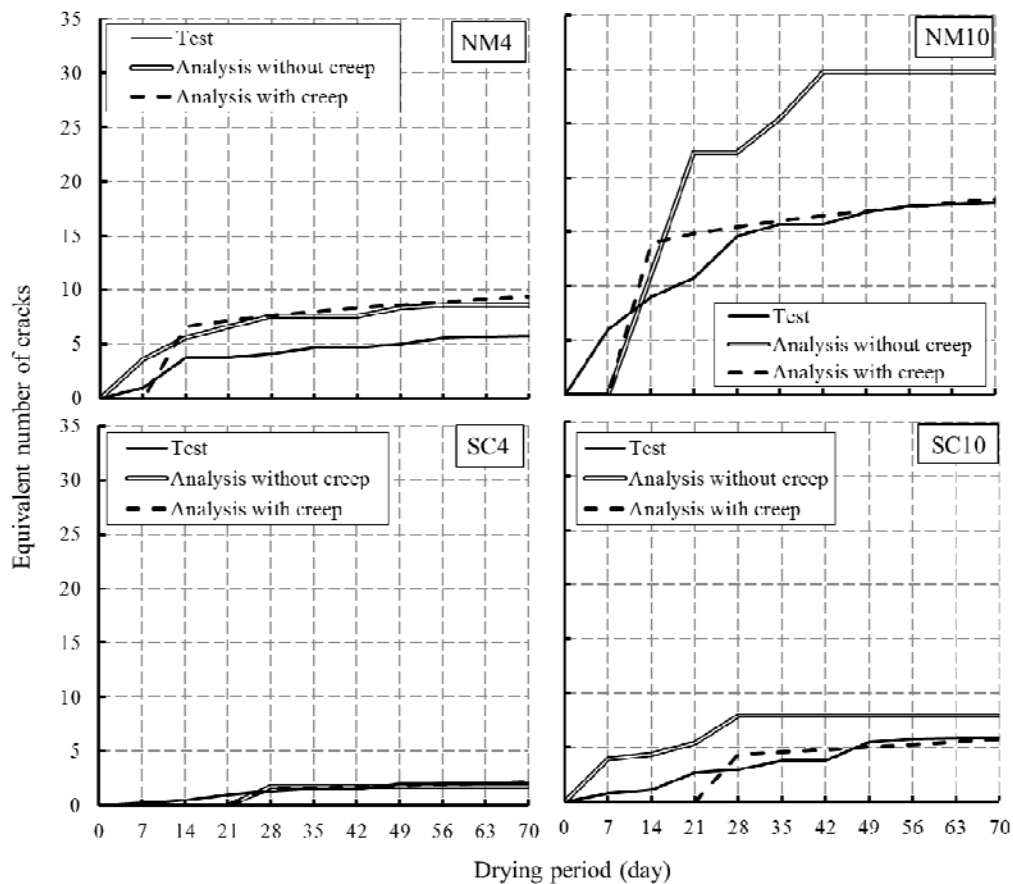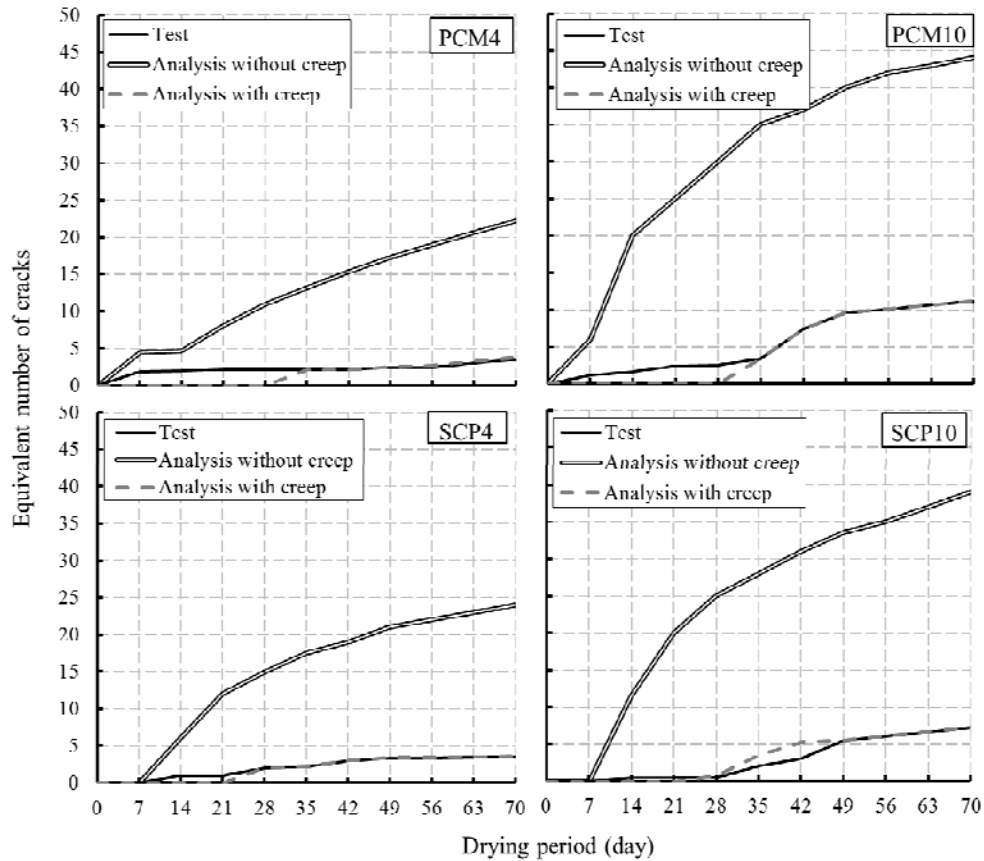
Figure 7.11 Equivalent number of cracks-drying period relationships of PCM and SCP (considered creep)

7.3.3 Concluding remarks of prediction of drying shrinkage crack of SCRPCC

In this section, the number of cracks was predicted by modeling the drying shrinkage strain of SCRPCC and the specific creep coefficient based on the test results. The following remarks are obtained.

1) According to the superposition method used in this study, appropriate modeling can be achieved by changing the coefficient in the specific creep formula of CEB-FIP Model Code 1990 to a new coefficient.

2) The equivalent number of cracks was predicted by analyzing the bond behavior of the steel bars and binder in the member using the specific creep model and drying shrinkage strain model which was proposed in this paper. The result nearly matched the number of cracks obtained by the experiments.

7.4 Conclusions

In this chapter, the drying shrinkage cracking behaviors of SCRCC and SCRPCC part of walls with steel bars inside members are evaluated considering the tensile creep. Creep tests were simultaneously performed. In addition, the equivalent number of cracks was predicted by modeling the drying shrinkage strain of SCRCC and SCRPCC and the specific creep coefficient based on the test results. The following conclusions were obtained from the results.

1) Drying shrinkage of NM and PCM was reduced by reinforcing with steel chip.

2) The equivalent numbers of cracks of SCRCC and SCRPCC wall specimens were less than those of NM and PCM.

3) According to the superposition method used in this study, appropriate modeling can be achieved by changing the coefficient in the specific creep formula of CEB-FIP Model Code 1990 (CEB-FIP 1990) to a new coefficient.

4) The equivalent number of cracks was predicted by analyzing the bond behavior of the steel bars and binder in the member using the specific creep model and drying shrinkage strain model which was proposed in this paper. The result nearly matched the number of cracks obtained by the experiments.

Chapter 8 Conclusions

8.1 Summary and concluding remarks

Concrete is relatively brittle, and its tensile strength is typically only about one tenths of its compressive strength. Therefore, for many applications, it is becoming increasingly popular to reinforce the concrete with small, randomly distributed fibers.

Over the years, numerous attempts have been made to reuse the waste produced by the iron and steel industry. Among them, the use of steel chips which are waste products of the iron and steel industry as a substitution material of steel fiber is economically efficient and environmentally sound because it reduces the total amount of industrial waste.

The usage of polymer cement mortar is one of the promising solutions to enhance strength, adhesion, waterproofness and durability of building structures

In this study, in order to verify the long-period durability of steel chip reinforced cementitious composites (SCRCC) and steel chip reinforced polymer cementitious composites (SCRPCC), various studies were conducted through from previous studies and experimental studies to analysis researches to predict the drying shrinkage cracking.

Chapter 1 is the background of this study, Chapter 2 summarizes the previous researches on fiber reinforced cementitious composites, steel chip, concrete-polymer composites and shrinkage cracking. And Chapter 8 is the summary and conclusions. Chapter 3 to 7 constitute the main part of the dissertation: (1) compressive and flexural strength properties, (2) drying shrinkage cracking characteristics through the free and restrained shrinkage test, (3) bond characteristics through the pull-out and uniaxial tension test, (4) creep characteristics to predict the drying shrinkage crack. (5) prediction of drying shrinkage cracking behavior based on the experiment results. The contents of the five chapters are summarized as follows.

Mechanical Properties of SCRPCC

In Chapter 3, compression test and three point flexural test were conducted to examine the material properties and fracture mode of SCRCC (SC) and SCRPCC (SCP). The following conclusions were obtained from the results.

1) It was confirmed that the spalling of NM specimens was surely prevented by reinforcing with steel chip in the compressive strength test.

2) Flexural strengths of NM specimens were improved by reinforcing with steel chip at every curing days. And it was confirmed that SC specimen was not broken in spite of large crack in contrast with NM specimen.

3) Regardless of reinforcing with steel chip, brittle fracture didn't occur in the PCM and SCP specimens after compressive strength test. Also, it was confirmed that the ductility of PCM specimens was improved by reinforcing with steel chip.

4) It was confirmed that SCP specimen was not broken in spite of large crack in contrast with PCM specimen. It is attributed to the bridging effect by reinforcing with steel chip.

Drying Shrinkage Characteristics of SCRPCC

In Chapter 4, the drying shrinkage properties and the cracking characteristics of SCRCC and SCRPCC with large scale wall specimen were investigated. The following conclusions were obtained from the results.

1) The drying shrinkage strain of SCRCC was smaller than that of normal mortar.

2) The number of cracks by drying shrinkage of SCRCC was smaller than that of normal mortar. In addition, increasing the reinforcement ratio caused a decrease in crack widths and an increase in the number of cracks.

3) Drying shrinkage of PCM was decreased by reinforcing with steel chip at the outdoor condition. Influence of curing and drying condition on drying shrinkage is that drying shrinkage of outdoor specimens was lower than that of indoor specimens.

4) Drying shrinkage of restrained PCM specimens was reduced by reinforcing with steel chip. And in the case of specimens with high reinforcement ratio, the occurrence of cracks of restrained SCRPCC specimen was less than that of PCM specimen.

5) Average crack width of restrained specimen was decreased by increasing of the amount of reinforcing bar.

Bond Characteristics of SCRPCC

In Chapter 5, the stress-slip relationships between steel bar and steel chip reinforced cementitious composite (SCRCC) and steel chip reinforced polymer cementitious composite (SCRPCC) were investigated by conducting the pull-out tests. Also, uniaxial tension tests were conducted to examine the cracking characteristics of SCRCC and SCRPCC. The following conclusions were obtained from the results.

1) Maximum bond stresses at failure of non-reinforced NM showed a tendency to be higher than that of SCRCC. It was also higher than that of SCRCC before yielding of steel bars.

2) Maximum bond stresses before yielding of steel bars of PCM showed a tendency to be higher than that of SCRPCC.

3) Average crack width of PCM was decreased by reinforcing with steel chip at failure and before yielding of steel bars. And average crack width of NM showed a tendency to be lower than that of SCRCC.

Creep Characteristics of SCRPCC

In Chapter 6, flexural creep test was conducted to examine the creep behaviors of SCRCC under a constant temperature and humidity (20 ℃, 60% R.H.). The following conclusions were obtained from the test results.

1) Strains of NM and PCM showed a tendency to decrease by reinforcing with steel chip.

2) Creep strains of NM and PCM were reduced by reinforcing with steel chip.

3) The earlier loading start, the bigger increment of creep is. Because sufficient strength of specimen wasn't developed by loading day.

4) In the case of not notched specimens, the increments of strain were smaller than those of notched specimens

5) In the test results, some specimens showed irregular tendency. It needs to be examined additionally on this problem.

Prediction of Drying Shrinkage Crack of SCRPCC

In Chapter 7, the drying shrinkage cracking behaviors of SCRCC and SCRPCC walls with steel bars inside members are evaluated considering the tensile creep. Creep tests were simultaneously performed. In addition, the equivalent number of cracks was predicted by modeling the drying shrinkage strain of SCRCC and SCRPCC and the specific creep coefficient based on the test results. The following conclusions were obtained from the results.

1) Drying shrinkage of NM and PCM was reduced by reinforcing with steel chip.

2) The equivalent numbers of cracks of SCRCC and SCRPCC wall specimens were less than those of NM and PCM.

3) According to the superposition method used in this study, appropriate modeling can be achieved by changing the coefficient in the specific creep formula of CEB-FIP Model Code 1990 to a new coefficient.

4) The equivalent number of cracks was predicted by analyzing the bond behavior of the steel bars and binder in the member using the specific creep model and drying shrinkage strain model which was proposed in this paper. The result nearly matched the number of cracks obtained by the experiments.

8.2 Future works

In this study, high strength mortar with silica fume for SCRCC and ordinary strength mortar without silica fume for SCRPCC were used as base mortars. Because of the difference in their strengths, it could not sufficiently compare SCRCC with SCRPCC on the influence of modification with polymer. Therefore, it needs to be examined about ordinary strength mortar-based SCRCC and SCRPCC not used silica fume.

Also, steel chips should be uniform in shape because non-uniform shape of steel chip caused variation of real volume fraction of steel chips in the specimens. And the variation of real fraction of steel chips in the specimens causes the variation of test results in all the tests.

Finally, the applications of steel chip to geopolymer composites made with supplementary cementing materials need to be examined. If steel chip reinforced geopolymer composites are possible to use, an innovative construction material that both binder and reinforcing material are eco-friendly can be developed.

REFERENCES

ACI committee 446, (1999). *446.1R Fracture Mechanics of Concrete: Concepts, Models and Determination of Material Properties*

ACI Committee 544, (1973). "Revision of State-of-the-Art Report (ACI 544 TR-73) on Fiber Reinforced Concrete," *ACI Journal Proceedings*, 70(11), 727-744

ACI committee 544, (1996). *544.1R Report on Fiber Reinforced Concrete*

ACI committee 548, (2009). *548.3R Report on Polymer-Modified Concrete*

Afridi, M. U. K., Ohama, Y., Demura, K., and Iqbal, M. Z., (2003) "Development of Polymer Films by the Coalescence of Polymer Particles in Powdered and Aqueous Polymer-Modified Mortars," *Cement and Concrete Research*, 33, 1715-1721

Architectural Institute of Japan, (2008). "*Recommendations for Environmentally Conscious Practice of Reinforced Concrete Buildings*" (in Japanese)

Architectural Institute of Japan, (2011). "*Recommendation for Practice of Concrete-Polymer Composites*" (in Japanese)

Alwaeli, M. and Nadziakiewicz, J., (2012). "Recycling of Scale and Steel Chips Waste as a Partial Replacement of Sand in Concrete." *Construction and Building Materials*, 28(1), 157-163

Balaguru, P., and Ramakrishnan, V., (1987). "Comparison of Slump Cone and V-B Tests as Measures of Workability for Fiber Reinforced and Plain Concrete," *Cement, Concrete and Aggregates*, 9(1), 3-11

Balaguru, P., and Ramakrishnan, V., (1988). "Properties of Fiber Reinforced Concrete: Workability Behavior under Long Term Loading and Air-Void Characteristics," *ACI Materials Journal*, 85(3), 189-196

Barluenga, G., and Hernández-Olivares, F., (2004). "SBR Latex Modified Mortar Rheology and Mechanical Behavior," *Cement and Concrete Research*, 34(3), 527-535

Beeldens, A., Monteny, J., Vincke, E., De Belie, N., Van Gemert, D., Taerwe, L., and Verstraete, W., (2001). "Resistance to Biogenic Sulfuric Acid Corrosion of Polymer-Modified Mortars," *Cement and Concrete Composites*, 23(1), 47-56

Bettelle Memorial Institute, (1969). *United States Patent 3,429,094*

Bettelle Memorial Institute, (1970). *United States Patent 3,500,728*

Biryukovich, K. L., Biryukovich, Yu. L. and Biryukovich, D. L. (1965). "Glass Fiber Reinforced Cement," *CERA Translation*, No. 12

Bond, A. E., (1932). *British Patent 369,561*

Bureau, L., Alliche, A., Pilvin, P., and Pascal, S., (2001). "Mechanical Characterization of a Styrene-Butadiene Modified Mortar," *Materials Science and Engineering A*, 308(1-2), 233-240

Cao, J., and Chung, D. D. L., (2001). "Carbon Fiber Reinforced Cement Mortar Improved by Using Acrylic Dispersion as an Admixture" *Cement and Concrete Research*, 31(11), 1633-1637

Carlson, R. W., (1938). "Drying Shrinkage of Concrete as Affected by Many Factors," *ASTM Proceeding*, 38, Part 2, 419-437

CEB-FIP, (1990). "Model Code for Concrete Structures"

Chandra, S., and Ohama, Y., (1994). *Polymers in Concrete*

Chou, Y.-S., Mecholsky, J. J., and Silsbee, M., (1990). "Fracture Toughness of Macro-Defect-Free Cement Using Small Crack Techniques," *Journal of Materials Research*, 5(8), 1774-1780

Cooke, G. B., (1941). *United States Patent* 2,227,533

Cresson, L., (1923). *British Patent* 191,474

Darwin, D., Browning, J., and Lindquist, W. D., (2004). "Control of Cracking in Bridge Decks: Observations from the Field," Cement, Concrete and Aggregates, *ASTM International*, 26(2), 148-154

Davis, H. E., (1940). "Autogenous Volume Change of Concrete," *ASTM Proceeding*, 40, 1103-1110.

De Puy, G. W., (1996). "Polymer Modified Concrete—Properties and Applications," *International ICPIC Workshop on Polymers in Concrete for Central Europe*, 63-67

Dixon, J., and Mayfield, B., (1971). "Concrete Reinforced with Fibrous Wire," *Journal of the Concrete Society*, 5(3), 73-76

Fessenden, R. J., and Fessenden, J. S, (1998). *Organic Chemistry*, sixth edition

fib, (2010). "fib Model Code 2010," 233-239

Geist, J. M., Amagna, S. V., and Mellor, B. B., (1953). "Improved Portland Cement Mortars with Polyvinyl Acetate Emulsions," *Industrial and Engineering Chemistry*, 45(4), 759-767

Goldfein, S., (1963). "Plastic Fibrous Reinforcement for Portland Cement," *Technical Report No. 1757-TR, U.S. Army Research and Development Laboratories*, 1-16

Gray, R. J., and Johnston, C. D., (1984). "The Effect of Matrix Composition on Fibre/Matrix Interfacial Bond Shear Strength in Fibre-Reinforced Mortar," *Cement and Concrete Research*, 14, 285-296

Griffiths, L. H., (1951). "Floor Surfacing for Food Processing Plants," *Food Manufacture*, 26(9), 369-372

Hannant, D. J., (1978). "Fibre Cements and Fibre Concretes", 53

Hoff, George C., (1986). "Use of Steel Fiber Reinforced Concrete in Bridge Decks and Pavements," *Steel Fiber Concrete*, 67-108

Hong, S., Kimura, S., Tanaka, D., Sato, Y., and Kaneko, Y., (2014). "Drying shrinkage and creep characteristics of steel chip reinforced cementitious composite." *Proceedings of Annual Research Meeting, Materials and Construction, Kinki Branch, Architectural Institute of Japan*, 54, 9-20 (in Japanese)

Houk, I. E., Borge, O. E., and Houghton, D. L., (1969). "Studies of Autogenous Volume Change in Concrete in Dworshak Dam," *ACI Journal Proceedings*, 66(7), 560-568

Issa, M. A., Alhassan, M. A., and Ramos, J., (2007). "Glass Fiber Reinforced Latex-Modified Concrete Using a Volumetric Mixer for Production of Overlays," *Concrete International*, 29(3), 48-52

Jaenicke, J., Knoop, H., Miedel, H., and Schweitzer, O, (1943). *United States Patent* 2,311,233

Jenni, A., Zurbriggen, R., Holzer, L., and Herwegh, M., (2006). "Changes in Microstructures and Physical Properties of Polymer-Modified Mortars during Wet Storage" *Cement and Concrete Research*, 36, 79-90

Johnston, C. D., (1974). "Steel Fibre Reinforced Mortar and Concrete – A Review of Mechanical Properties," *Fiber Reinforced Concrete ACI Special Publication*, 44, 127-142

Johnston, C. D., (1984). "Measures of the Workability of Steel Fiber Reinforced Concrete and Their Precision," *Cement, Concrete and Aggregates*, 6(2), 74-83

Johnston, C. D., (1989). "Effects on Flexural Performance of Sawing Plain Concrete and of Sawing and Other Methods of Altering Fiber Alignment in Fiber Reinforced Concrete," *Cement, Concrete and Aggregates*, 11(1), 23-29

Kanada, M., Sato, Y., and Kaneko, Y., (2011). "Seismic Retrofit of Exposed Column Basement Using Steel Chip Reinforced Cementitious Composite." *Proceedings of Constructional Steel*, 19, 155-162 (in Japanese)

Kanada, M., (2012). "Development of Steel Chip Reinforced Cementitious Composites and Application to Steel Column Basement" *Master's Thesis, Department of Architecture, Graduate School of Engineering, Kyoto University*

Kardon, J. B., (1997). "Polymer-Modified Concrete: Review," *Journal of Materials in Civil Engineering*, 9(2), 85-92

Kheder, G. F., (1997). "A New Look at the Control of Volume Change Cracking of Base-Restrained Concrete Walls." *ACI Structural Journal*, 94(3), 262-270

Kim, J., Robertson, R. E., and Naaman, A. E., (1999). "Structure and Properties of Poly(vinyl alcohol)-Modified Mortar and Concrete," *Cement and Concrete Research*, 19(3), 407-415

Kirkpatrick, S. M., (1925) *British Patent* 242,345

Kormeling, H. A., Reinhardt, H. W., and Shah, S. P., (1980). "Static and Fatigue Properties of Concrete Beams Reinforced with Continuous Bars and with Fibers," *ACI Journal Proceedings*, 77(1), 36-43

Kojima, K. and Nakamura, N., (2008). "Experiment of Tensile Creep and Tensile Relaxation for High Strength Mortar in Early Age." *Proceedings of the Japan Concrete Institute*, 30(1), 441-446 (in Japanese)

Koyanagi, M., Masuda, Y., and Nakane, S., (1990). "A Study on Shrinkage Cracks in Reinforced Concrete Walls (Part 4) -Prediction Analysis of Cracking Widths due to Restrained Volume Change in One-Way Concrete Members-." *Report of Obayashi Corporation Technical Research Institute*, 41, 73-79 (in Japanese)

Kumano, T., Nishibayashi, S., Inoue, S., and Yoshino, A., (1999). "A Study on the Prediction Model of Tensile Creep Strain of Concrete Based on Micro Pore Behavior." *Journal of Japan Society of Civil Engineers*, 42(613), 121-135

Krenchel, H., and Shah, S., (1985). "Applications of Polypropylene Fibers in Scandinavia" Concrete International, 7(3), 32-34

Lavelle, J. A., (1988). "Acrylic Latex Modified Portland Cement" *ACI Materials Journal*, 85(1), 41-48

Lefebure, V., (1924). *British Patent* 217,279

Lezy, R., and Paillere, A., (1967). "Concrete, Mortars and Grouts—Improvements by Addition of a Resin," *Synthetic Resins in Building Construction* Vol. 1 *RILEM Symposium*, 127-140 (in French)

Majumdar, A. J., (1975). "Properties of Fiber Cement Composites," *Proceedings of RILEM Symposium,* 279-314

Maultzsch, M., (1989). "Studies on the Durability of Polymer Modified Cement Concrete for the Repair of Concrete Structures," *Materials Engineering Journal*, 1(1), 77-84

Mindess, S., Young, J. F., and Darwin, D., (2003). *Concrete*, 2nd Edition

Mirza, J., Mirza, M. S., and Lapointe, R., (2002). "Laboratory and Field Performance of Polymer-Modified Cement-Based Repair Mortars in Cold Climates," *Construction and Building Materials*, 16(6), 365-374

Monfore, G. E., (1968). "A Review of Fiber Reinforced Portland Cement Paste, Mortar, and Concrete," *Journal of the PCA Research and Development Laboratories*, 10(3), 36-42

Morgan, D. R., Deill, J., McAskill, D., and Duke, N., (1987). "Evaluation of Silica Fume Shotcrete," *Proceedings of CANMET/CSCE International Workshop on Silica Fume in Concrete*, 34

Morrison, J., Shah, S. P., and Jeng, Y. S., (1988). "Analysis of the Debonding and Pullout Process in Fiber Composites," *Journal of Engineering Mechanics*, 114(2), 277-294

Naaman, A. E., and Shah, S. P., (1975). "Bond Studies of Oriented and Aligned Fibers," *Proceedings of RILEM Symposium on Fiber Reinforced Concrete*, 171-178

Naaman, A. E., and Shah, S. P., (1976). "Pullout Mechanism in Steel Fiber Reinforced Concrete," *Journal of Structural Division*, 102(8), 1537-1548

Naaman, A.E., Shah. S., and Throne, J., (1982). "Some Developments in Polypropylene Fibers for Concrete", *Fiber Reinforced Concrete International Symposium ACI Special Publication*, 81, 375-396

Naaman, A.E., (1985). "Fiber Reinforcement for Concrete." *Concrete International: Design and Construction,* 7(3), 21-25

Ohama, Y., (1973). "Study on Properties and Mix Proportioning of Polymer-Modified Mortars for Buildings," *Report of the Building Research Institute*, 65 (in Japanese)

Ohama, Y., Notoya, K., and Miyake, M., (1985). "Chloride Permeability of Polymer-Modified Concretes," *Transactions, Japan Concrete Institute*, 7, 165-172

Ohama, Y., (1987). "Principle of Latex Modification and Some Typical Properties of Latex-Modified Mortars and Concretes", *ACI Materials Journal*, 84(6), 511-518

Ohama, Y., (1995a). *Handbook of Polymer-Modified Concrete and Mortars Properties and Process Technology*, 1

Ohama, Y., (1995b). "Polymer-Modified Mortars and Concretes," *Concrete Admixtures Handbook: Properties, Science and Technology,* Second Edition, Chapter 7

Ohama, Y., (2007). *Bibliography on Polymers in Concrete*, Third edition, International Congress on Polymers in Concrete (ICPIC), Vol.1 and 2. (CD-ROM)

Ohama, Y., and Shiroishida, K., (1983). "Freeze-Thaw Durability of Polymer-Modified Mortars," *Proceedings of Annual Research Meeting, Materials and Construction, Tohoku Branch, Architectural Institute of Japan*, 41, 165-168 (in Japanese)

Okba, S. H., El-Dieb, A. S., and Reda, M. M., (1997). "Evaluation of the Corrosion Resistance of Latex Modified Concrete (LMC)" *Cement and Concrete Research*, 27(6), 861-868

PCI Committee on Glass Fiber Reinforced Concrete Panels, (1991). "Manual for Quality Control for Plants and Production of Glass Fiber Reinforced Concrete Products."

PCI Committee on Glass Fiber Reinforced Concrete Panels, (1993). "Recommended Practice for Glass Fiber Reinforced Concrete Panels."

Pickett, G., (1956). "Effect of Aggregate on Shrinkage of Concrete," *ACI Journal Proceedings*, 52(5), 581-590

Popovics, S., and Tamas, F., (1978). "Investigation on Portland Cement Pastes and Mortars Modified by the Addition of Epoxy," *Polymers in Concrete—International Symposium ACI Special Publication*, 58, 357-366

Price, W. H., (1982). "Control of Cracking During Construction," *Concrete International*, 4(1), 40-43

Puterman, M., and Malorny, W., (1998). "Some Doubts and Ideas on the Microstructure Formation of PCC," *Proceedings of the IXth International Congress on Polymers in Concrete*, 166-178

Ramakrishnan, V., Coyle, W. V., Kopac, Peter A., and Pasko, T. J., Jr., (1981). "Performance Characteristics of Steel Fiber Reinforced Superplasticized Concrete," *Developments in the Use of Superplasticizers ACI Special Publication*, 68, 515-534

Ramakrishnan, V., (1987). "Materials and Properties of Fibre Concrete," *Proceedings of the International Symposium on Fibre Reinforced Concrete*, 1, 2.3-2.23.

Ranaivomanana, N., Multon, S., and Turatsinze, A., (2013). "Tensile, compressive and flexural basic creep of concrete at different stress levels." *Cement and Concrete Research*, 52, 1-10

Rehm, G., (1961). "Über die Grundlagen des Verbundes zwischen Stahl und Beton," Deutscher Ausshcuss für Stahlbeton, Nr. 138

RILEM Technical Committee 19-FRC, (1977). "Fibre Concrete Materials," *Materials and Structures*, 10(56), 103-120

Rodwell, A. G., (1939). *German Patent* 680,312

Romualdi, J.P., and Batson, G. B., (1963). "Mechanics of Crack Arrest in Concrete." *Journal of the Engineering Mechanics Division*, 89(3), 147-168

Schmitt, T. R., and Darwin D., (1999). "Effect of Material Properties on Cracking in Bridge Decks," *Journal of Bridge Engineering*, 4(1), 8-13

Shah, S. P., and Rangan, B.V., (1970). "Ductility of Concrete Reinforced with Stirrups, Fibers and Compression Reinforcement," *Journal of Structural Division*, 96(6), 1167-1184

Shah, S. P., and Rangan, B.V., (1971). "Fiber Reinforced Concrete Properties," *ACI Journal Proceedings*, 68(2), 126-135

Shah, S. P., and McGarry, F. J., (1971). "Griffith Fracture Criterition and Concrete," *Journal of the Engineering Mechanics Division*, 97(6), 1663-1676

Shah, S. P., (1974). "New Reinforcing Materials in Concrete Construction," *ACI Journal Proceedings*, 71(5), 257-262

Shah, S. P., and Naaman, A. E., (1976). "Mechanical Properties of Steel and Glass Fiber Reinforced Concrete," *ACI Journal Proceedings*, 73(1), 50-53

Shah, S. P., (1983). "Fiber Reinforced Concrete," *Handbook of Structural Concrete*

Shaker, F. A., El-Dieb, A. S., and Reda, M. M., (1997). "Durability of Styrene-Butadiene Latex Modified Concrete," Cement and Concrete Research, 27(5), 711-720

Snyder, M. L., and Lankard, D. R., (1972). "Factors Affecting the Strength of Steel Fibrous Concrete," *ACI Journal Proceedings*, 69(2), 96-100

Sprinkel, M. M., (1999). "Very-Early-Strength Latex-Modified Concrete Overlay," *Transportation Research Record,* 18-23

Su, Z., Bijen, J. M., and Larbi, J. A., (1991). "The Interface between Polymer-Modified Cement Paste and Aggregate" *Cement and Concrete Research*, 21(6), 983-990

Su, Z., Sujata, K., Bijen, J. M., Jennings, H. M., and Fraaij, A. L. A., (1996). "The Evolution of the Microstructure in Styrene Acrylate Polymer Modified Cement Paste at the Early Stage of Cement Hydration," *Advanced Cement Based Materials*, 3(3-4), 87-93

Stang, H., and Shah, S. P., (1986). "Failure of Fiber Reinforced Composites by Pullout Fracture," *Journal of Materials Science,* 21(3), 953-957

Stevens, W. H., (1948) "Latex Processes and Potentialities" *Rubber Developments*, 1(3), 10-13.

Swamy, R. N. and Stavrides, H., (1979). "Influence of Fiber Reinforcement on Restrained Shrinkage and Cracking." *ACI Journal Proceedings*, 94(3), 262-270

U.S. Steel Corporation, (1972). *United States Patent* 3,650,785

Vecchio,F. J., (1999). "Towards Cyclic Load Modeling of Reinforced Concrete", *ACI Structural Journal*, 96(2), 193-202

Wakatsuki, T., Sato, H., Watanabe, Y., and Maruyama, T., (2006). "Development of Fe-Mn-Si-Cr Shape Memory Alloy Machining Chips Reinforced Smart Composite." *Journal of the Iron and Steel Institute of Japan (Tetsu-to-Hagane)*, 92(9), 562-566 (in Japanese)

Works, R. H., and Untrauer, R. E., (1964). Discussion of "Tensile Strength of Concrete Affected by Uniformly Distributed and Closely Spaced Short Lengths of Wire Reinforcement," *ACI Journal Proceedings*, 61(12), 1653-1656

Xu, H.; Mindess, S.; and Banthia, N., (2004), "Toughness of Polymer Modified, Fiber Reinforced High Strength Concrete: Beam Tests vs. Round Panel Tests," *Proceedings of International RILEM Symposium on Concrete Science and Engineering: A Tribute to Arnon Bentur, J. Weiss et al., eds.*, 1

Yannapouos, P. J. and Tassios, T. P., (1991). "Reinforced Concrete Axial Elements Analyzed under Monotonic and Cyclic Actions." *ACI Structural Journal*, 8(1), 3-11

Zainab, Z. I. and Enas, A. A., (2008). "Reuse of Waste Iron as a Partial Replacement of Sand in Concrete," *Waste Management*, 28(11), 2048-2053

LIST OF PUBLICATIONS

Peer-reviewed papers

[1] **Hong S**, Kimura S, Sato Y, Kaneko Y, "Experimental study on drying shrinkage cracking characteristics of steel chip reinforced cementitious composite", *Proceedings of JCI*, 2013, 35(1), 601-606

[2] **Hong S**, Kimura S, Sato Y, Kaneko Y, "Experimental study on drying shrinkage cracking characteristics of steel chip reinforced polymer cementitious composite", *Proceedings of JCI*, 2014, 36(1), 460-465

[3] **Hong S**, Kimura S, Sato Y, Kaneko Y, "Study on drying shrinkage cracking characteristics of steel chip reinforced polymer cementitious composite", *Construction Materials and Structures: Proceedings of the First International Conference on Construction Materials and Structures*, Johannesburg, South Africa, November 2014, 196-201

[4] Kimura S, **Hong S**, Tanaka D, Sato Y, Kaneko Y, "Prediction of drying shrinkage cracking of steel chip reinforced cementitious composite considering tensile creep", *Journal of the Society of Materials Science, Japan* (in press, in Japanese)

[5] **Hong S**, Sato Y, Kaneko Y, Kimura S, "Prediction of drying shrinkage cracking of eco-efficient steel chip reinforced cementitious composite considering tensile creep", *Journal of Advanced Concrete Technology*, 2015, 13(8), 393-402

International conference papers

[6] **Hong S**, Kimura S, Sato Y, Kaneko Y, "Study on drying shrinkage cracking characteristics of steel chip reinforced cementitious composite", *Proceedings of the 2013 World Congress on Advances in Structural Engineering and Mechanics(ASEM13)*, Jeju, Korea, September 2013, 432-443

[7] **Hong S**, Kimura S, Sato Y, Kaneko Y, "Experimental study on free and restrained shrinkage of steel chip reinforced cementitious composite", *Environmentally Friendly Concrete Eco-Crete: Proceedings of the International Symposium on Eco-Crete*, Reykjavik, Iceland, August 2014, 155-162

[8] **Hong S**, Kimura S, Sato Y, Kaneko Y, "Study on free and restrained shrinkage of steel chip reinforced cementitious composite", *Proceedings of the 6th International Conference of Asian Concrete Federation*, Seoul, Korea, September 2014, 827-833

Domestic conference paper

[9] Kimura S, **Hong S**, Kaneko Y, Sato Y, "Drying shrinkage cracking characteristics of steel chip reinforced cementitious composite: Part 1. Test plan", *Summaries of Technical papers of Annual Meeting AIJ*, August 2013, 79-80

[10] **Hong S**, Kimura S, Sato Y, Kaneko Y, "Drying shrinkage cracking characteristics of steel chip reinforced cementitious composite: Part 2. Test results", *Summaries of Technical papers of Annual Meeting AIJ*, August 2013, 81-82

[11] **Hong S**, Kimura S, Tanaka D, Sato Y, Kaneko Y, "Drying shrinkage and creep characteristics of steel chip reinforced cementitious composite: Part 1. Test results of restrained and free drying shrinkage specimens", *Summaries of Technical papers of Annual Meeting Kinki Branch AIJ,* May 2014, 9-12 (in Japanese)

[12] Tanaka D, **Hong S**, Kimura S, Sato Y, Kaneko Y, "Drying shrinkage and creep characteristics of steel chip reinforced cementitious composite: Part 2. Flexural creep test", *Summaries of Technical papers of Annual Meeting Kinki Branch AIJ,* May 2014, 13-16 (in Japanese)

[13] Kimura S, Tanaka D, **Hong S**, Sato Y, Kaneko Y, "Drying shrinkage and creep characteristics of steel chip reinforced cementitious composite: Part 3. Analysis and modeling of crack propagation", *Summaries of Technical papers of Annual Meeting Kinki Branch AIJ,* May 2014, 17-20 (in Japanese)

[14] **Hong S**, Kimura S, Tanaka D, Sato Y, Kaneko Y, "Characteristics of drying shrinkage and creep of steel chip reinforced cementitious composite: Part 1. Test results of restrained and free drying shrinkage specimens", *Summaries of Technical papers of Annual Meeting AIJ,* September 2014, 73-74 (in Japanese)

[15] Tanaka D, **Hong S**, Kimura S, Sato Y, Kaneko Y, "Characteristics of drying shrinkage and creep of steel chip reinforced cementitious composite: Part 2. Test results of restrained and free drying shrinkage specimens", *Summaries of Technical papers of Annual Meeting AIJ,* September 2014, 75-76 (in Japanese)

[16] Sato Y, Tanaka D, **Hong S**, Kimura S, Kaneko Y, "Characteristics of drying shrinkage and creep of steel chip reinforced cementitious composite: Part 3. Modeling of creep characteristics", *Summaries of Technical papers of Annual Meeting AIJ,* September 2014, 77-78 (in Japanese)

[17] Kimura S, Tanaka D, **Hong S**, Sato Y, Kaneko Y, "Characteristics of drying shrinkage and creep of steel chip reinforced cementitious composite: Part 4. Analysis and modeling of crack propagation", *Summaries of Technical papers of Annual Meeting AIJ,* September 2014, 79-80 (in Japanese)

[18] Ida Y, Kato R, Kimura S, Mori K, **Hong S**, Sato Y, Kaneko Y, "Drying shrinkage and creep characteristics of steel chip reinforced cementitious composite: Part 4. Flexural creep of polymer cement mortar", *Summaries of Technical papers of Annual Meeting Kinki Branch AIJ,* June 2015, 13-16 (in Japanese)

[19] Kato R, **Hong S**, Kimura S, Ida Y, Mori K, Sato Y, Kaneko Y, "Bond characteristics of steel chip reinforced polymer cementitious composite: Part 1. Pull-out test of steel bar of small diameter", *Summaries of Technical papers of Annual Meeting Kinki Branch AIJ,* June 2015, 17-20 (in Japanese)

[20] **Hong S**, Kato R, Ida Y, Kimura S, Mori K, Sato Y, Kaneko Y, "Bond characteristics of

steel chip reinforced polymer cementitious composite: Part 2. Uniaxial tension test of steel bar of small diameter", *Summaries of Technical papers of Annual Meeting Kinki Branch AIJ,* June 2015, 21-24

[21] Kato R, **Hong S**, Kimura S, Ida Y, Mori K, Sato Y, Kaneko Y, "Structural test of mortar-based fiber reinforced cementitious composites and steel chip reinforced cementitious composite: Part 6. Pull-out test of polymer cementitious material and small diameter steel bar", *Summaries of Technical papers of Annual Meeting AIJ, September* 2015 (in Japanese)

[22] **Hong S**, Kato R, Ida Y, Kimura S, Mori K, Sato Y, Kaneko Y, "Structural test of mortar-based fiber reinforced cementitious composites and steel chip reinforced cementitious composite: Part 7. Uniaxial tension test of polymer cementitious material and small diameter steel bar", *Summaries of Technical papers of Annual Meeting AIJ, September* 2015

ACKNOWLEDGEMENTS

This dissertation has been completed under the guidance of my advisor, Professor Yoshio Kaneko. First, I would like to express my sincere gratitude to him. I could have learned not only the professional knowledge, but also the way to do a research through creative thinking. I am deeply indebted to him for his guidance, inspiration, and encouragement in the past three years. It is a great honor to work with him and I will keep those things I have learned in my mind and take them as my guideline for my future.

I would like to give special thanks to Assistant Professor Yuichi Sato. Without his support, I could have never completed this work. From the early stage of this study, his guidance, comments and patience led me to conduct this research. I appreciate a lot of useful help on solving the met difficulties from when I was a research student, both in my research and life in Japan. I will never forget your kindness to me.

Great thanks go to my dissertation committee member, Professor Hitoshi Tanaka and Professor Izuru Takewaki for their valuable comments and encouragement.

Very special thanks go to Professor Wanki Kim of Hyupsung University (Korea), my former supervisor, for his encouragement and kindness over these years.

I would also like to thank Emeritus Professor Yoshihiko Ohama of Nihon University. His enthusiastic working attitude and determination always inspire me as a researcher.

Sincere thanks go to Mr. Shinya Kimura (OB), Mr. Daiki Tanaka, Miss. Yuika Ida and Mr. Ryohei Kato. Without their great efforts and kind support, this work are not possible to complete.

I would like to thank Mr. Mori Koji for his helpful comments and support, Mr. Takahiro Chujo, Mr. Yuhei Yamagami, Mr. Takamasa Terashima, Mr. Ryo Inoue, Miss. Eri Fujioka, Mr. Junya Watanabe and all members of Kaneko Laboratory including OB members since 2012, Mr. Namikawa Genki, Mr. Tatsuya Okada, Mr. Kazuya Matsushita and Mr. Tetsuya Kida, Miss. Nanohana Ikeuchi for their kind support.

I must acknowledge the Japan Society for the Promotion of Science (JSPS) for granting me the research fellowship for young scientists (DC1) which made this study possible.

Finally, I would like to thank my family, especially my parents and all my friends for their love and support and encouragement.

August, 2015

Sunhee Hong